University of Alberta
Department of Civil &
Environmental Engineering

Structural Engineering Report No. 191

Cyclic Behavior of Steel Gusset Plate Connections

by

Jeffrey S. Rabinovitch

and

J.J. Roger Cheng

August 1993

Structural Engineering Report No. 191

CYCLIC BEHAVIOR OF STEEL GUSSET PLATE CONNECTIONS

by

Jeffrey S. Rabinovitch

and

J.J Roger Cheng

Department of Civil Engineering

University of Alberta

Edmonton, Alberta

August, 1993

ABSTRACT

The cyclic behavior of steel gusset plates has been examined by an experimental investigation of full-scale gusset plate connections of a diagonal bracing member at the joint of a beam and column. The frame model examined considers a concentric braced frame where the brace member is designed not to buckle. The energy of the system is designed to be absorbed by the gusset plate connection. The experimental program considered the effect of the gusset plate thickness, plate edge stiffeners, gusset plate geometry, and connection bolt slip on the energy absorption characteristics of the system. A total of five gusset plate specimens were tested under reverse loading conditions. The test results were compared to current design practices and to the results of a monotonic gusset plate test series. The finite element program ANSYS was used to provide an analytical reference to the observed test results.

Based on the test results it was revealed that the ultimate tensile behavior of the gusset plate specimens was not significantly adversely affected by the cyclic loading history. In contrast, it was observed that cyclic loading significantly reduces the ultimate compressive strength of gusset plates. The tensile strength of gusset plates under cyclic loads can be accurately determined using the block shear tear-out model. The equivalent column method provides a conservative estimate of the ultimate compressive capacity of gusset plates under cyclic loads. Unstiffened gusset plate specimens experienced an unstable drop in compressive load carrying capacity once overall plate buckling occurs. However, stiffened gusset plates reveal a stable post-buckling response. It was determined that there is no rationale for providing for the free formation of a plastic hinge in the geometry of a gusset plate connected to the framing members on two sides. The gusset plate required to accommodate the free formation of a plastic hinge results in a reduced stiffness and buckling load. It is concluded that properly designed and detailed gusset plate

connections appear capable of absorbing significant amounts of energy to validate the proposed 'strong braced, weak gusset' concentric braced frame model.

ACKNOWLEDGEMENTS

This report is a reprint of a thesis by the same name, written by the first author under the supervision of the second author.

Financial support for the project was provided by the Natural Sciences and Engineering Research Council of Canada to Dr. J.J. Cheng under grant No. 4727 and the Central Research Fund of the University of Alberta. Financial support was provided to the first author by the Natural Sciences and Engineering Research Council of Canada and by the Walter H. Johns Graduate Fellowship.

The assistance of the technical staff of the I.F. Morrison Structural Laboratory at the University of Alberta is acknowledged.

A special gratitude of thanks goes to Michael Yam for his helpful advice and suggestions.

TABLE OF CONTENTS

LIST OF TABLES

LIST OF FIGURES

1. INTRODUCTION

1.1 General

Concentric braced frames are one of the most common lateral load-resisting systems for steel buildings. In a concentric braced frame the lateral loads applied to the structure are resisted by a network of inclined bracing members. Depending on the configuration of the braced frame, either tensile or compressive loads can be accommodated by the bracing members. These loads are commonly transferred to the beam and column members of the frame by gusset plate connections. The gusset plate receives the load from the diagonal bracing member and transfers it to the main framing members. The delivery of load into and out of the gusset plate will produce bending, shear, and normal forces in the gusset plate. Some common configurations of concentric braced frames are shown in Figure 1.1. When a structure is subjected to reverse lateral load conditions, the bracing members and the gusset plate connections can be subject to both tensile and compressive load conditions.

1.2 Seismic Design Considerations

When a steel structure is required to resist seismic load conditions, the design of the concentric braced frame is governed in Canada by the National Building Code of Canada 1990 (NRCC, 1990) and the provisions of CAN/CSA-S16.1 - Limit States Design of Steel Structures (CSA, 1989). The National Building Code outlines the procedure for determining the minimum lateral seismic force that is to be applied to the structure. The determination of the lateral seismic force considers, among others, the nature of the design seismic event, the fundamental period of the structure, the foundation substrate conditions, and the type of lateral load resisting system. The type of lateral load resisting system is included in the design by a force reduction factor, R. Depending on the strength and ductility of the framing system, the calculated elastic lateral seismic force is reduced by the

force reduction factor to reflect the inelastic response of the structure. The National Building Code classifies concentric braced frames as either ductile, nominally ductile, or in a third category for which no special provisions are made for ductile behavior.

CAN/CSA-S16.1 (CSA, 1989) provides detailed provisions for ductile and nominally ductile braced frames. The CSA standard defines the design loading to be applied to the components of the framing system and as well imposes specific member limitations. The expected behavior for braced frames with concentric bracing is that ductility is provided by braces yielding in tension or in flexure under compression. In general, the other members of the framing system are designed to remain essentially elastic. A further discussion of the energy absorbing mechanism in lateral load resisting systems will be considered in the next section.

1.3 Energy Absorption in Braced Frames

It is the requirement of the CSA code that ductile braced frames with concentric bracing have the capacity to absorb energy through the yielding of braces. It will be proposed in the current research, that an alternate design philosophy is worthy of consideration.

The energy absorption characteristics of traditional braced frames is best understood by observing the behavior under cyclic loads. A typical horizontal load versus displacement plot for a one-bay, one-story X-braced frame is shown in Figure 1.2 (Wakabayashi, et al., 1974). The solid curve line represents the actual test frame behavior under reversed loading conditions. The observed hysteresis loops are pinched and begin to deteriorate as the loading cycles increase. This reduced energy absorbing response is a result of the post-buckling behavior of the compression bracing and the behavior of bent tension bracing. A more stable inelastic compressive response would be required to improve the energy absorption characteristic of the frame. In addition, the figure shows the monotonic

test behavior of the frame specimen (heavy dotted line) and an analytical prediction of the frame response (light dotted line).

Eccentric braced frames absorb energy in an entirely different manner than concentric braced frames. The distinguishing characteristic of an eccentric braced frame is that at least one end of every brace is connected so that the brace force is transmitted either to another brace or to a column through shear and bending in a beam segment called a link (Figure 1.3). Inelastic activity under severe cyclic loading is restricted primarily to the links, which are designed and detailed to sustain large inelastic deformations without loss of strength. In contrast to concentric braced frames, the braces are designed not to buckle, regardless of the severity of lateral loading on the frame. Because brace buckling is prevented and because the link can sustain large deformations without strength loss, full and stable hysteretic loops similar to those of moment resisting frames are obtained (Popov and Engelhardt, 1988).

Figure 1.4, reprinted from Popov and Engelhardt (1988), provides a crude comparison between the hysteresis behavior of a moment resisting frame (MRF), a concentric braced frame (CBF), and an eccentric braced frame (EBF). The observed difference in cyclic load behavior is recognized by the National Building Code of Canada (NRCC, 1990). The favorable energy absorption behavior of ductile moment resisting frames is assigned a force reduction factor of R = 4.0. Eccentric braced frames are designed using an R value of 3.5, while the reduced energy absorption behavior of concentric braced frames is evidenced by an assigned R value of 3.0 or less.

The experience gained from eccentric braced frames can be applied to concentric frames in an effort to improve their energy absorption characteristics. The behavior of concentric braced frames can be improved if brace buckling can be avoided and the inelastic activity

can be confined to an element designed and detailed to sustain large inelastic deformations without significant loss of strength. The current research attempts to do just that. The frame model to be examined considers a concentric braced frame where the brace member is designed not to buckle. The energy of the system is designed to be absorbed by the gusset plate connection. The gusset plate is designed to yield in tension and to buckle in compression. In compression, a stable post-buckling behavior is desired for the gusset plate if an improved energy absorption behavior is to be obtained. It is the behavior of the gusset plate element under severe cyclic loads that is the focus of this investigation.

1.4 Current Gusset Plate Design

Design specifications in North America currently provide very little guidance for the design of steel gusset plates. Generally, only design philosophy is provided, with no specific formulas for evaluating the dimension and thickness of a gusset plate. As such, the design of gusset plates often draws upon the experience of the structural engineer.

When gusset plates are designed to resist strictly monotonic tension or compression, CAN/CSA-S6-88 - Design of Highway Bridges (CSA, 1988) states only that gusset plates shall be of ample thickness to resist shear, direct load, and flexure, acting on the weakest or critical section. A simple design equation is provided to determine the factored shear resistance of the gross area of the gusset plate. In addition, a provision is provided to avoid local buckling of the unsupported edge of a gusset plate. CAN/CSA-S6-88 states that if the unsupported edge of a gusset plate that may be subjected to compression exceeds $945/\sqrt{Fy}$ times its thickness, the edge shall be stiffened. Similar provisions are also provided in the 1989 Standard Specifications for Highway Bridges (AASHTO, 1989).

The Load and Resistance Factor Design Specification for Structural Steel Buildings (AISC, 1986) suggests that, if practicable, intersecting axially stressed members shall have

their gravity axes intersect at one point, otherwise, provisions shall be made for bending and shearing stresses due to the eccentricity. Design strength for gusset plates is only considered for tension loading conditions. It is stated that the design strength shall be the lower value obtained according to the limit states of yielding, fracture of the gusset plate element, and block shear rupture of the connection. Provisions relating specifically to the design of gusset plates under seismic conditions are provided in the Seismic Provisions for Structural Steel Buildings (AISC, 1992). A distinction is made between gusset plates that are connected to brace members that buckle in-plane or out-of-plane of the gusset plate. When the brace member buckles out-of-plane it is required that the brace terminate on the gusset a minimum of two times the gusset thickness from the theoretical line of bending which is unrestrained by the column or beam joints. This detail is provided to permit the formation of a hinge line in the gusset plate.

Under seismic loading conditions, CAN/CSA-S16.1-M89 - Limit States Design of Steel Structures (CSA, 1989) provides detailed provisions for the design of braced frames. A required factored resistance for the design of bracing connections is provided. The resistance of the bolted gusset plate connection is based on the ultimate tensile strength due to block shear considerations. In addition, it is suggested that gusset plates shall be detailed to avoid brittle failures due to rotation of the brace when it buckles. This specific design recommendation, and its origins, will be considered in detail in Chapter 5.

It is evident that the available design specifications provide only minimal support to the structural designer in his task of conventional gusset plate design. What guidance is provided is based on the design philosophy that ductile braced frames with concentric bracing have the capacity to absorb energy through the yielding of braces. This assumes that the other frame elements, including the gusset plates, remain essentially elastic. However, when the gusset plate is to be designed as the primary energy absorption

element, undergoing large inelastic deformations, no design guidelines exist.

1.5 Objectives and Scope

In order for the proposed 'strong brace, weak gusset' concentric braced frame to be effective under seismic loading conditions, the gusset plate must be capable of sustaining large inelastic deformations without significant loss of load. Therefore, the current research project was initiated to investigate the behavior of steel gusset plates under cyclic loads. The main objectives of the project are as follows:

1. Observe the general behavior of gusset plates under cyclic loading conditions
2. Provide experimental data for the various design parameters
3. Improve the compressive behavior of gusset plates under cyclic compressive loads
4. Determine if the ultimate gusset plate capacity under tension is affected by severe compressive inelastic deformations, and vice versa
5. Determine the feasibility of having the gusset plate as the primary energy absorption element in a concentric braced frame
6. Establish preliminary design rules, if possible
7. Identify areas requiring further investigation

Because of the complexity of the problem, the research program developed to fulfill these purposes was primarily experimental in nature. The test results are compared both with the current design practices and the results of tests performed on gusset plates under monotonic loading conditions. A limited finite element study was conducted to provide a basis of comparison for the observed test results. The scope of the investigation is limited to the following:

1. Single gusset plate connections of a concentric braced steel frame were used

2. All gusset plates were connected to the main framing members along two plate boundary edges
3. The diagonal bracing member was prevented from buckling
4. Forces that exist in the beam and column were neglected in the test program
5. The gusset plate variables that were chosen for investigation under cyclic loads are plate thickness, gusset plate geometry such that the formation of a plastic hinge is facilitated, and the stiffness of the plate free edges

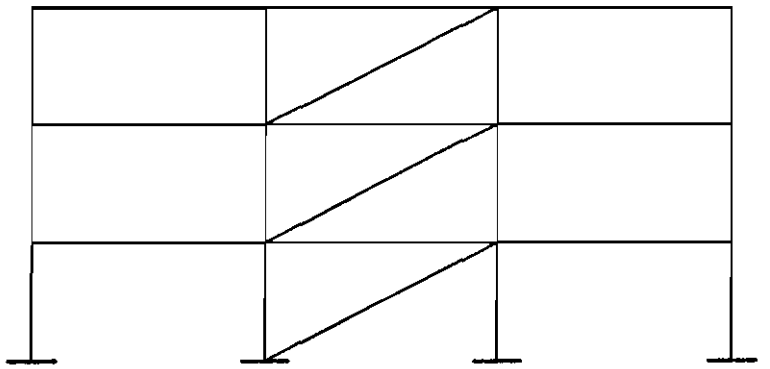

a) Diagonal Bracing

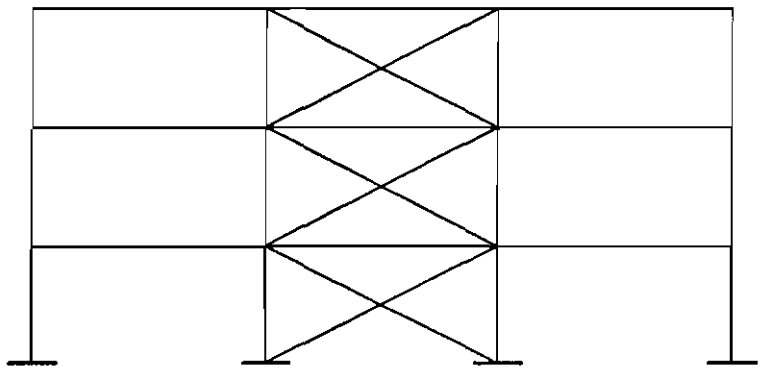

b) X-bracing

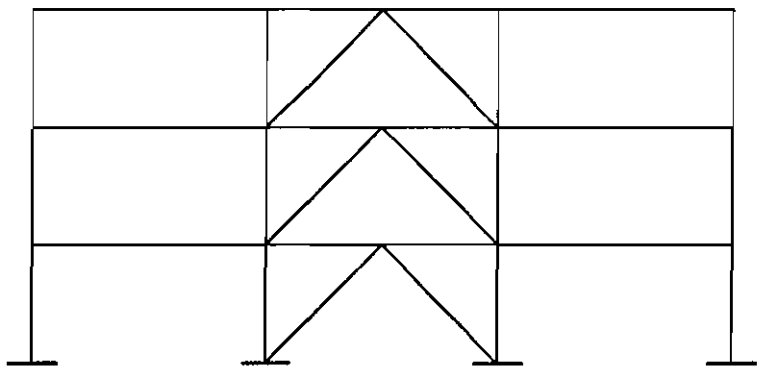

c) Chevron Bracing (V-bracing)

Figure 1.1. Basic Configurations of Concentric Braced Frames

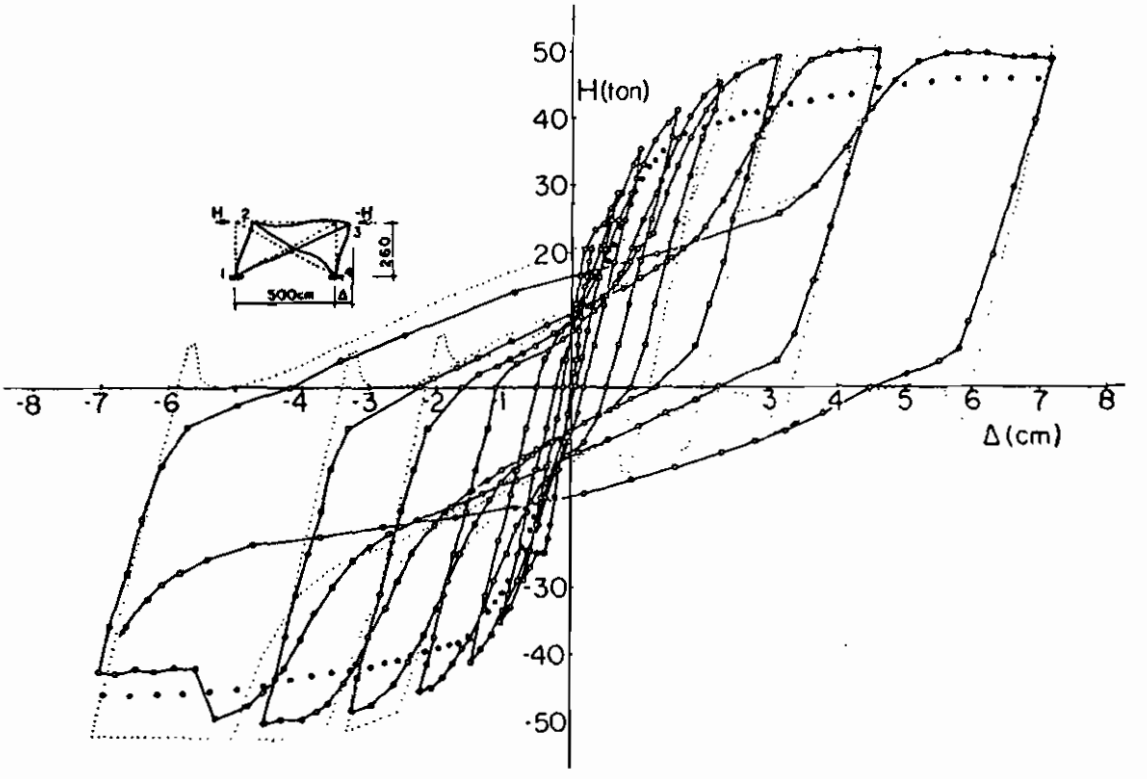

Figure 1.2. Hystereris Loops - Concentric Braced Frame
(Wakabayashi, et al, 1974))

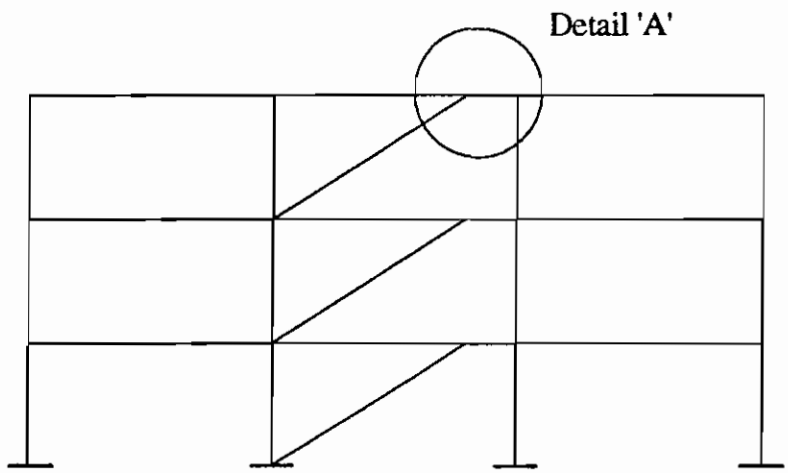

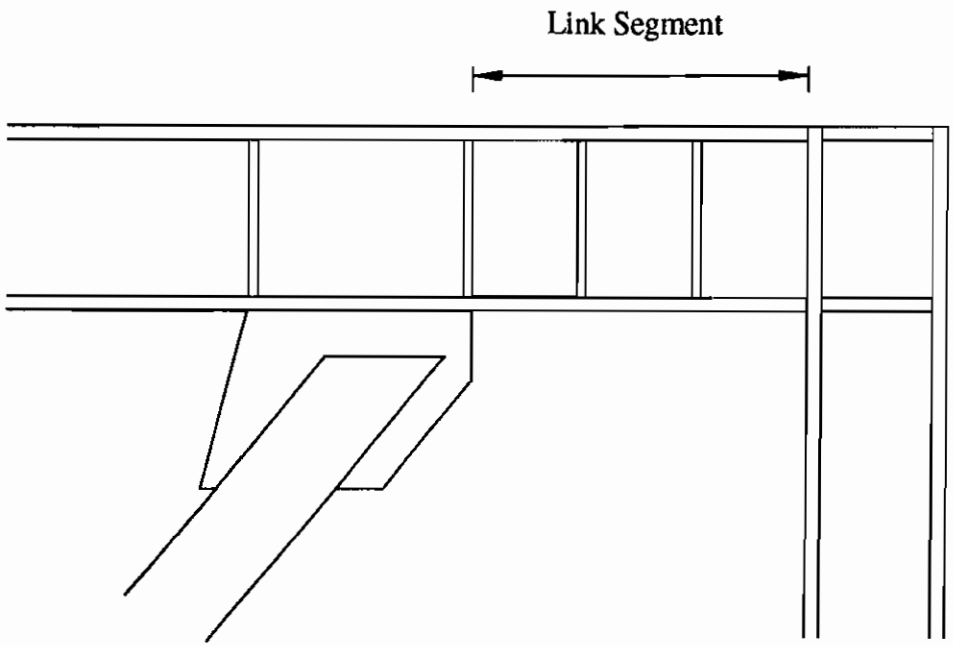

Detail 'A'

Figure 1.3. Eccentric Braced Frame - Link Segment

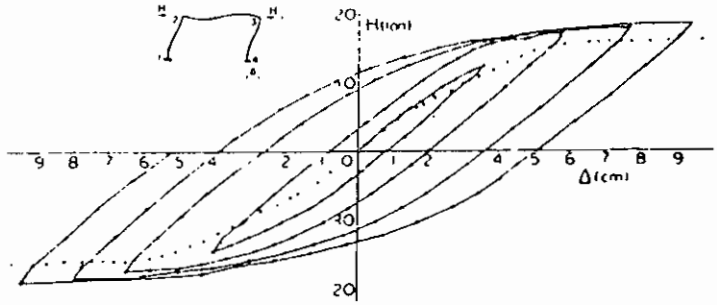

(a)

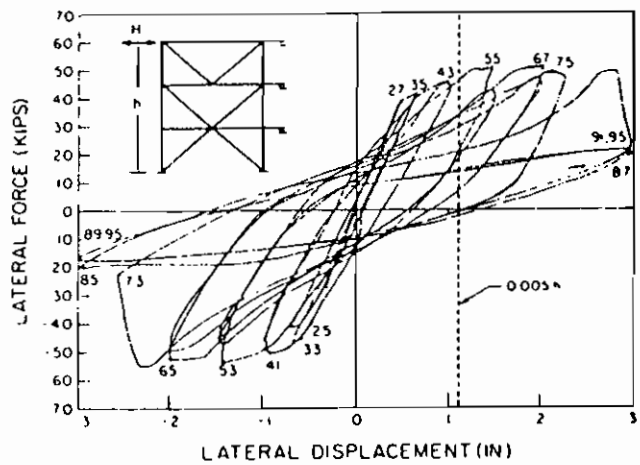

(b)

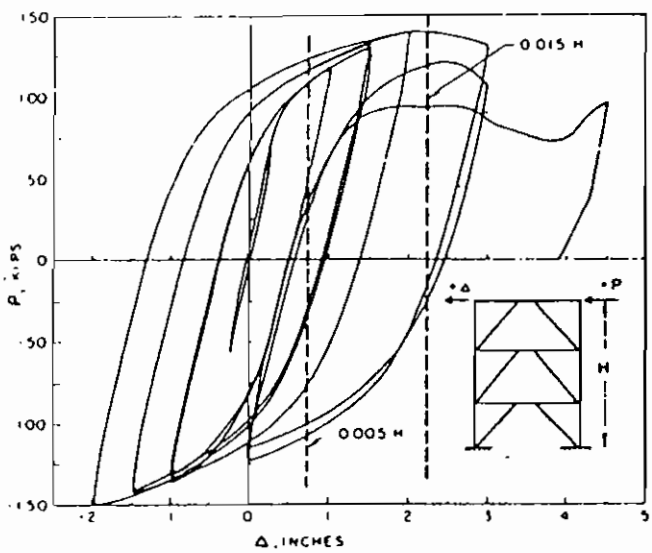

(c)

Figure 1.4. Typical Experimental Frame Behavior under Cyclic Lateral Load. (a) MRF; (b) CBF; (c) EBF
(Popov and Engelhardt, 1988)

2. LITERATURE REVIEW

2.1 Introduction

The current design method for gusset plates is mainly the result of experience, general practice, and the engineer's intuition. Recent research has attempted to improve the knowledge of the behavior of gusset plates in an effort to provide a rational design approach. However, the focus has been only on the behavior under either monotonic tension or compression. Research into the behavior of steel gusset plates under cyclic loads is severely lacking.

In this chapter, past work done on gusset plate connections is reviewed. Section 2.2 examines gusset plate research from an historical perspective, while Section 2.3 reviews recent research into the ultimate load behavior of gusset plates under both monotonic tensile and compressive loads. The limited investigations of the behavior of gusset plates under cyclic loads is considered in Section 2.4.

2.2 Early Gusset Plate Research

Early research focused on determining the general elastic stress distribution in gusset plates. One of the early gusset plate studies that was to prove significant was conducted by Whitmore (1952). Whitmore tested a one-quarter scale model of a gusset plate connection from the lower chord of a Warren Truss. A schematic drawing of the gusset plate prototype is shown in Figure 2.1. Experimental tests were performed on aluminum gusset plate models and stresscoat tests were performed using masonite specimens. Based on his experiments, Whitmore determined that the location of the maximum tensile stress is near the end of the tension diagonal and the maximum compressive stress is near the end of the compressive diagonal. Whitmore also concluded that using beam formulas to determine the direct, bending, and shearing stresses on a plane through the ends of the

diagonals does not accurately reflect the stress condition in gusset plates. Based on his observations, Whitmore found that the maximum tensile and compressive stresses could be approximated quite closely by assuming the force in each diagonal to be uniformly distributed over an area obtained by multiplying the plate thickness by an effective length normal to the axis of the diagonal. This effective length is obtained by drawing 30° lines from the outside bolts of the first row, to intersect with a line perpendicular to the member through the bottom row of bolts. This concept compares quite well to test results and has since been used as one of the primary tools in gusset plate design. An estimate of the gusset plate yield load can be determined by multiplying the yield stress by the plate area at the effective width section. The method of determining the 'effective width' is illustrated in Figure 2.2.

Subsequent investigations attempted to confirm Whitmore's findings. Irvan (1957) investigated the primary stress in the double gusset plates of a Pratt truss. The locations of the maximum stresses were similar to Whitmore's. However, his method of estimating the maximum stress was slightly different than Whitmore's. A further study by Hardin (1958) of a gusset connection of a Pratt truss confirmed Irvan's findings. Finite element studies were first performed by Davis (1967) and Vasarhelyi (1971) to determine the elastic stress distribution in gusset plates. Davis performed his study on the gusset plate model used by Whitmore and confirmed his results. Vasarhelyi performed tests and elastic finite element analyses on a scale model of a Warren truss. He found that the maximum stress determined by various simplified analytical methods are only slightly different; the only deviations are in the location of the maximums.

2.3 Monotonic Gusset Plate Behavior

More recent research has concentrated on the behavior of gusset plates under ultimate load conditions. This section will consider the body of research that has addressed the

problem of ultimate gusset plate capacity under monotonic loads, both tensile and compressive.

Thornton (1984) presented an approach to the design of vertical bracing connections based on satisfying the dual requirement of equilibrium and yield, with sufficient attention given to stiffness to preclude buckling and failure. Thornton considered all components of a typical bracing connection. To determine the gusset plate ultimate strength under tension, he considered the tear-out of the gusset plate. The capacity is related to the block shear requirements of the 1978 AISC Specification. The tear-out capacity is based on the net section with hole size taken as bolt diameter plus 1/16 inch. In compression, Thornton considered gusset plate buckling by establishing the capacity of an equivalent column section. This method considers an imaginary fixed-fixed column strip (effective length coefficient, k=0.65) of unit width below the Whitmore section. The length of the column strip may be taken as the largest of L_1, L_2, and L_3 as defined in Figure 2.3. This strip is used to determine an equivalent slenderness ratio. Alternately, Thornton suggests that a shorter length, such as the average of L_1, L_2, and L_3, may give a more reasonable approximation of the buckling strength. Thornton originally presented his approach as an allowable stress method. From an ultimate strength perspective, the compressive buckling resistance of the gusset plate can be evaluated according to the column curves in the CAN/CSA-S16.1-M89 standard (CSA, 1989) using the Whitmore effective width (Whitmore, 1952) as the column area and the equivalent slenderness from the fixed-fixed column strip. Thornton states that this approach is conservative because it ignores plate action and the post-buckling strength of plates.

The behavior of gusset plates under tensile loads was isolated by Bjorhovde and Chakrabarti (1985). The joints that were tested were full-scale single gusset plate connections of a diagonal bracing member at the joint of a beam and column. Six tests

were performed, with three tests each at two different plate thicknesses and three different bracing member angles. For the type of bracing connection examined, the primary failure mode of the gusset plate was a tear across the bottom bolt holes of the splice connection. It was also determined that the type and location of the gusset plate boundaries, combined with the load transfer mechanism into the plate, have important secondary effects on plate buckling and associated out-of-plane bending.

Hardash and Bjorhovde (1985) continued the study of gusset plate capacity under tensile loads. In order to develop an ultimate strength approach to the design of gusset plates, test results from the University of Arizona, the University of Illinois, and the University of Alberta were incorporated into the evaluation. For all 42 gusset plate specimens, a tensile tear across the last row of bolts was observed, regardless of the strength parameters, hole size, or plate material. It was concluded that the governing block shear model is one incorporating the tensile ultimate strength, F_u, on the net area between the last row of bolts, and a uniform effective shear stress, F_{eff}, acting on the gross area along the outside bolt holes (Figure 2.4). The set of equations developed to give the nominal ultimate resistance, R_n, of a gusset plate loaded in tension are as follows:

$$R_n = F_u S_{net} t + 1.15 F_{eff} L t$$

$$F_{eff} = (1-C_1)F_y + C_1 F_u$$

$$C_1 = 0.95 - 0.047\ L\ (\text{L in inches})$$

It was discovered that the shear stress distribution is not uniform, but rather depends on the particular connection geometry and material. The variation in the shear stress distribution is accounted for by a connection length factor, C_1. If C_1 equals zero, then the effective shear stress equals the shear yield stress, and if C_1 equals one, then the effective shear stress equals the shear ultimate strength.

Williams and Richard (1986) conducted analytical and experimental studies to develop

design procedures for steel gusset plates in diagonally braced frames. The study considered both the tensile and compressive behavior of gusset plates. The analysis included the nonlinear behavior of the fasteners and the frame to which the gusset plate is attached. Finite element results demonstrated that the additional stiffness provided by the gusset plate cause the beam to develop end moments equivalent to a haunched fixed-end beam. To determine the tensile capacity, Richard developed a block shear model in which it is assumed that the plate will fail along the gross section of the bolt pattern in large diagonal connections. The strength of the gusset plate in tension may be determined by combining the tensile stress resultant acting at the end of the bolt pattern with the shear stress resultants acting along the sides of the bolts. In the case of bracing connections with less than six rows of bolts, it is suggested that it may be appropriate to use the net shear area, as opposed to the gross shear area, in the block shear model. Design equations were also generated to predict the gusset-to-frame fastener force distribution. It was determined that fastener forces do not act in pure shear as is commonly assumed in current design procedures. In compression, the finite element analysis was limited to linearly elastic behavior.

Full-scale diagonal bracing members were tested by Cheng and Hu (1987) at the University of Alberta. The compressive behavior and elastic buckling strength were examined. The gusset plate parameters considered in the investigation were plate thickness, geometric configuration, boundary condition, and out-of-plane eccentricity. All concentrically loaded tests failed in plate buckling. The eccentrically loaded specimens failed in plate bending of the splice plates. Attempts were made to correlate the eccentric loading tests with beam-column formulas and the concentric loading test results with the finite element program BASP (Akay, et al., 1977). The analytical predictions were in reasonable agreement with the test results. The available design methods were found to be inappropriate for determining the compressive behavior and failure of gusset plates.

Additional analysis of the test results was performed by Cheng, et al. (1993). A finite element analysis by the program ANSYS gave reasonable predictions of the elastic buckling strength of the gusset plate test specimens. Furthermore, the splice member connection length and the thickness of the splice member were found to affect the elastic buckling strength of the specimens. Increasing the length of the splice member connection, or the thickness of the splice member, results in an increase in the elastic buckling strength.

An experimental program was undertaken by Gross (1990) to determine 1) the influence of the members framing into the connection on the behavior and strength of the connection, 2) the effect of connection eccentricity on gusset plate capacity and the distribution of forces to the framing members, and 3) the difference in performance between a connection made to the column flange and one made to the column web. The behavior of three nearly full-scale braced steel subassemblies were studied experimentally. It was determined that computing gusset plate buckling using the equivalent column method with a value of k=0.5 appears to be conservative. Additionally, gusset tear-out capacity is predicted very closely using the block shear approach. It was found that the eccentric connection, which had a compact gusset plate, had a higher buckling capacity than larger concentric gusset plates, and that the gusset plates produced a nearly fixed condition for the beam to column connection.

Additional gusset plate research was performed at the University of Alberta by Cheng and Yam (1991). Test were performed on five gusset plate specimens in order to determine the inelastic behavior of gusset plates under compressive loads. Each specimen was tested under two conditions, the free case and the fixed case. For the free case, the diagonal bracing member was allowed to move out-of-plane relative to the test frame. For the fixed case, both the test frame and the diagonal bracing member were restrained from

moving out-of-plane. The paper presents the results of the inelastic specimens tested by Cheng and Yam and reviews the test results of the elastic specimens tested by Cheng and Hu (1987). It was determined that the plate thickness and plate size affect the buckling strength of the gusset plate significantly. The failure mode for the free case tests was sway buckling of the gusset plate connection, while the failure mode for the fixed case was local buckling of the free edges of the plate. The out-of-plane restraint had a lesser effect on the inelastic buckling strength of the specimens while the elastic buckling strength was greatly affected by the restraint. The test results show that the Whitmore effective width concept overestimates the strength of the specimens that failed in elastic buckling, but underestimates the inelastic buckling strength. In addition, the Thornton equivalent column method produced a large margin of safety for the gusset plate specimens that failed in inelastic buckling.

Cheng and Yam are considering the effect of the framing members, brace angle, and eccentric loading conditions on the compressive behavior of gusset plates. This phase of the research is currently in progress at the University of Alberta.

2.4 Cyclic Gusset Plate Behavior

Research into the cyclic behavior of steel gusset plates in concentrically braced frames is severely lacking. One of the most relevant studies in this area is a series of experimental investigations conducted at the University of Michigan. Astaneh-Asl, et al. (1981) conducted an experimental study to investigate the cyclic behavior of bracing members made of double angles connected to end gusset plates by fillet welds or high strength bolts. However, only the preliminary results from the welded specimens are included in this report. Two types of specimens were made. Brace angle specimens with long legs back-to-back buckled out-of-plane, whereas specimens with short legs back-to-back buckled in-plane. The specimens were tested under quasi-static cyclic deformations to

simulate the effects of strong earthquakes. Although the study focused on the brace member behavior, gusset plate behavior was also monitored. Observations from the in-plane specimen tests revealed that no major plastification occurred in the gusset plates and they behaved mostly elastic until the end of the test. Observations from the out-of-plane specimen tests showed that during post-buckling deformations the rotation of the plastic hinges in the gusset plate is about an axis normal to the axis of the brace member. From the study, it was discovered that the portion of the gusset plate connected to the angles must be allowed to rotate freely about the axis of the hinge. Any restriction to this freedom would cause early fractures in the gusset plate. As such, it was concluded from the tests that an optimum free length of 2t, where t is the thickness of the gusset plate, was necessary for the free space in the gusset to prevent its premature fracture. Figure 2.5 shows the type of gusset plate employed in this study and the recommended free length of gusset plate required to allow free rotation about the plastic hinge.

A further research paper by Astaneh-Asl, et al. (1985) focuses on the out-of-plane specimen tests. The results of both the welded and bolted specimens are included in this report. It was observed that three plastic hinges formed in all test specimens. One hinge formed at midspan of the brace and one in each end gusset plate. The formation of plastic hinges in the end gusset plates was due to the relatively small strength and stiffness of the gusset plate in out-of-plane bending, compared to that of the double-angle member. The combined effect of bending and axial load in the post-buckling region caused yielding in the gusset plate before the angles. It was noticed that the brace buckling load decreased significantly from the first to second cycle. In further cycles, however, the rate of decrease in buckling capacity was reduced. The conclusions of Astaneh-Asl, et al. (1981) are reiterated. It is stated that not only must plastic hinges in the gusset plate be free to form, but there must be enough free length of the gusset between the ends of the angles and the corner of the gusset. The free length of 2t is again advised.

The cyclic behavior of gusset plate connections in V-braced frames was studied by Astaneh (1992). To improve the behavior of V-braced frames, this study suggests that shear inelasticity of the gusset plate connection be utilized as a reliable and stable source of ductility and energy dissipation. The experimental part of the research consisted of subjecting three gusset plate connections to cyclic loading. It was observed that the specimen with the largest eccentricity of point of intersection of members behaved in the most desirable manner, while the behavior of the typical concentric connection used in V-braced frames was relatively brittle and undesirable. In the specimen with the largest eccentricity, the governing failure mode was the shear yielding of the gusset plate which was a very ductile and stable energy dissipating mechanism. Additionally, a capacity design approach is proposed. The main component of the design philosophy is to make the shear yielding of the gusset plate the weakest link in the system. It is expected that the gusset plate will yield before the buckling of the bracing member and that the inelastic shear deformation of the gusset will result in a more ductile bracing system.

Research into the behavior of connections for seismic-resistant eccentrically braced frames (EBFs) is described by Engelhardt and Popov (1989). Although brace connections in EBFs may be subject to a significantly different stress environment than brace connections in concentrically braced frames, the observed gusset plate behavior is worthy of note. It was observed that large compressive stresses were produced along the edge of the gusset plate nearest the link region. In order to preclude gusset plate buckling, stiffeners were provided along the edge of the gusset plate. The improved gusset plate detail performed well under cyclic loading.

The current test program by the author is a continuation of the gusset plate research conducted at the University of Alberta. Cheng and Hu (1987) considered the elastic buckling of gusset plates, while Cheng and Yam (1991) are currently considering the

inelastic compressive behavior. The current study on the cyclic behavior of steel gusset plates draws upon the experienced gained in these previous investigations.

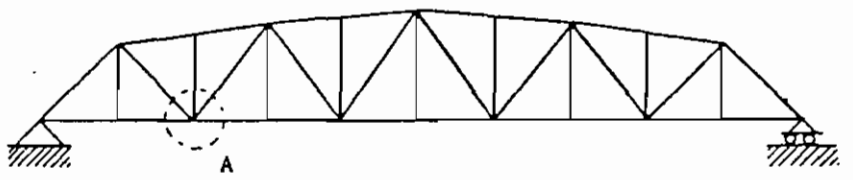

Truss Outline

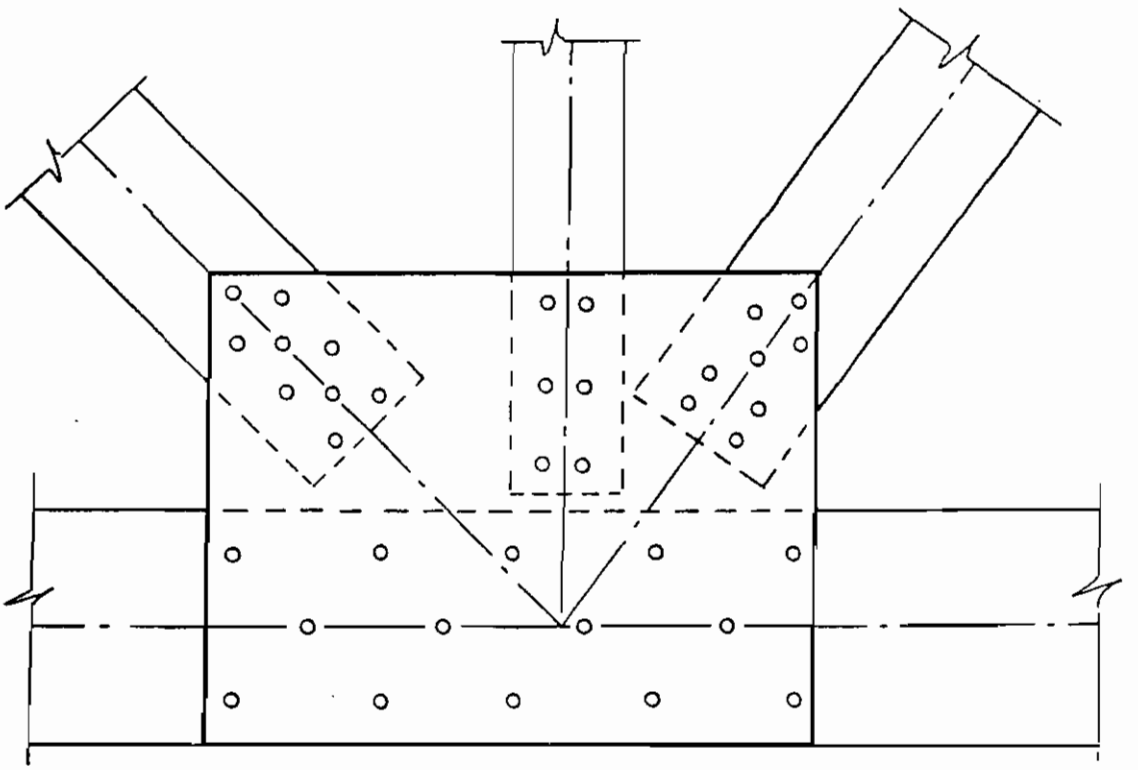

Connection A

Figure 2.1. Whitmore Gusset Plate Prototype

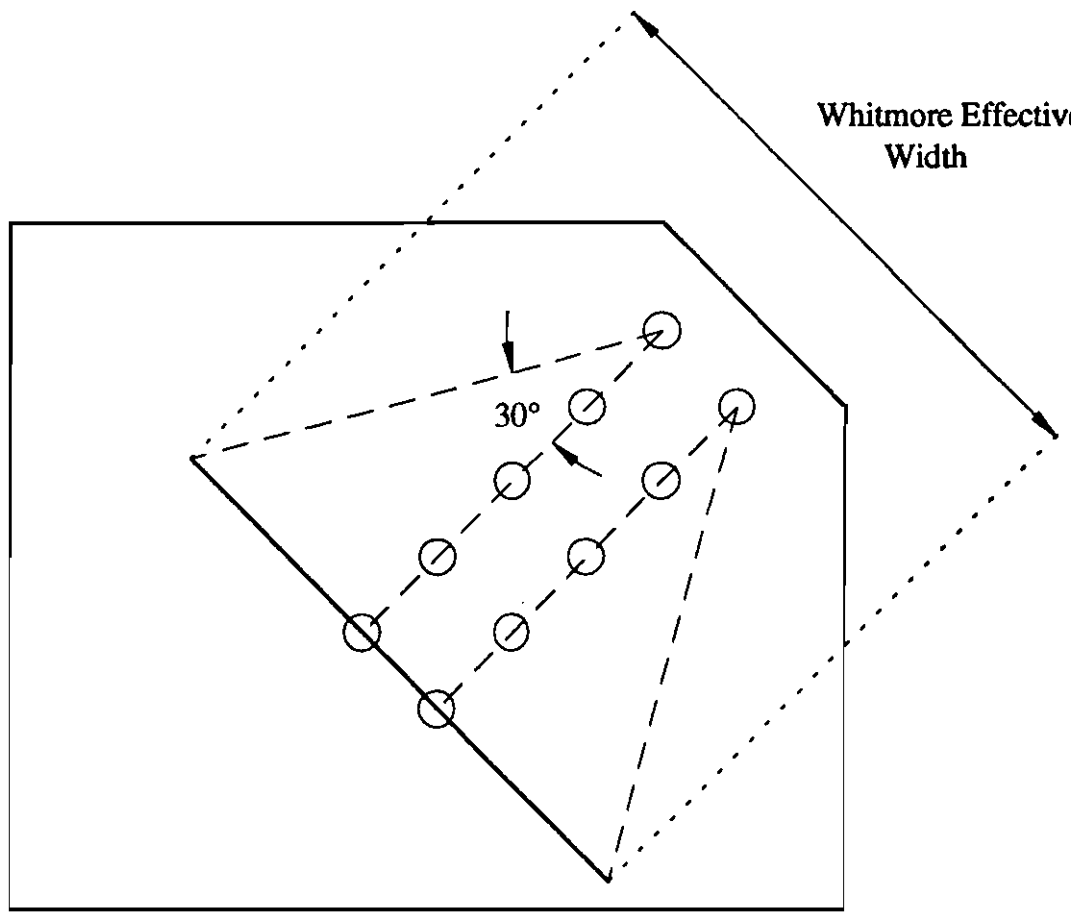

Figure 2.2. Whitmore Effective Width

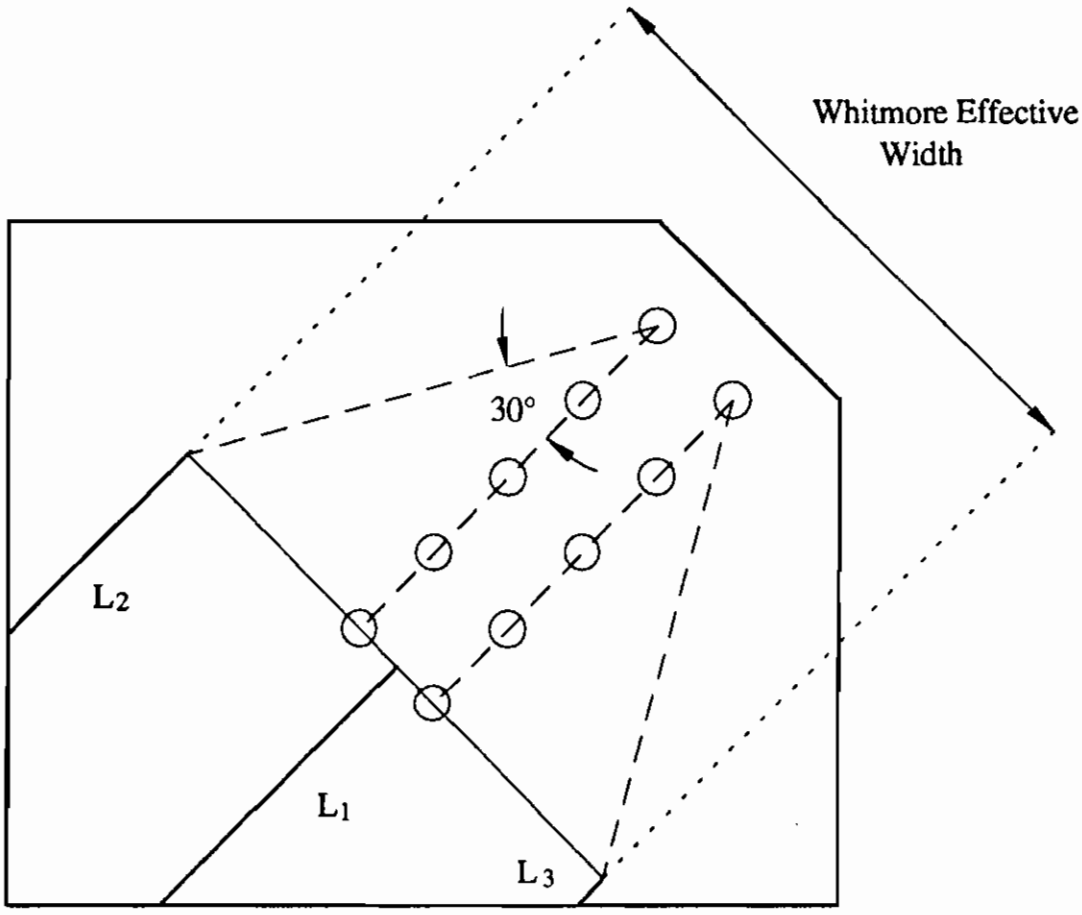

Imaginary Fixed-Fixed Column Strip: k = 0.65

Equivalent slenderness = $\frac{kL}{r}$

Figure 2.3. Thornton Equivalent Column Method

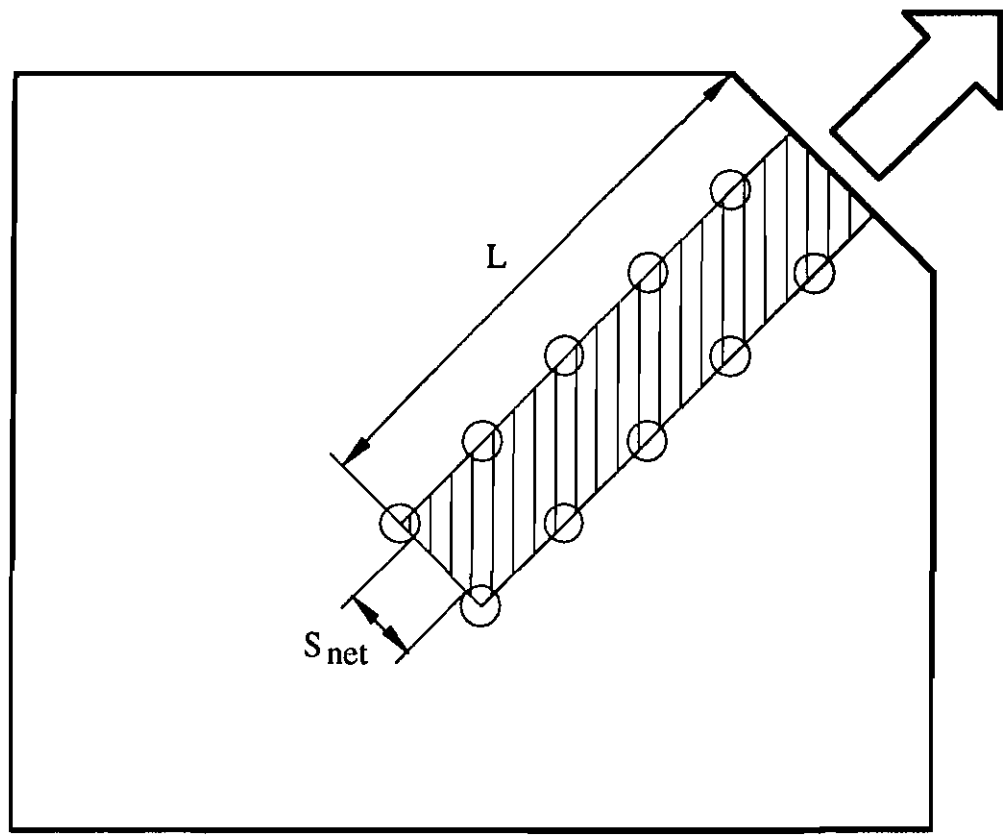

Ultmate Tear-out Resistance, R_n :
(Hardash and Bjorhovde, 1985)

$$R_n = F_u S_{net} t + 1.15 F_{eff} L t$$

Figure 2.4. Block Shear Tear-out Model

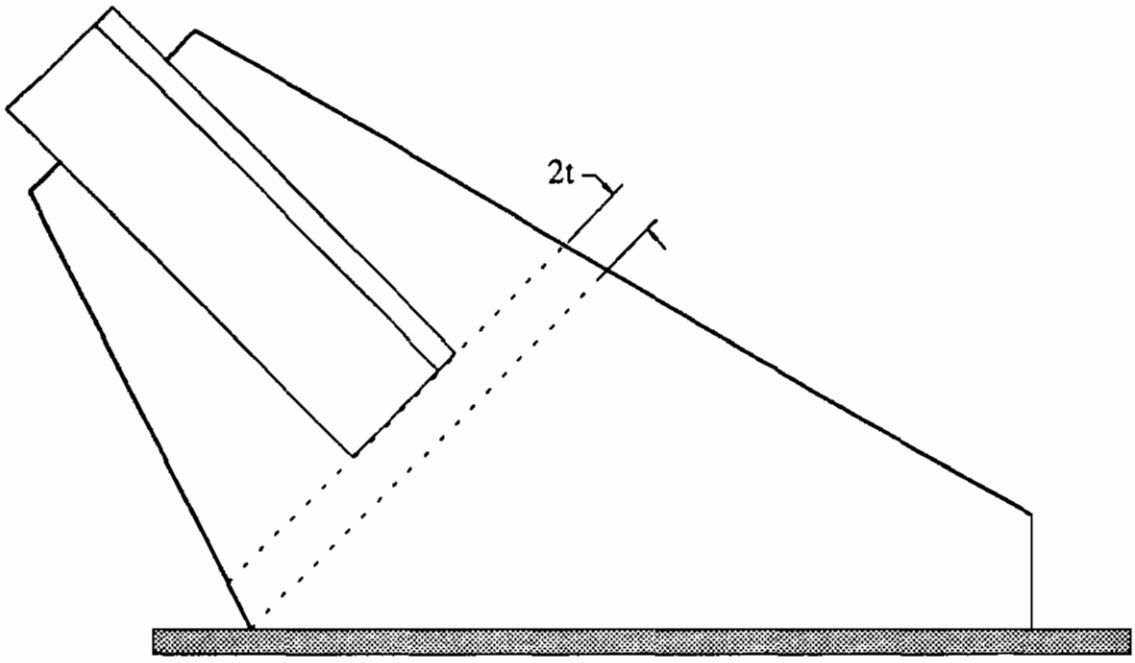

Figure 2.5. Gusset Plate Studied by Astaneh-Asl, et al. (1981)

3. EXPERIMENTAL PROGRAM

3.1 Introduction

The purpose of the experimental program was to investigate the general behavior of gusset plate connections in a braced steel frame under cyclic loading conditions. A bracing system subjected to cyclic loads may fail either in the bracing member itself or in the gusset plate which connects the bracing member to the beam and column. The proposed 'strong brace, weak gusset' model to be examined in this investigation considers a concentric braced frame where the brace member is designed not to buckle. In such a case, the bracing member acts as a restraining member to provide rotational restraint to the gusset plate. The assumption was made in designing the present experimental program that the gusset plate would fail prior to the bracing member and that the rotational restraint provided by the bracing member is effectively infinite.

3.2 Preliminary Considerations

The experimental program was designed to represent the conditions of actual gusset plate connections. Thus, full-scale single gusset plate connections of a diagonal bracing member at the joint of a beam and column were used. The variables of this kind of connection include plate thickness, plate size and configuration, plate boundary conditions, angle of bracing, type of connection (welded or bolted), cross-section of bracing member, length of splice member. In order to simplify the problem, the test parameters considered were gusset plate thickness, stiffness of the free edge of the gusset plate, and the geometry of the gusset plate such that the free formation of a plastic hinge is facilitated. These parameters were considered to be the most significant in examining the overall behavior of the connection under cyclic loading.

The connection details that were maintained constant throughout the test program were

designed to best represent the conditions of actual gusset plate connections. The most common bracing angles in practice range from 30 to 60 degrees. As such, a 45 degree bracing angle was used in this program. It was chosen to connect the brace member to the gusset plate through the use of a splice member. A bolted connection was used to connect the splice member to the gusset plate and the gusset plate itself was directly welded to the beam and column members in the braced frame assembly. All gusset plates were loaded concentrically through the brace member.

3.3 Specimen Description

A series of five specimens was tested in the experimental program. The plate size and thickness of the test specimens are listed in Table 3.1 and a typical gusset plate specimen is shown in Figure 3.1. All specimens were fabricated from CSA G40.21-M 300W structural quality steel. Two different thicknesses of gusset plate, 9.32 mm and 6.18 mm, were used in the test program. The test specimens were rectangular in shape with the exception of Specimen A-5, which was designed to allow the free formation of a plastic hinge under compressive buckling deformations. Based on the recommendation of a previous research investigation (Astaneh-Asl, et al., 1985), a plastic hinge region of width of 2t, where t is the thickness of the test specimen, was provided for at the base of the splice member connection. The modified geometry of Specimen A-5 is illustrated in Figure 3.2.

In order to investigate the effect of the stiffness of the free edge of a gusset plate, stiffeners were welded onto the free edges of Specimen A-3 and A-4. 50 x 9.32 mm stiffeners were used on Specimen A-3, while 50 x 6.18 mm stiffeners were used for Specimen A-4. The dimensions of the plate stiffeners were designed such that the strong axis (out-of-plane) bending stiffness of the stiffener was proportional to the thickness of the individual test specimen. Free edge stiffeners were added in an attempt to increase the

energy absorbing capacity of these specimens.

In all cases, two Tee-sections (WT125x22.5) and two 10 mm thick plates were used as a splice member to ensure that the gusset plate failed prior to the splice assembly. The 9.32 mm specimens were connected to the splice member with five rows of 7/8" diameter ASTM A325 high strength bolts designed for bearing. Due to the loads anticipated in the connection, all 9.32 mm thick specimens were expected to experience bolt slip in the gusset plate to splice member connection during the cyclic loading history. The 6.18 mm thick specimens utilized 7/8" diameter ASTM A490 bolts in order to achieve a slip-critical connection. All bolts were pretensioned using turn-of-nut tightening as specified in CAN/CSA-S16.1-M89, Clause 23.5 (CSA, 1989). The calculated slip-resistance of all gusset plate to splice member connections are recorded in Table 3.2. All specimens were designed to be loaded at 45 degrees by the bracing member and all specimens were directly welded to the beam and column members. In the design of the weld connection, the force distribution between the gusset plate and the beam and column members was based on a model proposed by Williams and Richard (1986). In connecting the gusset plate specimens to the frame members, a 10 mm fillet weld was used for the 9.32 mm specimens and an 8 mm fillet weld was used for the 6.18 mm specimens.

3.4 Test Set-up

A gusset plate connection under cyclic loading conditions might deform out-of-plane due to compressive loading as shown in Figure 3.3(a). The upper end of the gusset plate, which is connected to the brace member, moves out-of-plane. However, the lower end of the gusset plate, which is welded to the frame members, remains in-plane due to the restraint provided by the steel frame. This boundary condition can be simulated by the frame assembly shown in Figure 3.3(b). In this case, the bracing member and the upper end of the gusset plate remain fixed in-plane, while the lower end of the gusset plate is

allowed to move out-of-plane along with the frame assembly. To simplify the test set-up, the simulation of Figure 3.3(b) was used. To further simplify the test set-up, the forces that would normally exist in the framing members under lateral loading conditions were neglected in the testing program.

The test set-up is shown schematically in Figure 3.4. The cyclic test loads were applied by the MTS 6000 testing machine. Two W310x129 steel sections were used as the beam and column members in the test frame assembly. The frame assembly was then bolted to a WWF400x202 distributing beam in order to transfer the specimen loads out to the test set-up reactions. The diagonal bracing member (W250x67) was restricted to vertical displacements in the plane of the test specimen by the restraint provided by two lateral bracing roller assemblies. The roller assemblies were fixed to the frame of the MTS testing machine and restrained the brace member at the contact points shown in Figure 3.4. The test frame, with the specimen in place, was then sandwiched between a set of rollers at each end of the set-up to allow it to sway laterally out-of-plane under both compressive and tensile loading (Figure 3.5). The compressive reactions were transferred directly to the strong floor of the test lab, while the tensile reactions were resisted by a tension reaction frame as shown in Figure 3.6. To prevent a sudden kicking out of the test frame a guided rod mechanism was affixed to each end of the distributing beam. The movement of the guided rod mechanism was monitored throughout the testing to allow unrestrained sway of the test frame. Figure 3.7 is a photograph of the assembled test set-up, with the tension reaction frames removed.

3.5 Instrumentation

The specimens were instrumented using linear variable displacement transducers (LVDT), cable transducers, strain gages, and dial gages. In order to measure the strain distribution in the gusset plate, strain gages were placed on each specimen in pairs, one on either side

of the gusset plate. The location of the strain gages was decided on the basis of previous gusset plate test experience. In addition, a pair of rosette strain gages were placed on either side of the test specimens at the possible location of the maximum normal stress. The strain gage locations were the same for Specimens A-1 through A-4, while the gage locations were modified for Specimen A-5 due to the unique geometry of that specimen. The locations of the specimen strain gages are shown in Figures 3.8 and 3.9.

LVDTs were used to monitor both the out-of-plane and in-plane displacements of the gusset plate specimens and the test frame assembly. The out-of-plane buckled shape of the specimen plates were monitored by three sets of LVDTs which recorded the deformed shapes of the two free edges of the gusset plates and the center line of the loading path (Figure 3.10 and 3.11). In the in-plane direction, a pair of LVDTs were used to record the axial displacement of the gusset plate itself. An additional pair of LVDTs were used to monitor the axial displacement of the splice member and to observe the behavior of the proposed fixed boundary condition. By monitoring the axial displacement of both the gusset plate and the splice member, the deformation and bolt slip in the splice member to gusset plate connection could be isolated. In addition, an LVDT was used to record the axial displacement of the brace member relative to the distributing beam to confirm that the brace member to splice member connection was performing adequately. The locations of the axial displacement LVDTs are shown in Figure 3.12. All axial displacement LVDTs were referenced to the distributing beam.

In order to monitor the effectiveness of the out-of-plane restraint provided to the brace member, a pair of LVDTs were used to record the out-of-plane displacement of the brace member at the lateral brace location. In order to record the out-of-plane sway of the test frame, an LVDT was positioned on the distributing beam at the point of load application. In addition, dial gages were positioned at each end of the distributing beam to monitor the

lateral and longitudinal twist that might develop in the test frame. Finally, the centerline deflection of the distributing beam was recorded using a cable transducer. The location of the test frame instrumentation is detailed in Figure 3.13. All in-plane LVDTs and most out-of-plane LVDTs were placed on a support frame affixed to the distributing beam at the point of load application, as shown in Figure 3.14. The remaining LVDTs were affixed to the frame of the MTS testing machine.

The cyclic load applied to the test specimens was monitored by the internal load cell of the MTS 6000. Furthermore, load cells were incorporated into the tension reaction at both ends of the test set-up. Under tension loading, the MTS load was compared to the sum of the loads recorded at the tension reactions. The MTS load was in strong agreement with the loads recorded at the reactions. Therefore, the statics of the systems are confirmed and all loads are accounted for. The specimen load as recorded by the MTS 6000 testing machine was used in the test results. Load cells were not incorporated into the compression reactions due to stability considerations.

The electronic readings generated from the strain gages, LVDTs, load cells, and the MTS testing machine were continuously monitored by the Fluke data acquisition system. Dial gage readings were monitored manually at regular intervals throughout the testing. In addition, a whitewash coating was applied to all specimens in order to visually observe the yielding process.

3.6 Test Procedure

The cyclic test loads were applied and controlled by using the MTS 6000 testing machine. All specimens were tested under reverse loading conditions. Each test began with a series of cycles in the elastic range. Elastic cycles were conducted at 10% and 50% of the expected tensile yield load based on the Whitmore yield capacity and the nominal material

properties (F_y=300 MPa). The procedure for calculating the Whitmore yield capacity of a gusset plate is outlined in Section 2.2. During each cycle, the specimen was initially loaded in tension to the desired maximum cycle load level. The specimen was then unloaded from tension and cycled through zero to the same load level in compression. Two cycles were conducted at each elastic load level. The first cycle was loaded in a start-stop fashion with the testing stopped at regular intervals for electronic data acquisition. The second cycle at each load level was tested under continuous loading conditions; the loading was only stopped at the peak tensile load, zero load, and the peak compressive load during each cycle so that qualitative specimen observations and dial gage readings could be recorded.

The inelastic loading sequence for all specimens began with a set of yield level cycles at 100% of the expected nominal tensile yield load. The loading procedure in the inelastic range varied slightly between the specimens tested. In general, subsequent inelastic cycles were conducted under increasing levels of specimen axial deformation. The specimen axial deformation was monitored using the LVDTs attached to the splice member, such that the bolt slip in the connection, if any, would be included in the determination of the cycle axial deformation level.

During each cycle, a specimen was initially loaded in tension to a predetermined level of axial deformation. The specimen was unloaded from tension and then deformed in compression to the same axial deformation level, as referenced to the specimen deformation level recorded after tension unloading of the same cycle. For the 6.18 mm thick specimens (Specimen A-2 and A-4) the axial deformation level for all inelastic cycles was based on intervals of a yield load deformation, Δ_y, as computed from the maximum tensile deformation attained during the nominal yield level cycles. Since bolt slip was anticipated in the 9.32 mm specimens (Specimen A-1, A-3, and A-5), no reference could

be made to a nominal yield level deformation. As such, the cycle axial deformation level was increased in roughly evenly spaced intervals over the course of the inelastic loading. The level of axial deformation was increased in subsequent cycles until the tensile failure of the specimen was achieved. Failure in tension was signified by a decrease in specimen load carrying capacity under increasing MTS machine stroke. The test was concluded by loading the specimen in compression until an excessive level of compressive plate deformation was obtained. The test loading was limited by the level of out-of-plane deformation that was able to be accommodated by the test set-up.

All inelastic cycles were tested under continuous loading conditions, with the exception of the testing of Specimen A-1. It was originally thought that the effect of continuous versus stop-start loading on the specimen behavior could be investigated in the test program. As such, the loading scheme for Specimen A-1 involved a set of three cycles at each axial deformation level in the inelastic range. The first cycle was loaded in a stop-start fashion with the testing stopped at regular intervals for electronic data acquisition. The other two cycles of the set were loaded continuously. However, when the axial deformation level is held constant for successive inelastic cycles, there is inadvertently an observed drop in the load carrying capacity due to inelastic straining and residual deformations. Consequently, no significant information could be obtained from this cycle loading scheme. Therefore, inelastic loading cycles of increasing axial deformation, with no cycle repeats, were employed in the testing of all remaining specimens.

The test loading for all elastic cycles, including the yield level cycle, were conducted under MTS load control, while the inelastic cycles were conducted under MTS stroke control. The cycle loading rate under load control ranged from 25 kN/min to 100 kN/min. Under stroke control, the stroke loading rate ranged from 0.5 mm/min to 2.0 mm/min, as measured by the stroke of the MTS 6000 testing machine. It has been shown that the

behavior of steel structures is relatively unaffected by moderate variations in the loading rate within the range of loading rates employed in this investigation (Davis, et al., 1982). Therefore, the loading rates chosen reflects values that enabled careful and controlled observation of the specimen throughout the testing process.

Table 3.1. Specimen Description

Test Specimen	Plate Size (mm x mm)	Thickness (mm)	Specimen Test Parameter
A-1	550 x 450	9.32	Basic Plate
A-2	550 x 450	6.18	Basic Plate
A-3	550 x 450	9.32	Stiffened Free Edge
A-4	550 x 450	6.18	Stiffened Free Edge
A-5	550 x 450	9.32	Free Formation of Plastic Hinge Facilitated

Table 3.2. Slip Resistance of Gusset Plate to Splice Member Connection

Test Specimen	Connection Details	Slip Resistance (kN) 5% Probability of Slip *	
		Class A Surface Clean mill scale	Class B Surface Blast-cleaned
9.32 mm Specimens	10 - ASTM A325 7/8 in. Bolts	918	1510
6.18 mm Specimens	10 - ASTM A490 7/8 in. Bolts	1096	1810

* As per CAN/CSA-S16.1-M89, Clause 13.12

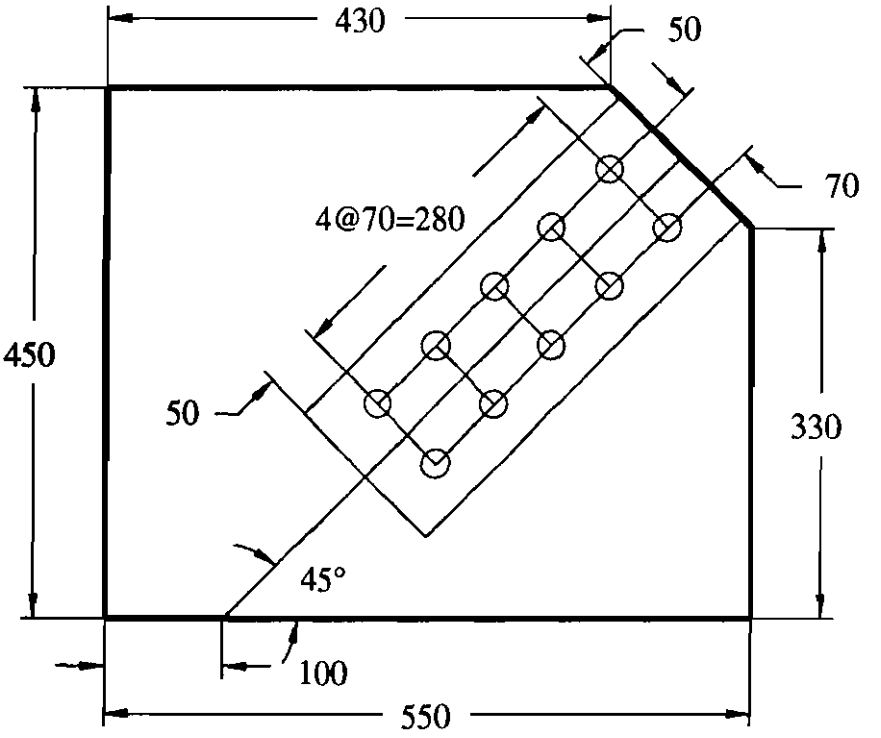

Figure 3.1. Typical Test Specimen Geometry
Specimens A-1 to A-4

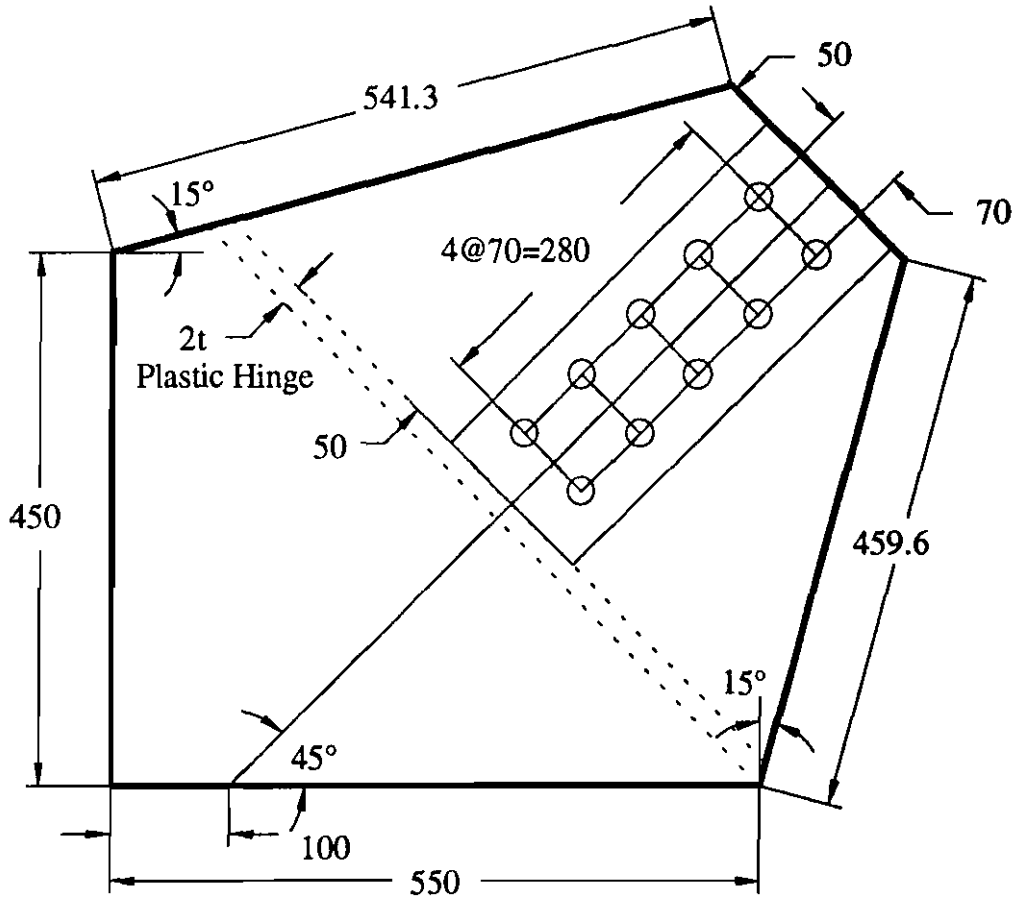

Figure 3.2. Geometry of Specimen A-5

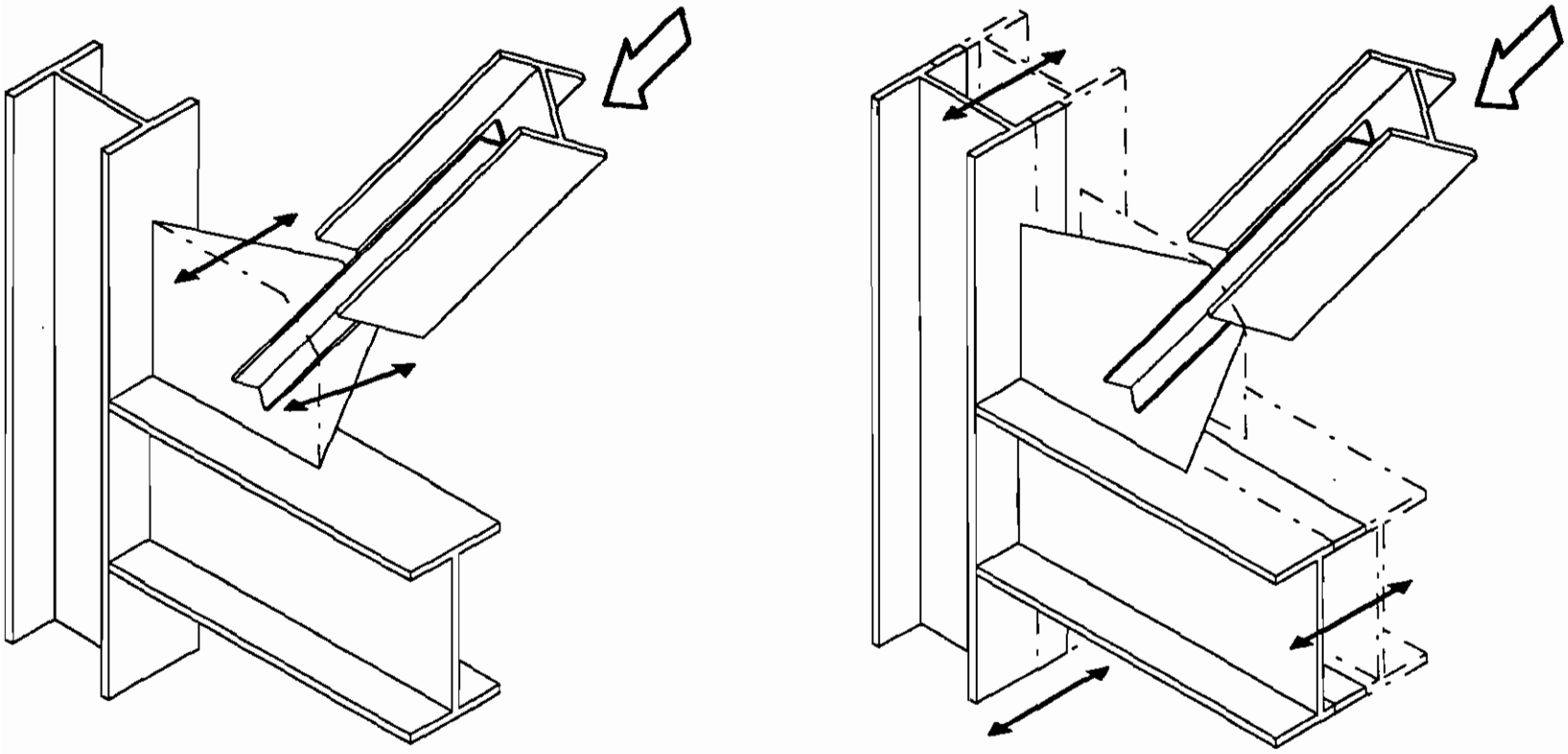

(a) Bracing member and upper end of gusset plate deform out-of-plane due to buckling

(b) Steel frame and lower end of gusset plate move out-of-plane

Figure 3.3. Simulation of Boundary Conditions

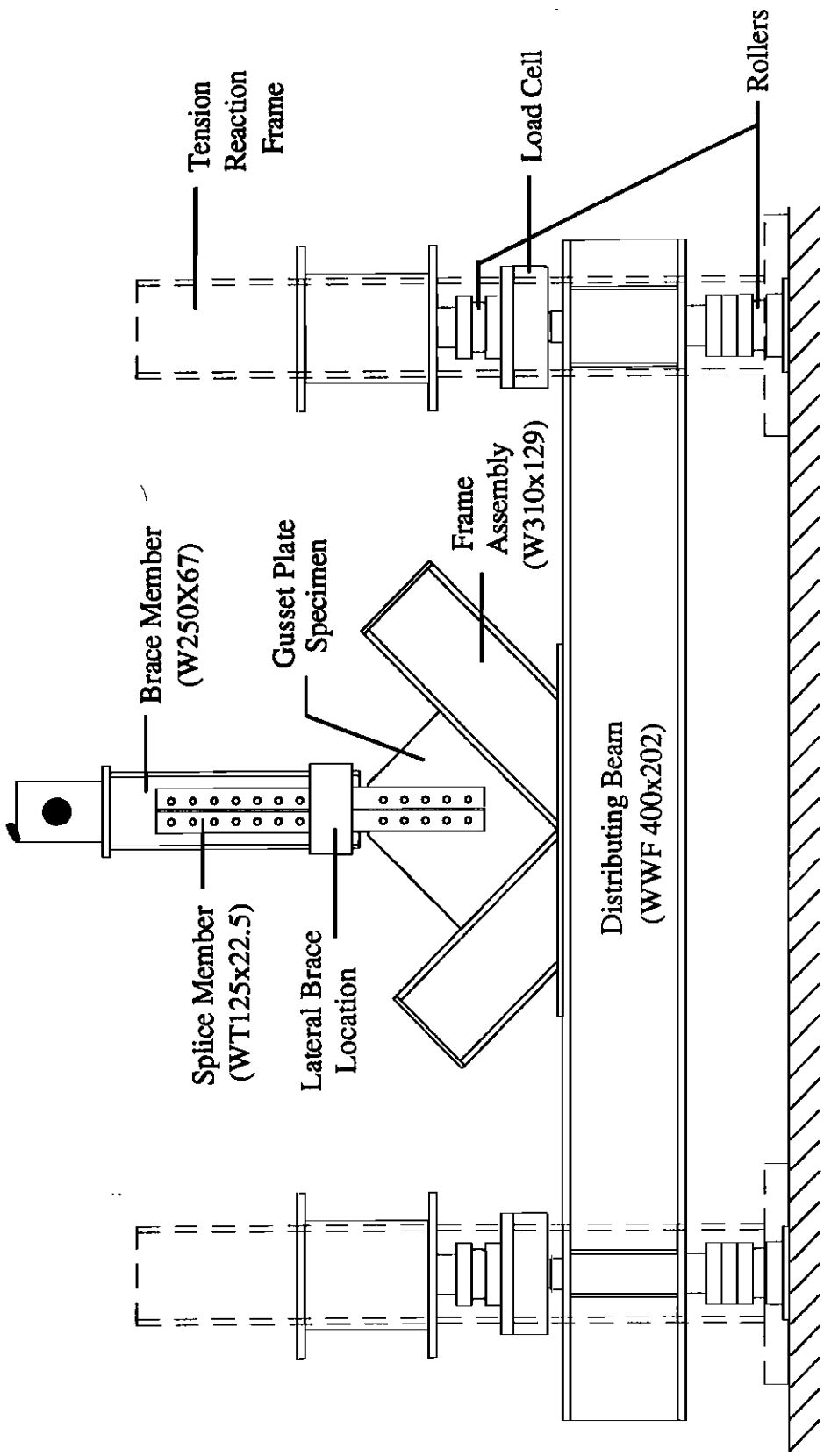

Figure 3.4. Schematic of Test Set-up

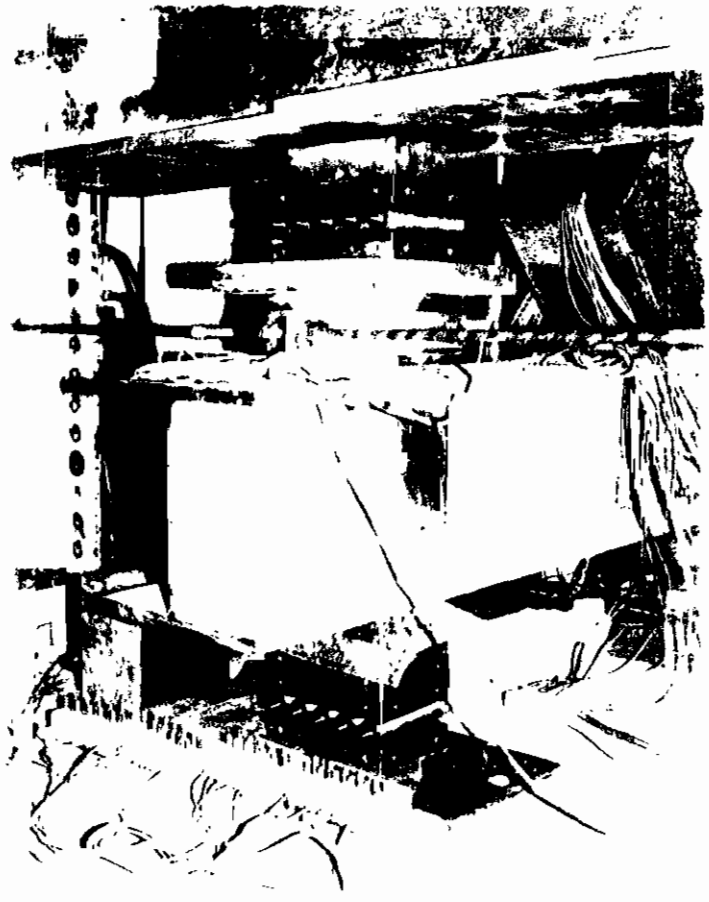

Figure 3.5. Test Set-up Reactions

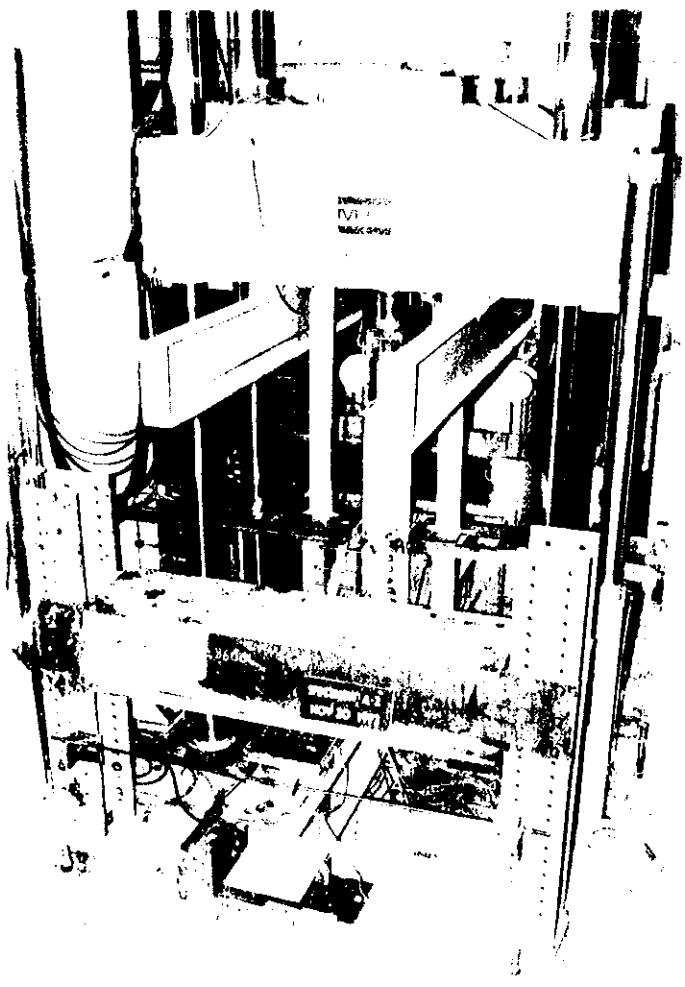

Figure 3.6. Tension Reaction Frame

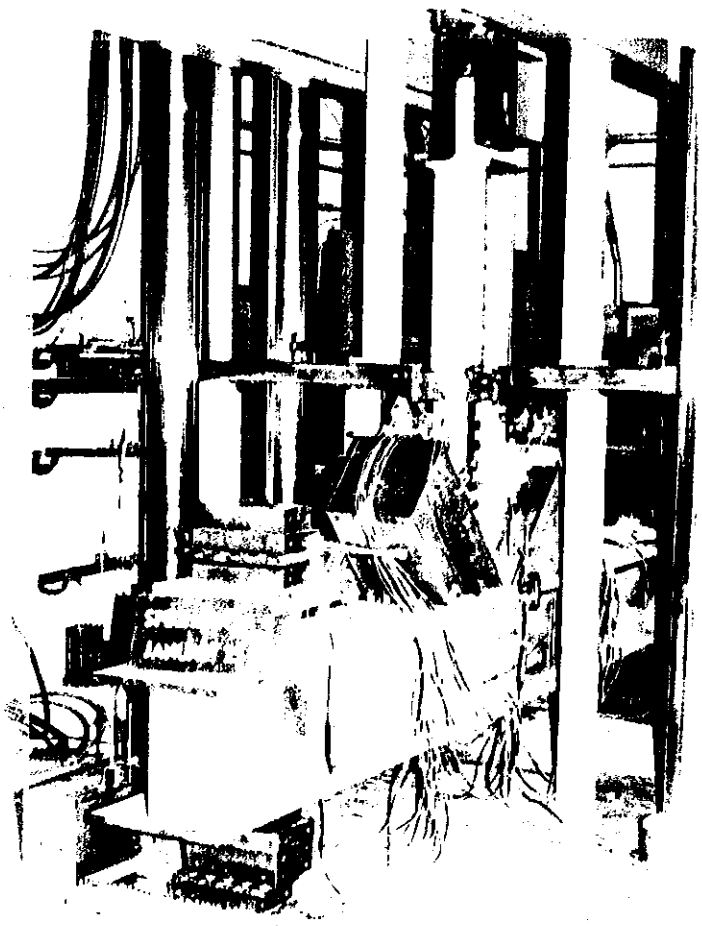

Figure 3.7. Test Set-up - Tension Reaction Frame Removed

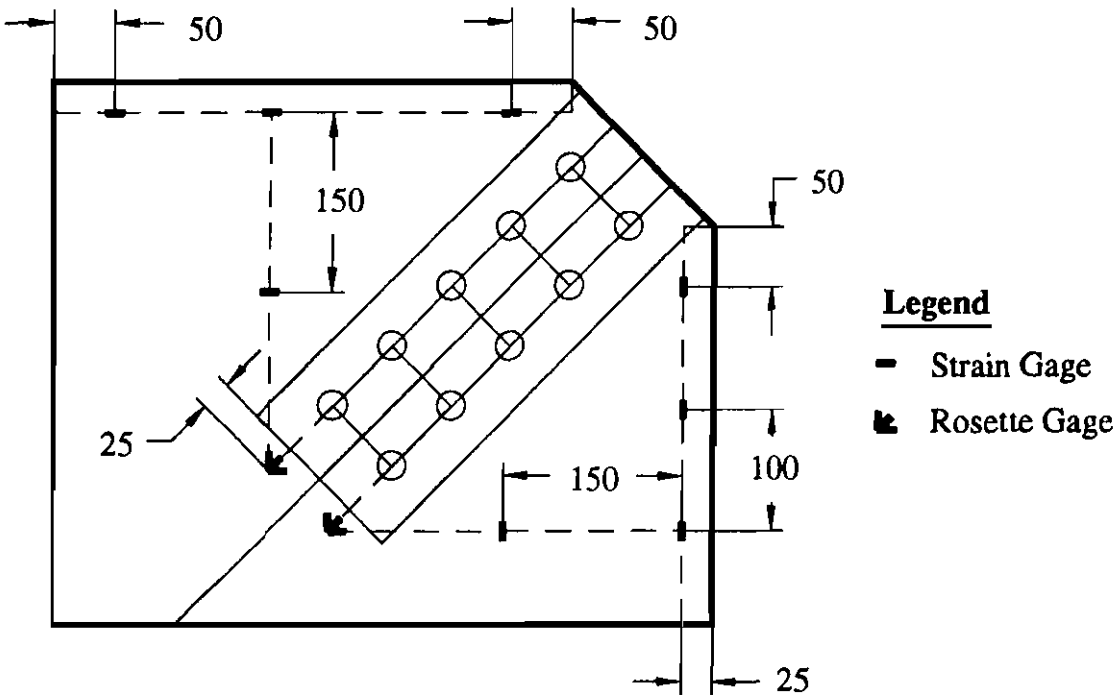

Figure 3.8. Typical Strain Gage Locations
Specimens A-1 to A-4

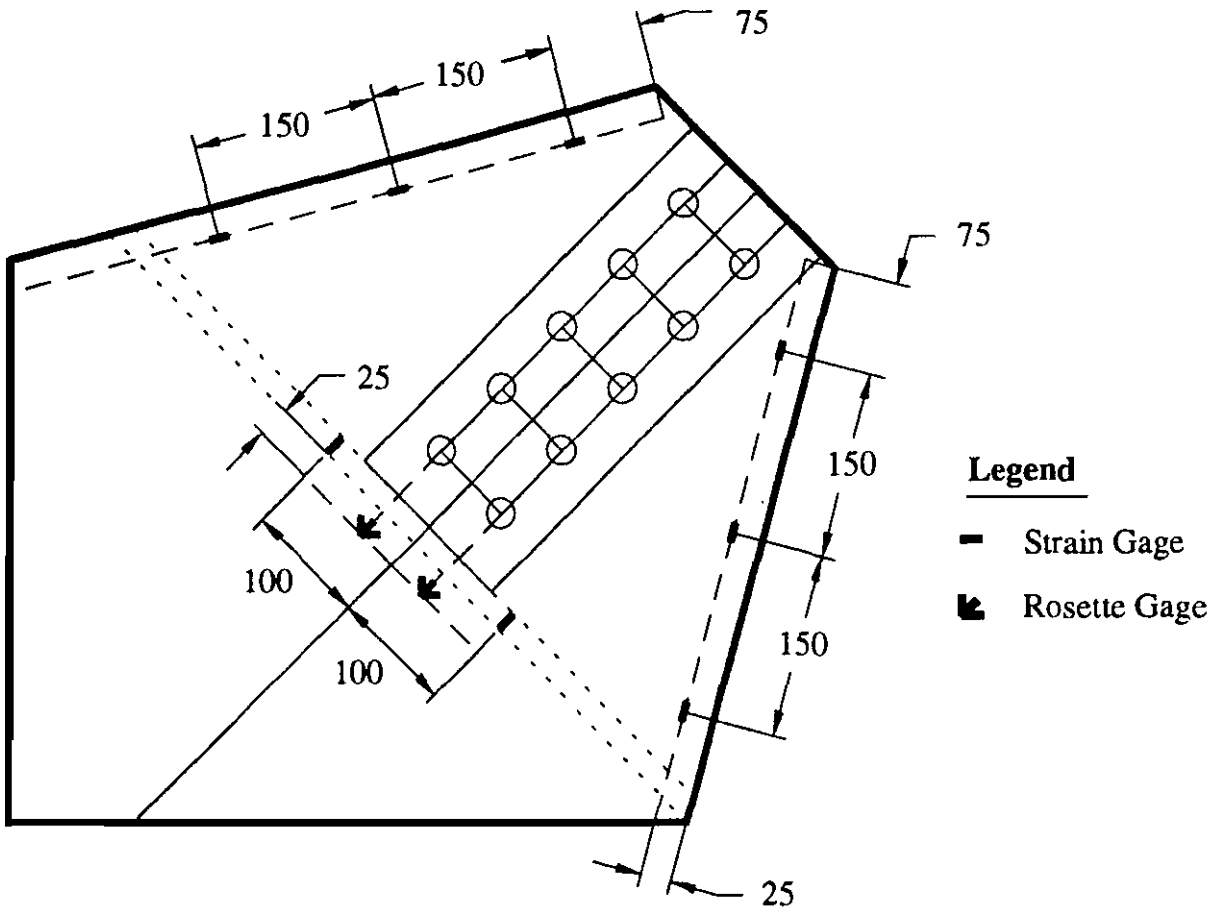

Figure 3.9. Strain Gage Layout of Specimen A-5

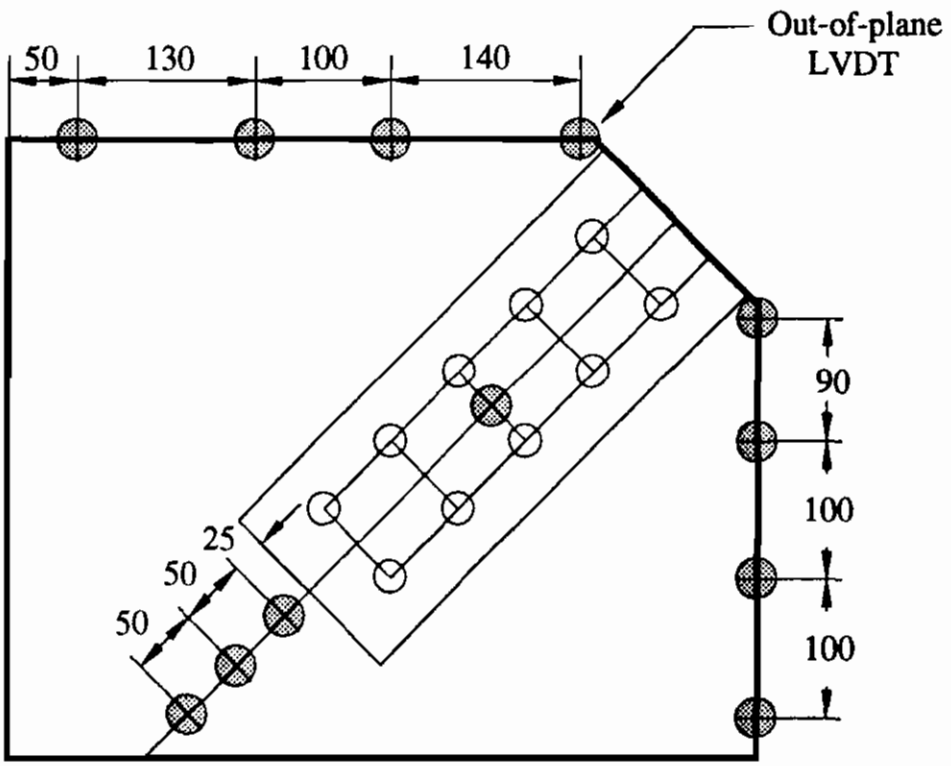

Figure 3.10. Out-of-plane LVDT Locations
Specimens A-1 to A-4

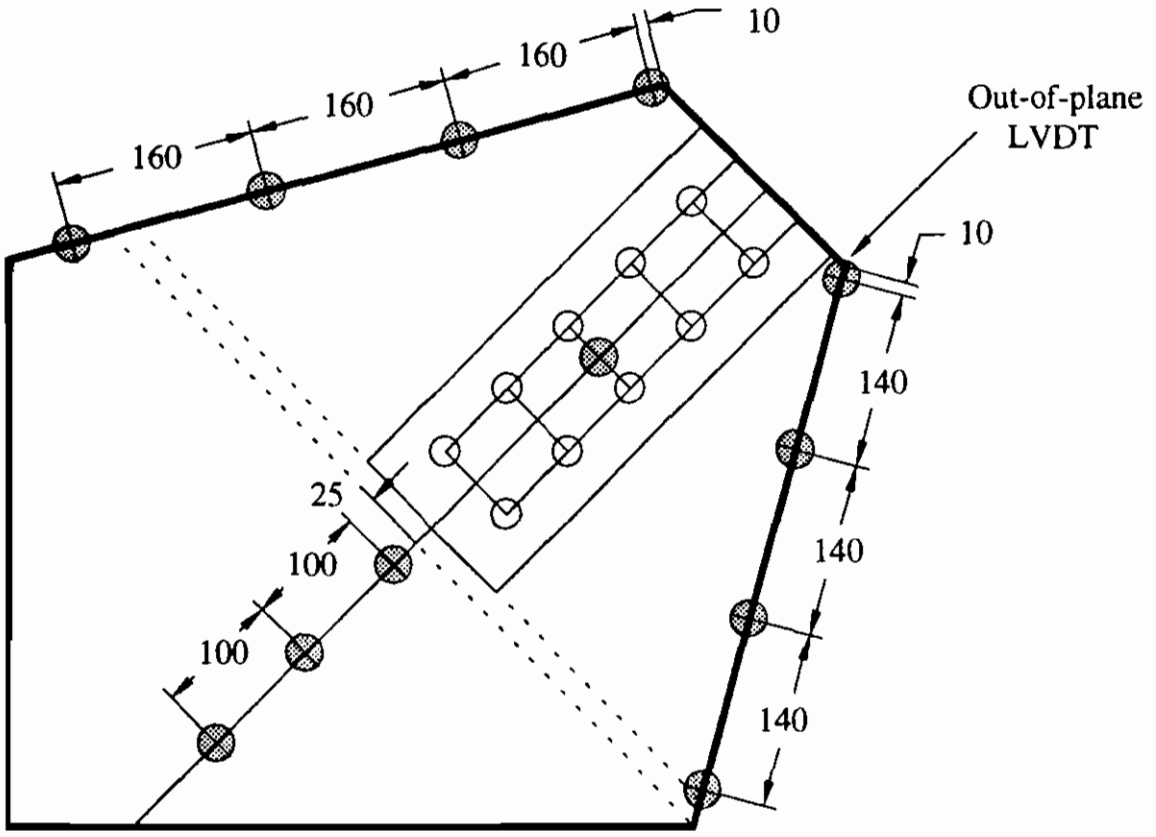

Figure 3.11. Out-of-plane LVDT Locations for Specimen A-5

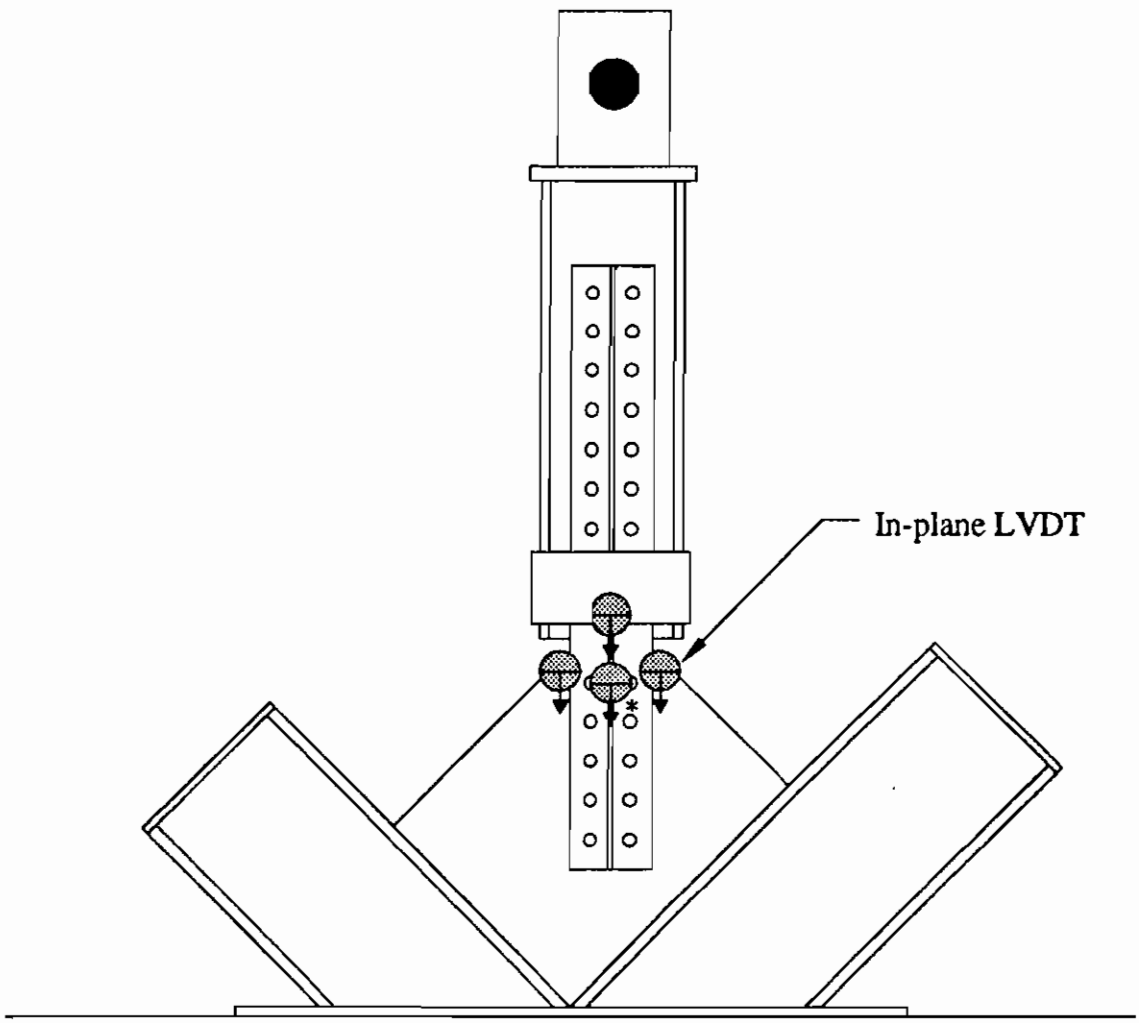

* LVDT on both sides of splice member

Figure 3.12. Axial Displacement LVDT Locations

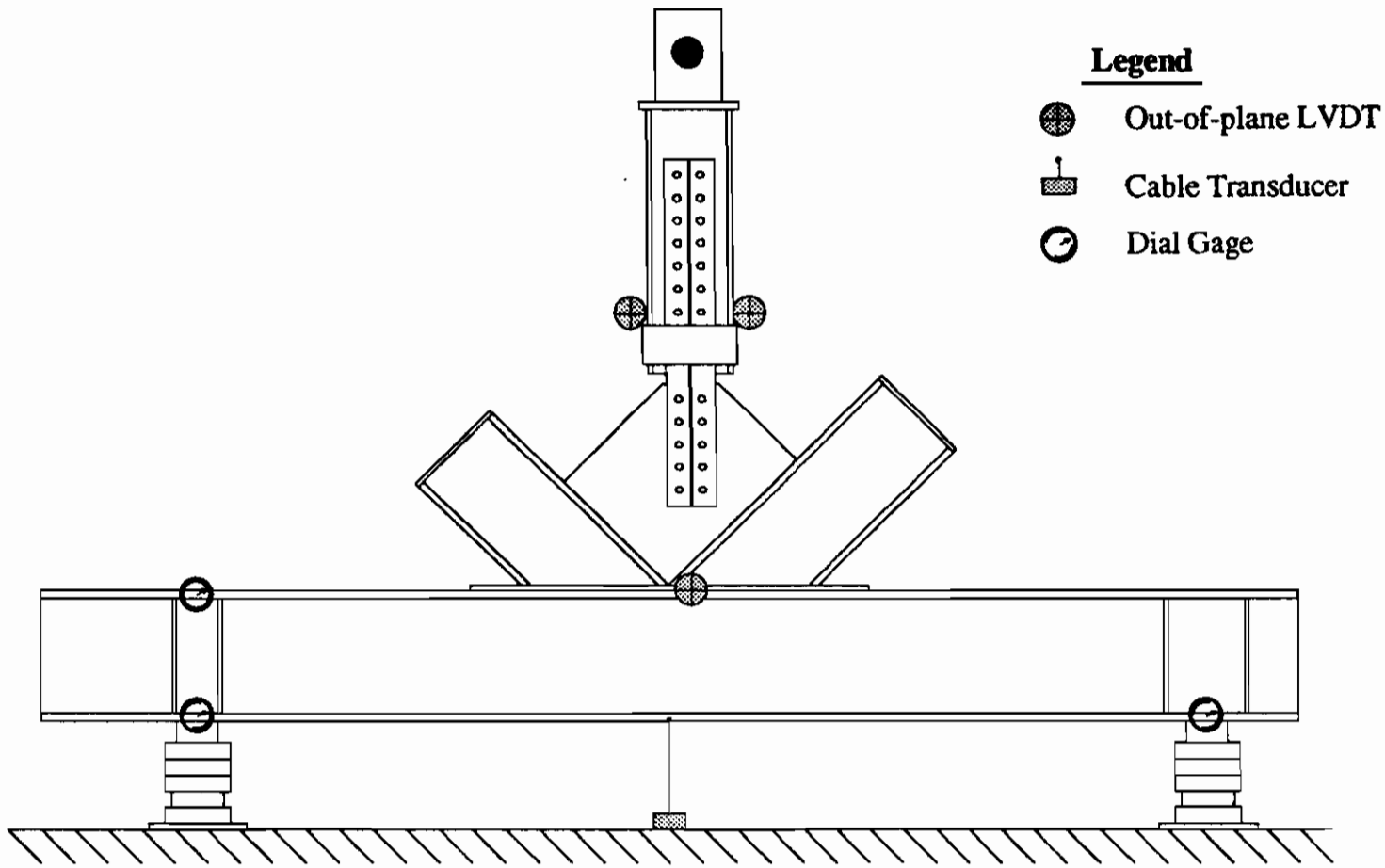

Figure 3.13. Test Frame Instrumentation

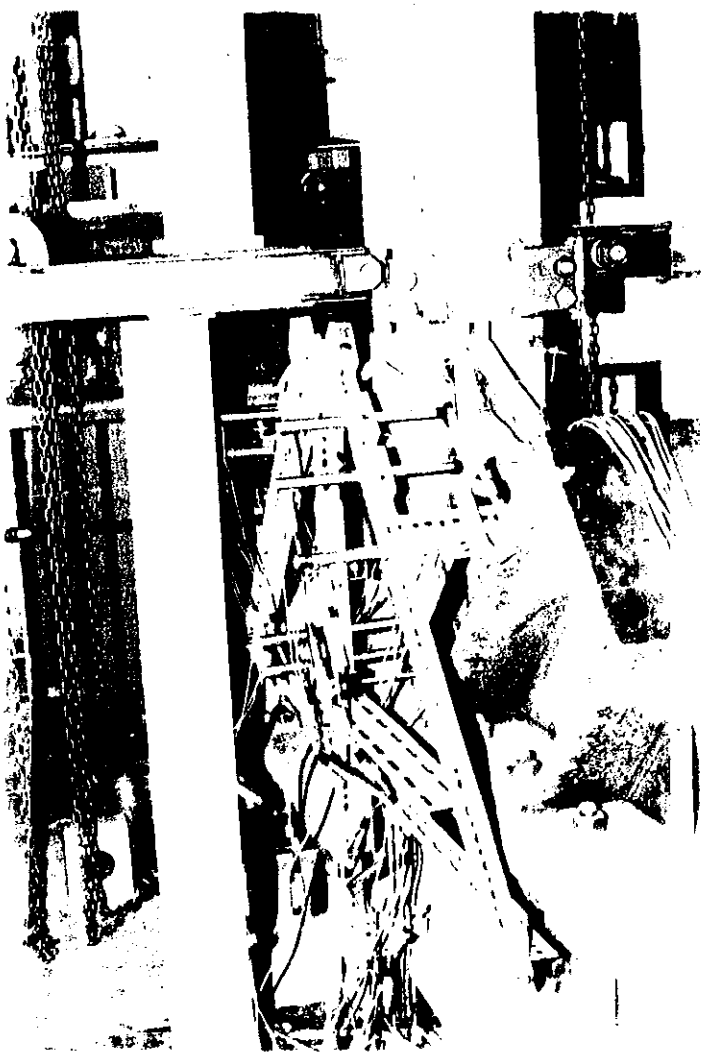

Figure 3.14. LVDT Support Frame

4. EXPERIMENTAL RESULTS

4.1 Introduction

The results of the experimental program are presented in this chapter. The material properties of the test specimen are discussed in Section 4.2. The results of the gusset plate tests are presented in Section 4.3. The full test behavior of each specimen will be presented. This chapter will focus on the physical behavior of the specimens during the cyclic loading as well as consider the load versus deformation response, the buckled configuration, and the observed strain distribution of the specimens. Further discussion of the test results in relations to the test parameters will be covered in Chapter 5.

4.2 Material Properties

Table 4.1 lists the values of the elastic modulus, the static and dynamic yield levels, and the dynamic ultimate strength as determined from tensile tests on coupons taken from the material used in the test specimens. Four coupons were fabricated from each of the plate thicknesses utilized. A 200 mm gage length was used for all material tests. Two coupons from each plate were tested in the direction parallel to the sheet steel rolling direction (a), while the remaining two coupons were tested in the perpendicular direction (b). The test values from each plate direction and the average values from the four coupons tested are reported. As expected, higher strengths were observed from the coupons tested parallel to the rolled direction of the steel plate. However, the response of the specimens should not be significantly affected by the orientation of the plate material with respect to the rolled direction since a 45 degree brace angle was chosen for the testing program. Consequently, average material properties will be utilized in the analysis of the gusset plate test results. A typical plot of stress versus strain for the material tested is shown in Figure 4.1 and reveals the characteristic behavior of mild structural steel. All coupon tests were conducted in accordance with ASTM standard A370-92 (ASTM, 1992).

4.3 Test Results

The ultimate tensile and compressive loads attained during testing are recorded in Table 4.2. The ultimate load is defined as the maximum load level reached by a specimen throughout its cyclic loading history. The test results of each specimen are presented in turn in Section 4.3.1 through Section 4.3.5. The discussion of each specimen will first focus on the physical response of the specimen during testing and will then consider the load versus deformation response, the buckled configuration, and the observed strain distribution within the specimen. Additional test data, including the gusset plate load versus deformation response and the load versus out-of-plane displacement of the test frame, is provided in Appendix A.

4.3.1 Specimen A-1

Specimen A-1 is a basic, unreinforced gusset plate specimen of 9.32 mm thickness. Ten 7/8" diameter ASTM A325 high strength bolts designed for bearing were used to connect the splice member to the gusset plate.

The load versus axial displacement response of Specimen A-1 throughout its loading history is shown in Figure 4.2. The area under the load-deformation curve is a measure of the energy absorbed by the gusset plate throughout the cyclic loading. Plotted here is the average axial displacement of the gusset plate assembly. The displacement was recorded by the LVDTs attached to the splice member and referenced to the distributing beam. The recorded displacement includes the deformation of the gusset plate, the splice member, and the slip in the splice member to gusset plate connection, if any. The same general specimen behavior can be observed from a plot of the load versus axial displacement behavior of the gusset plate itself (Appendix A, Figure A-1). Although the influences of the splice member to gusset plate connection slip and the local bearing deformations in the gusset plate are absent, the same general specimen response is observed.

By examining the tension portion of the loading in Figure 4.2, it is observed that the specimen response under tension is relatively stable; as the axial deformation level is increased the load carrying capacity of the specimen is maintained. Conversely, in compression, the overall plate buckling of the specimen is accompanied by a sudden increase in axial deformation and a significant drop in load carrying capacity. Although, the cyclic specimen loading was not continued very far into the post-buckling range, it can still be observed that there is a deterioration of the compressive load carrying capacity as the cyclic axial deformation level and the specimen out-of-plane deformations increase. A photograph of the failed specimen and the final yield line pattern is shown in Figure 4.3.

Figure 4.4(a) shows the specimen load versus deformation response of the gusset plate assembly during the elastic portion of loading, Cycle #1-7. As expected, no yield lines were observed on the specimen during the elastic cycles. During the tension loading of Cycle #5, at a load of approximately 1000 kN, bolt slip occurred in the fasteners in the splice member to gusset plate bolted connection. Due to the slack created in the loading system, the observed load dropped during the slip process. Upon completion of the initial bolt slip, the specimen once again began to pick up load.

As the testing progressed, the splice member to gusset plate connection underwent slippage twice during every test cycle, once during tension loading, and once again when the specimen was cycled through into compression. The connection slipped in several small steps as various portions of the connection were each brought into bearing in turn. In the load versus axial displacement plot of Figure 4.2, the bolt slip experienced during the tensile and compressive portions of each loading cycle appear as a series of plateaus on the loading curve. Although the overall response of the specimen varies with the cycle axial deformation level, the load at which slip occurs, and consequently the dynamic slip level, appears roughly constant throughout the loading history.

Figure 4.4(b) shows the load versus deformation response of the specimen during the inelastic loading cycles up to the onset of plate buckling, Cycle #8-13. The first visible signs of yielding were recorded on the specimen along the welded boundary between the gusset plate and the frame assembly. Yielding was indicated by the flaking of the whitewash coating on the specimen. Yielding in this region appeared to be due to the restraint provided by the welded boundary as the specimen began to deform out-of-plane. As the cycle axial deformation level increased, yield lines developed on the gusset plate about the sides of the splice member at the mid-height of the connection. This indicated the yielding of plate material in the connection under both tensile and compressive bolt bearing deformations. Yield lines about the base of the splice member revealed the beginning of a plate buckle stretching from the bottom corner of one free edge, extending beneath the splice member, to the bottom corner of the other free edge.

During the compressive loading of Cycle #13, overall plate buckling occurred. The long free edge of the gusset plate buckled, allowing the specimen to deform significantly out-of-plane. The load carrying capacity of the specimen dropped significantly after overall plate buckling occurred. As a result, the maximum load of 1682 kN reached during Cycle #11 is the compressive capacity of this specimen.

Once overall plate buckling had occurred, the remaining loading cycles for Specimen A-1 involved only an increase in the axial deformation level for the tension loading portion of each cycle. Since the specimen had already buckled in compression, it was decided to stop the compressive loading during each cycle when the specimen load carrying capacity began to drop. Figure 4.4(c) shows the load versus deformation response of the specimen for the remainder of the cyclic loading. As the cycle axial deformation level increased, tensile yield line activity was observed to increase slowly on the gusset plate in the vicinity of the splice member connection. The test was concluded by loading to failure in tension

(Cycle #17). The specimen underwent significant tensile axial deformation until tensile failure was reached at a load of 1794 kN.

The gusset plate specimen was examined after the completion of the test. It was observed that the specimen failed in tension due a fracture of the plate material between the bolt holes in the bottom row of the connection. Figure 4.5 is a photograph of the failed plate material. This tensile failure mode was characteristic of all the specimens tested. The remaining bolt holes in the connection had been deformed in both tension and compression due to the bearing of the bolts under load, with the greatest deformations occurring in the first and last row of the connection.

The linear variable displacement transducers recorded the out-of-plane deflected shape of the specimen free edges and the center line deflection. Figure 4.6 depicts the displacements that existed in the specimen after overall plate buckling occurred in Cycle #13. It is observed that the deflected shape of the specimen center line closely resembles that of a fixed-fixed but guided column. The long free edge has buckled and the deformed shape indicates that the restraint provided to the top of the specimen by the splice member appears to be localized, and does not provide fixity to the free edges of the gusset plate. Figure 4.7 is a photograph of the long free edge of the specimen after overall plate buckling occurred.

In plotting the deflected shape of the specimen center line, an interpolation of the existing data was necessary. Only one LVDT recorded the out-of-plane displacement of the splice member along the gusset plate center line (Figure 3.10). Therefore, a linear interpolation was used to determine the displacement along the entire length of the splice member. The splice member was assumed to displace as a rigid body and a compatibility of specimen deformations was maintained at the top of the gusset plate. The displacement of the top

of the splice member was assumed to be roughly equal to the out-of-plane displacement at the top of the gusset plate free edges. Since the splice member is relatively rigid compared to the gusset plate, this assumption appears to be valid.

Specimen strain gage readings were recorded throughout the loading history. However, only strain levels obtained from the elastic portion of loading are relevant in an analysis of the strain distribution in the specimen. Once local yielding occurs and the stresses begin to redistribute in the plate, the strain readings are difficult to interpret. Strain gage values were investigated at the cycle maximum loads at both the 50% and 100% nominal Whitmore load levels, 530 kN and 1060 kN respectively. From this analysis it was observed that the peak strain levels in the specimen were recorded at the rosette locations beneath the splice member. Figure 4.8 shows both the tensile and compressive plate strain distributions at the 530 kN and 1060 kN levels. At the 530 kN load level there was no significant difference between the strain levels and pattern of distribution between the tension and compression stress states. This indicates that the elastic loading path within the specimen is generally the same under both tension and compression loading.

When the specimen load is increased to the +1060 kN level, strain levels are generally twice those recorded at the +530 kN load level. The linearity of strain supports the assumption that the material response is generally elastic at this load level. When the strain readings at the -1060 kN load level are analyzed, the strain levels are generally slightly more than twice those recorded at the -530 kN level. In addition, a comparison of the gage readings from both faces of the specimen indicate that plate bending strains are present along the long free edge of the plate and at the rosette locations under the splice member. This observation is in agreement with the onset of local yielding in the plate that was observed at the same load cycle level.

For the purpose of comparison, the maximum strain levels in the specimen, based on the Whitmore critical stress theory, should be approximately ±1500 microstrain at the Whitmore section at the 100% nominal yield load level (1060 kN). The Whitmore section runs through the bottom row of bolts in the splice member connection, slightly above the rosette gage locations.

4.3.2 Specimen A-2

Specimen A-2 is a basic, unreinforced gusset plate specimen of 6.18 mm thickness. Ten 7/8" diameter ASTM A490 high strength bolts were used to connect the splice member to the gusset plate in order to achieve a slip-resistant connection. No bolt slip was expected to occur during the testing of this specimen.

Figure 4.9 shows the load versus the axial displacement response of the gusset plate assembly throughout the loading of Specimen A-2. By examining the tension portion of the loading, it is observed that the specimen response under tension is stable. In compression, the buckling behavior of the specimen is revealed. The occurrence of overall plate buckling is well defined by the compressive peak load plotted in the figure. As observed during testing, the compressive capacity immediately drops significantly to a post-buckling load capacity level. The figure confirms that the post-buckling behavior is relatively stable; the post-buckling load capacity is seen to deteriorate very slowly as the axial plate deformations increase significantly. A photograph of the failed specimen and final yield line pattern is shown in Figure 4.10.

Figure 4.11(a) shows the specimen load versus deformation response of the gusset plate assembly during the elastic portion of loading, Cycle #1-6. The onset of yielding was observed during the compression loading of Cycle #4, at 50% of the nominal yield load level. A few yield lines were noted at the base of the specimen running parallel to the

long free edge of the plate. Yielding was likely due to the restraint provided by the welded boundary condition.

Figure 4.11(b) shows the load versus deformation response of the specimen during the inelastic loading cycles up to the onset of plate buckling, Cycle #7-8. As the cycle axial deformation level increased, a significant increase in compressive plate yielding was observed about the base of the splice member. The first signs of tension yielding were observed during Cycle #8 ($\pm 2.0\Delta_y$), when yield lines were noted about the sides of the splice member as the material in the connection region was beginning to yield. When the loading was cycled through to compression, overall plate buckling occurred at a load of 1128 kN. Immediately upon buckling, the load carried by the specimen dropped to 730 kN. The plate buckle extended from the midpoint of both free edges down to the base of the splice member. Both plate free edges buckled in order to enable the specimen to undergo significant out-of-plane deformation.

Figure 4.11(c) shows the specimen load versus deformation response for the remainder of the test loading. As the test proceeded under sequentially increasing levels of cyclic axial plate deformation, the tensile yield lines about the splice member connection increased. The maximum tensile loads reached continued to increase as the cycle axial deformation level increased. In compression, only minor deterioration was observed in the post-buckling behavior of the specimen. The compressive loads attained only decreased slightly with each successive cycle. As the compressive deformations increased, yield lines were observed along the outside edges of the gusset plate to frame assembly connection. Yielding in this region is likely due to the deformation reversals, as the plate buckles, then straightens under tension loading. As compressive deformations continued to increase, a secondary buckle was observed running from the bottom corner of one free edge, down beneath the base of the splice member, and up to the bottom corner of the other free edge

(Figure 4.10).

The tensile failure of the specimen occurred during Cycle #16 ($\pm 16.0\Delta_y$) when the load carrying capacity reached 1340 kN, then quickly began to drop as the MTS controlled axial deformation continued to increase. The test was concluded by loading the specimen in compression until an excessive level of deformation was achieved. Even at the extreme deformation level that was imposed during this final cycle, the compressive capacity was still 630 kN, only 100 kN less than the initial post-buckling capacity. The final deformed shape of the specimen (Figure 4.10) reveals the complex pattern of plate yielding and the associated plastic hinge locations. It is believed that the complex pattern of buckles allowed the specimen to redistribute the compressive load through a series of redundant load paths, resulting in a relatively stable post-buckling capacity.

The failure of the specimen in tension was a fracture of the plate material between the bolts in the bottom row of the connection. Only the bottom row of bolt holes appeared to be significantly deformed. Since no major connection slip occurred, bolt hole deformations observed were due to overall connection material yielding, not bolt bearing deformations. In addition, tensile yielding caused the plate to spread outwards and bulge upwards at the top of the splice member connection region.

The out-of-plane deflected shape of the plate free edges and the center line deflection of the specimen, as recorded immediately after overall plate buckling occurred, are shown in Figure 4.12. Unlike Specimen A-1, the deflected shape of the center line more closely resembles the buckled shape of a fixed-pinned but guided column. It appears that a plastic hinge region developed at the base of the splice member, thereby reducing the fixity provided to the gusset plate by the splice member at that location. The buckled shapes of the free edges also resemble that of a fixed-pinned but guided column. As the out-of-

plane deformations increased, the fixity of the free edges decreased as plastic hinges developed at the bottom corners of the free edges at the location of the weld connection to the frame assembly. Photographs of the free edges (Figure 4.13) show the deformed shapes, including the location of the plastic hinge lines that developed as the specimen buckled.

Strain gage values were investigated at the maximum cycle loads at both the 50% and 100% cycle levels. For Specimen A-2, this corresponds to 353 kN and 707 kN respectively. In general for Specimen A-2, the strains are highest at the rosette locations at the base of the splice member, and the edge strains are higher along the long free edge. The recorded plate strain distributions at both the 353 kN and 707 kN load levels are shown in Figure 4.14. At the +707 kN load level, the distribution of strains is roughly unchanged from the +353 kN level. In addition, strains have approximately doubled, indicating an elastic linearity of strains in tension. Under compressive loading, the strains have more than doubled at the rosette locations when the loading increased from the -353 kN to the -707 kN level. The strains at the rosette locations are approaching yield strain levels, which is in agreement with the whitewash flaking observed on the specimen at this load level.

4.3.3 Specimen A-3

Specimen A-3 is a 9.32 mm thick specimen with reinforced plate free edges. 50 mm x 9.32 mm stiffeners, of the same material as the specimen, were welded along the full length of each plate free edge. Ten 7/8" diameter ASTM A325 high strength bolts designed for bearing were used to connect the splice member to the gusset plate.

The load versus axial displacement response of the gusset plate assembly for Specimen A-3 is plotted in Figure 4.15. The specimen response under tension loading is similar to

Specimen A-1 in that as the axial deformation level is cyclically increased, the load carrying capacity of the specimen is stable. In compression, the enhanced behavior of Specimen A-3 is revealed. Not only is the ultimate compressive capacity increased over that of Specimen A-1, but the onset of overall plate buckling was not accompanied by a sudden increase in axial plate deformation nor a significant decrease in load carrying capacity. Since Figure 4.2 and Figure 4.15 are both plotted to the same scale, the increased energy absorption capacity of the reinforced plate, Specimen A-3, as compared to the basic plate, Specimen A-1, is evident. A photograph of the failed specimen and the final yield line pattern is shown in Figure 4.16.

Figure 4.17(a) shows the specimen load versus deformation response of the gusset plate assembly during the elastic portion of loading, Cycle #1-6. As expected, no yield lines were observed on the specimen during the elastic cycles. Figure 4.17(b) shows the load versus deformation response during the inelastic loading cycles up to the onset of plate buckling, Cycle #7-14. Connection bolt slip in Specimen A-3 first occurred during the tension loading of Cycle #7 at a load of 1290 kN. As in the testing of Specimen A-1, the splice member to gusset plate connection experiences slippage twice during every subsequent test cycle. The bolt slip experienced during each cycle of loading is evident in the load versus axial deformation response of Figure 4.15. The saw-tooth character of the slip on the load versus deformation curve is a function of the discrete nature of the data observations.

The first visible signs of yielding were observed on the specimen at the base of the gusset plate, near the gusset plate to frame assembly welded boundary. As the axial deformation level increased in subsequent loading cycles, yielding spread to the region of the gusset plate beneath the splice member. These yield lines can be associated with the compressive loading as the gusset plate begins to deform out-of-plane. Whitewash flaking due to

tensile yielding was first noticed on the specimen along the sides of the splice member as the plate material in the connection region began to yield. Yielding about the sides of the splice member connection was likely due to both tension and compressive loads. As the testing progressed, plate yielding spread out from the regions previously indicated.

During the compressive loading portion of Cycle #14, a maximum compressive load of 1990 kN was reached, accompanied by the first signs of yielding on the outside face of the plate edge stiffeners. This was a slight decrease from the maximum compressive load reached during the previous cycle. The slight decrease in maximum load and the onset of yielding in the stiffeners indicated that plate buckling or local plate crippling of the specimen had begun. The maximum load of 2004 kN reached during Cycle #13 is the compressive capacity of this specimen.

The test proceeded under sequentially increasing levels of cyclic axial plate deformation until tensile failure of the specimen was observed. Figure 4.17(c) shows the specimen load versus deformation response for the remainder of the test loading. The failure of the specimen in tension occurred during Cycle #15 just prior to reaching the desired cycle axial deformation level. The maximum tensile load reached prior to failure was 1850. This was slightly less than the ultimate specimen tensile capacity of 1884 kN attained during the previous cycle. The test was concluded by loading the specimen in compression until an excessive level of compressive deformation was achieved. During this final loading a peak compressive load of 1910 kN was reached prior to the slow deterioration of the load carrying capacity of the specimen under increasing axial and out-of-plane deformations.

The tensile failure mode and the behavior of the plate material in the connection region were similar to that of Specimen A-1. The tension tear-out deformations caused the plate

to spread outwards and to bulge upwards at the top of the connection. In addition, due to the high compressive loads realized, the compressive bolt hole deformations were more severe, resulting in some piling-up of material on the compressive side of some of the bolt holes.

Figure 4.18 shows the out-of-plane deflected shape of the stiffened plate edges and the center line deflection of the specimen after the onset of overall plate buckling in Cycle #14. The deflected shape of the center line again resembles that of a fixed-fixed but guided column. However, the presence of the edge stiffeners restricts the plate edges from experiencing any significant out-of-plane deformation at this load level. Only when severe compressive axial deformations were imposed during the final test cycle, do significant deformations become visible along the stiffened edges. As seen in Figure 4.19, the stiffener displacements are predominately confined to rotational deformations at the stiffener to frame weld locations while the rest of the stiffener remains relatively rigid.

Gusset plate strain distributions for Specimen A-3 were investigated at the same levels as Specimen A-1. Figure 4.20 shows the strain distributions at both the 530 kN and 1060 kN load levels for Specimen A-3. The general distribution of strains remains generally unchanged between the tensile and compressive load states. The peak specimen strains are recorded at the rosette locations beneath the splice plate, while the edge and interior strains are higher along the long edge side of the specimen. Along each reinforced edge, the strains are highest at the top of the specimen. When the specimen load is doubled to the 1060 kN level, plate strains in both tension and compression also approximately double. When compared with the strain readings from Specimen A-1 at the same load level, strains in Specimen A-3 are generally lower about the edges of the specimen, while roughly the same or slightly higher at the rosette locations. It appears that the effect of the plate edge stiffeners is to reduce the strains along the exterior plate edges. By welding

stiffeners onto the specimens, the plate stresses and strains are distributed over a larger area of material. In addition, at the -1060 kN load level, no significant bending is indicated by the strain readings in Specimen A-3. This observation supports the conclusion that the addition of stiffeners to Specimen A-3 delays the onset of yielding and out-of-plane buckling deformation in the gusset plate.

4.3.4 Specimen A-4

Specimen A-4 is a 6.18 mm thick specimen with reinforced plate free edges. 50 mm x 6.18 mm stiffeners, of the same material as the specimen, were welded along the full length of each plate free edge. Ten 7/8" diameter ASTM A490 high strength bolts were used to connect the splice member to the gusset plate in order to achieve a slip-resistant connection. No bolt slip was expected to occur during the testing of this specimen.

Figure 4.21 shows the load versus axial displacement response of Specimen A-4. The tensile portion of the cyclic loading curve shows the stable response of the specimen under tension loading. In compression, the effect of the edge stiffeners is observed. Although the compressive capacity of Specimen A-4 is not significantly higher than Specimen A-2, the presence of the plate edge stiffeners greatly affected the post-buckling behavior of the specimen. The attainment of the specimen compressive capacity was not followed by a sudden drop in load carrying capacity, but instead, a steady deterioration is observed. By comparing Figure 4.9 and Figure 4.21, the increased energy absorption capacity of the reinforced plate, Specimen A-4, as compared to the basic plate, Specimen A-2, is observed. The final yield line pattern observed on the failed specimen plate and the deformed plate edge stiffeners is shown in Figures 4.22 and 4.23.

Figure 4.24(a) shows the specimen load versus deformation response of the gusset plate assembly during the elastic portion of loading, Cycle #1-6. The onset of yielding was first

observed during Cycle #5, at the 100% nominal Whitmore yield load level. A few yield lines were noted running parallel to the long free edge at the base of the specimen. The onset of yielding was supported by the presence of residual plate strains at the completion of the cycle.

The testing proceeded with cycles of increasing axial plate deformation. Figure 4.24(b) shows the load versus deformation response of the specimen during the inelastic loading up to the onset of plate buckling, Cycle #7-10. During Cycle #9, at an axial deformation level of $2.5\Delta_y$, the first signs of tensile yield lines were observed on the plate about the sides of the splice member connection. In compression, yield lines increased about the base of the splice member as a localized buckle began to form at the base of the specimen plate. The onset of yielding was also observed on the outsides of the plate edge stiffeners at the bottom corner of each edge.

During Cycle #10 ($\pm 3.0\Delta_y$) the compressive capacity of the specimen was reached. A compressive load of 1149 kN was attained, accompanied by an increase in yield line activity about the base of the splice member and on the plate edge stiffeners. Although the compressive capacity had been reached, the plate appeared to have only buckled locally as overall plate buckling was being restrained by the plate edge stiffeners. Unlike Specimen A-2, the buckling of the specimen was not immediately followed by a significant drop in the specimen load carrying capacity.

As the test proceeded under sequentially increasing levels of axial plate deformation, the tensile yield lines about the splice member connection increased. Figure 4.24(c) shows the specimen load versus deformation response for the remainder of the test loading. It is observed that the maximum tensile loads attained increased as the cyclic axial deformation level increased. In compression, the maximum cycle loads reached deteriorated at a

steady pace as the testing cycles continued. There was an increase in yielding throughout the specimen as the plate continued to buckle under constraint from the plate edge stiffeners. Yield lines developed along the long edge of the gusset plate, just beneath the edge stiffener. Eventually, the buckled shape became more defined, stretching from the bottom corners of the splice member out towards the corners of the plate edges. Yield lines on the plate stiffeners increased significantly under cycles of increasing axial plate deformation. Ultimately, the plate edge stiffeners themselves deformed both in-plane and out-of-plane, allowing the outside edges of the specimen plate to buckle.

The tensile capacity of the specimen was reached during Cycle #17 ($\pm 21.0\Delta_y$) when a maximum load of 1265 kN was reached. However, the tensile failure of the specimen occurred during Cycle #18 when the tensile load carrying capacity began to drop under increasing axial plate deformation. During Cycle #18, a new region of yielding was observed along the gusset plate to frame assembly boundary due to the cyclic out-of-plane deformations in the specimen. The test was concluded by loading the specimen in compression. The test was stopped when the compressive capacity of the specimen had deteriorated to 680 kN.

The tensile failure mode of the specimen was a fracture of the plate material between the bolts in the bottom row of the connection. There was no sign of bolt slip in the connection region. Tensile yielding deformations were the most severe in the bottom row of bolts, while compressive deformations were the greatest in the top row of bolts. The compressive yielding in the connection caused the topmost bolt holes to deform downwards and outwards, in a direction approximately parallel to the plate free edges. In addition, overall connection yielding caused tension plate bulging and plate spreading at the top of the connection region, and compressive plate spreading at the bottom of the connection region. Figure 4.25 is a photograph of the bolt holes and deformation in the

connection region after the completion of testing.

Figure 4.26 shows the out-of-plane deflected shape of the stiffened plate edges and the center line deflection of the specimen during the compressive loading of Cycle #11. Initially, the deflected shape of the center line resembles the buckled shape of a fixed-fixed but guided column. The deflected shapes of the reinforced edges reveal that the edges themselves had not buckled at this load cycle level. As the compressive plate deformations increased, the deflected shape of the specimen center line began to resemble that of a fixed-pinned but guided column. As the stiffened edges began to buckle, overall plate buckling was facilitated. This created a plastic hinge region beneath the base of the splice member, thereby reducing the fixity provided by the relatively rigid splice member. Photographs of the final deformed shape of the plate edge stiffeners (Figure 4.23) show that the stiffeners have buckled.

Gusset plate strain distributions for Specimen A-4 were investigated at the same load levels as Specimen A-2. Figure 4.27 shows the tensile and compressive strain distributions at both the 353 kN and 707 kN level for Specimen A-4. In general, the plate strains are highest at the rosette locations beneath the splice member. The strain distribution is generally the same along both stiffened edges of the specimen, with slightly higher strains observed at the top corner of the long free edge. When the strain distribution under tensile and compressive loading is compared, the compressive loading state reveals lower strains along the plate edges and the interior points, but slightly higher strains at the rosette locations. Plate strains generally double when the specimen load is increased from the 353 kN to the 707 kN level. Under compression, at the 707 kN level, strains have become slightly higher along the short side of the plate. In addition, strains in the rosette locations are approaching yield levels and are indicating the onset of plate bending in that region. When compared to Specimen A-2, strains are significantly less along the plate

edges and within the interior of the plate, but are at similar levels at the rosette locations. By providing stiffeners to the plate edges, the stresses and strains in the edge regions of the plate are distributed over a greater area of material, thereby reducing the strain levels in those locations.

4.3.5 Specimen A-5

Specimen A-5 is a 9.32 mm thick specimen. The plate geometry was modified to accommodate the free formation of a plastic hinge under compressive loading deformations. Ten 7/8" diameter ASTM A325 high strength bolts designed for bearing were used to connect the splice member to the gusset plate.

The load versus axial displacement response of Specimen A-5 is plotted in Figure 4.28. Although the specimen geometry was significantly altered, the tensile response of Specimen A-5 is similar to the other test specimens. In contrast, the deteriorated compressive behavior is evident. The compressive capacity of Specimen A-5 is only a fraction of the compressive capacity of the other specimens of the same plate thickness (Table 4.2). By comparing the load deformation response of Specimen A-5 with the response of Specimens A-1 and A-3, the decreased energy absorption capacity of this specimen geometry is evident. A photograph of the final yield line pattern of the failed specimen is shown in Figure 4.29.

Figure 4.30(a) shows the specimen load versus deformation response of the gusset plate assembly during the initial portion of loading, Cycle #1-7. The specimen was to be subjected to a set of cycles, Cycle #5-6, each at 100% of the expected nominal tensile yield load, 1060 kN. However, during the compressive loading portion of Cycle #5, the loading was stopped at a maximum load of 907 kN in order to maintain the compatibility of axial deformations in both tension and compression. Observations at maximum

compression revealed the onset of yield lines along the specimen plate to frame assembly welded boundary. In addition, strain gage readings also indicated that yielding was occurring in the plate in the region beneath the splice member. Therefore compressive yielding had begun prior to reaching the expected nominal yield level. However, since the actual measured material yield level was significantly higher than the nominal value of 300 MPa, the 100% or nominal Whitmore yield level cycles were actually still well in the elastic range. Therefore, compressive yielding had begun well below the expected yield level based on the Whitmore critical stress theory.

Cycle #6 was loaded to the same axial deformation level as Cycle #5. Observations taken at the maximum compressive load of 905 kN revealed that the plate free edges were visibly deformed out-of-plane and the strain gage readings in the 'plastic hinge' region indicated significant plate bending. During compressive loading of Cycle #7, a maximum load of only 860 kN was reached. Specimen observations revealed the start of a plate buckle extending from the bottom corner of each free edge. The plate free edges themselves buckled in a region near the frame boundary, allowing the specimen to buckle out-of-plane.

The testing was continued with cycles of increasing axial plate deformation to observe the post-buckling behavior of the gusset plate and to reach the tensile capacity of the specimen. Figure 4.30(b) shows the specimen load versus deformation response for the remainder of the test loading. During the tension loading of Cycle #8, major bolt slip occurred in the splice member connection at a load of 1720 kN. Since the compressive capacity of the buckled specimen was less than the dynamic frictional resistance of the bolted connection, major slip did not occur during compressive loading. In fact, major slip was avoided throughout the remainder of the test as the splice member connection remained in tension bearing. The connection bolt slip that occurred is illustrated in the

plot of Figure 4.30(b).

As the testing progressed, the maximum tensile loads reached increased as the cycle axial deformation level increased. The first signs of tension yielding on the gusset plate were observed about the sides of the splice member as the bolt holes yielded under tensile bearing deformations. As the cycle axial deformation levels increased, the tensile yield lines about the connection region began extending outwards towards the free edges of the specimen. Under compression, the capacity of the buckled specimen deteriorated slowly but steadily from the peak capacity attained during Cycle #5. As the compressive deformations increased, yield lines indicated the presence of a secondary plate buckle extending from the base of the splice member out towards the middle of the plate free edges. In addition, the increase in cyclic out-of-plane deformations resulted in a fracture of the weld along the gusset plate to frame weld boundary, at the extreme outside edge of the long welded side. Initially, a fracture length of about 1 cm was visible. A photograph of the weld fracture under tension loading is shown in Figure 4.31.

The tensile failure of the specimen occurred during Cycle #14. However, the tensile capacity of the specimen was reached during the previous cycle when a maximum load of 1887 kN was attained. The test was concluded by loading the specimen in compression until an excessive level of compressive deformation was achieved. As the cyclic deformations increased, the length of the weld fracture grew as the plate was being pried off at that location.

The tensile failure mode and the behavior of the plate material in the connection region were similar to that of the previous specimens. However, since slip only occurred in tension, bolt hole bearing deformations occurred only in tension and material scaling due to slip was only evident on the tension side of all bolt holes.

Figure 4.32 shows the out-of-plane deflected shape of the plate free edges and the center line deflection of the specimen recorded during Cycle #7 once the compressive deformations had become significant. The deflected shape of the center line resembles that of a fixed-pinned but guided column. A hinge is evident on the gusset plate beneath the base of the splice member. At this load level, the deformed shape of the long free edge resembles the buckled shape of a fixed-pinned but guided column, while the deflected shape of the short free edge is closer to the buckled shape of fixed-fixed but guided column. The difference in deformation between the free edges is likely due to the increased fixity provided to the top of the short free edge by the close proximity of the splice member to that edge, as shown in the specimen geometry (Figure 3.2). Figure 4.33 is a photograph of the deformed plate free edges at the completion of the testing. It is observed that further deformation of the specimen caused hinges to form at the base of the plate edges along the frame member boundary.

An analysis of the specimen strain distribution during the assumed elastic cycles of loading confirms the poor response of Specimen A-5. Figure 4.34 illustrates the strain distribution of Specimen A-5 at both the 530 kN and +1060/-907 kN load level. At the +530 kN level, plate strains are highest under the splice member at the rosette locations. The strain distribution is similar along both free edges with slightly higher strains recorded at the middle of the edges. In compression, the magnitude and distribution of strains is relatively unchanged from the +530 kN load level. However, the strain readings indicate the onset of plate bending along the long edge, in the 'plastic hinge' region, and at the rosette locations. When the strains are examined at the +1060 kN level, the strains are approximately double those recorded at the +530 kN level, indicating elastic response under tension. In compression at a load of -907 kN, the overall buckling of the specimen is evident. Strains indicate significant plate bending at the gage locations along the length of the long edge, at the middle of the short edge, in the 'plastic hinge' region, and in the

rosette region. In addition, strain readings at the middle of the free edges, in the 'plastic hinge' region, and at the rosette locations are at or beyond yield levels. Gage readings appear distorted due the effects of significant plate bending.

Table 4.1. Material Properties

Plate Thickness (mm)	Elastic Modulus (MPa)	Yield Stress		Ultimate Strength (MPa)
		Static (MPa)	Dynamic (MPa)	
6.18 - (a)	213000	457	476	535
6.18 - (b)	199000	429	448	526
Average	206 000	443	462	530
9.32 - (a)	213000	460	480	543
9.32 - (b)	199000	438	458	532
Average	206000	449	469	537

Table 4.2. Ultimate Specimen Capacities

Specimen	Plate Size (mm)	Ultimate Tensile Load (kN)	Ultimate Compressive Load (kN)
A-1	550x450x9.32	1794	1682
A-2	550x450x6.18	1340	1128
A-3	550x450x9.32	1884	2004
A-4	550x450x6.18	1265	1149
A-5	550x450x9.32	1887	907

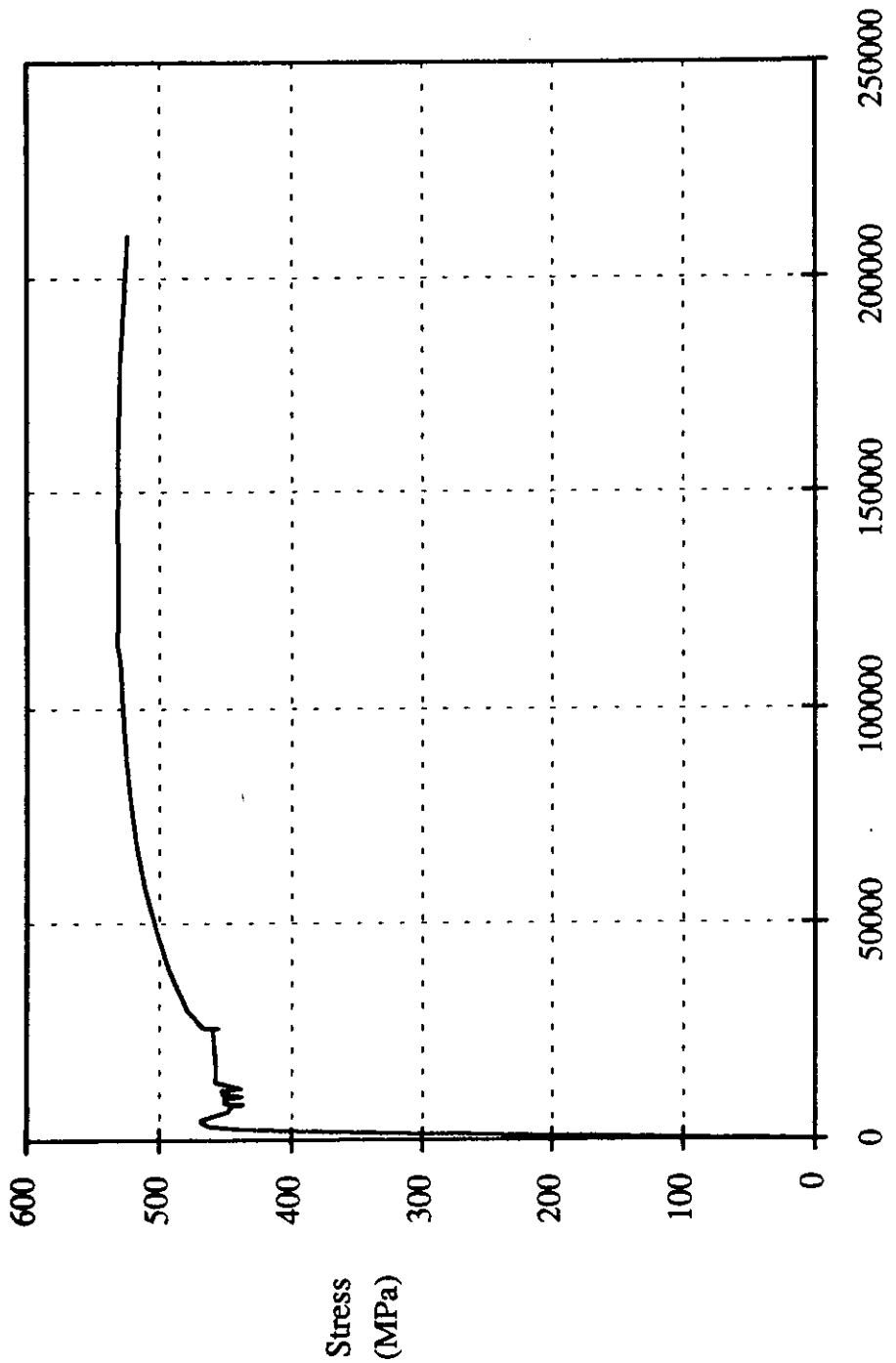

Figure 4.1. Typical Material Response

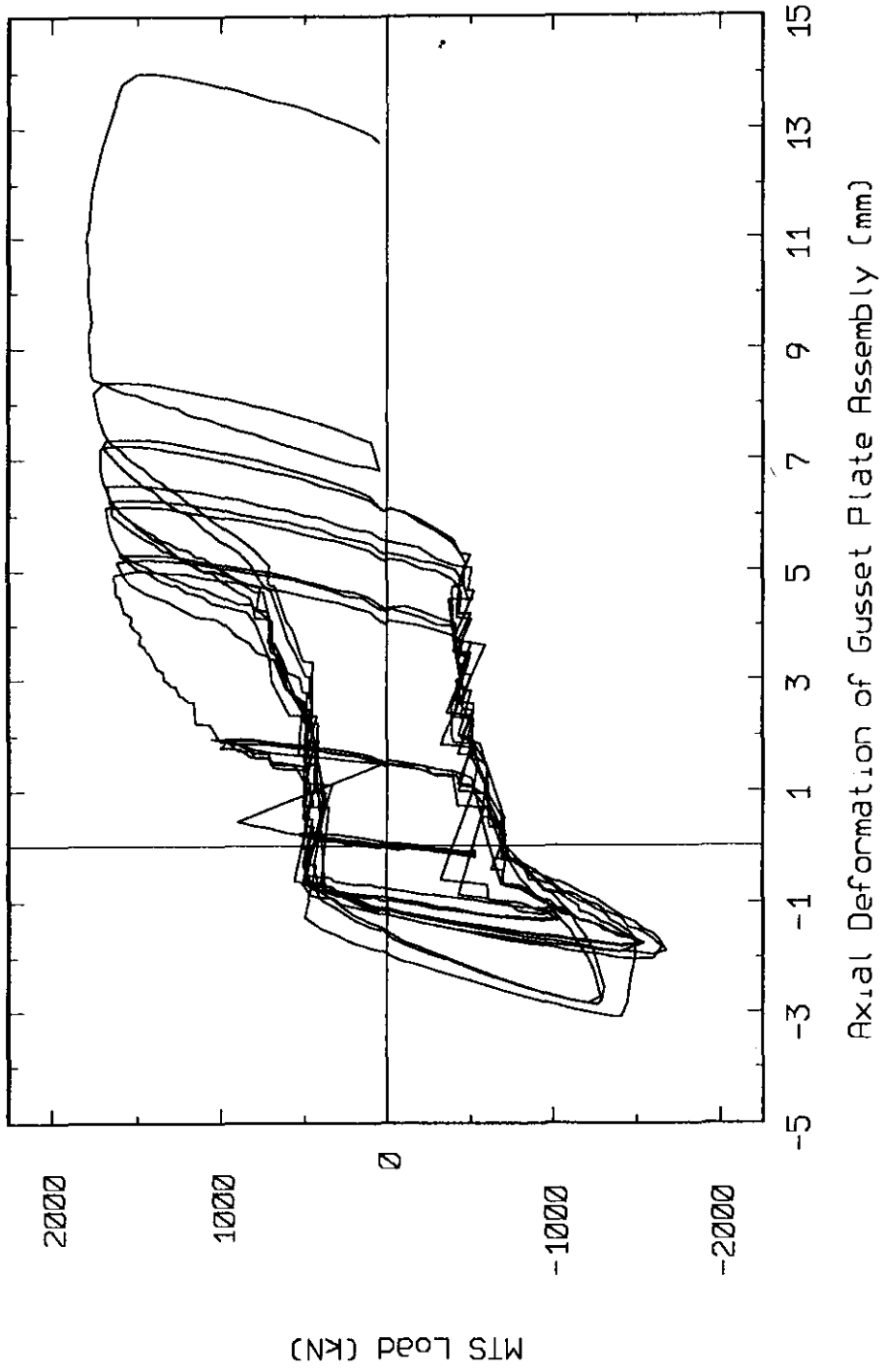

Figure 4.2. Load vs. Axial Displacement Response of the Gusset Plate Assembly - Specimen A-1

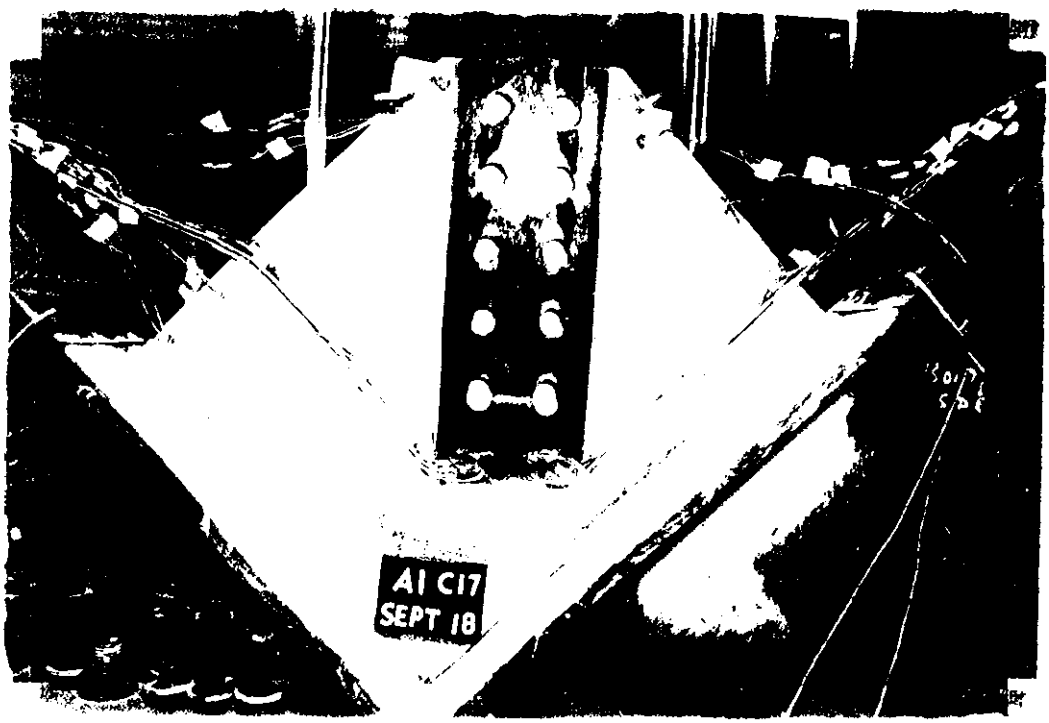

Figure 4.3. Final Specimen Yield Line Pattern - Specimen A-1

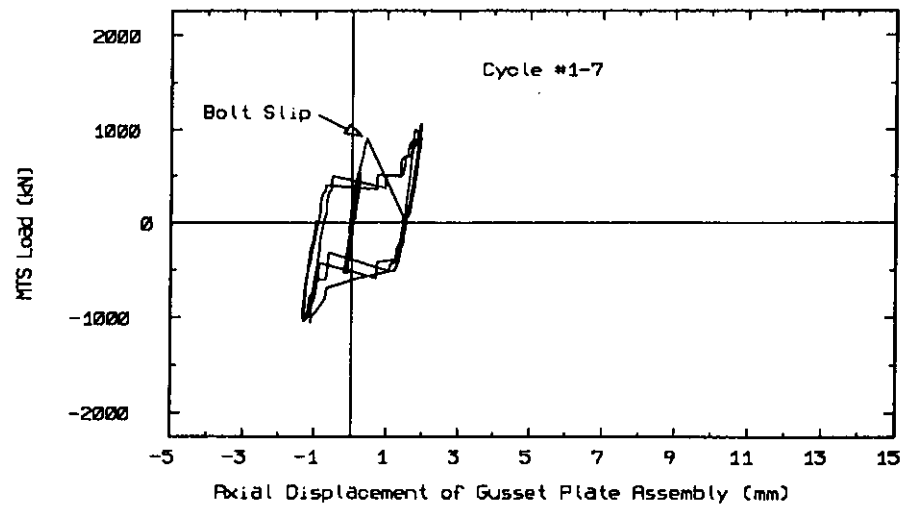

(a)

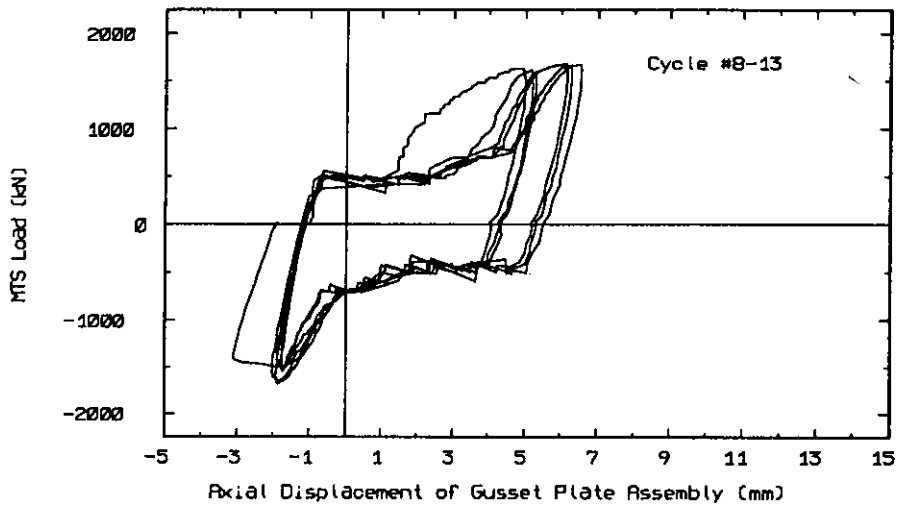

(b)

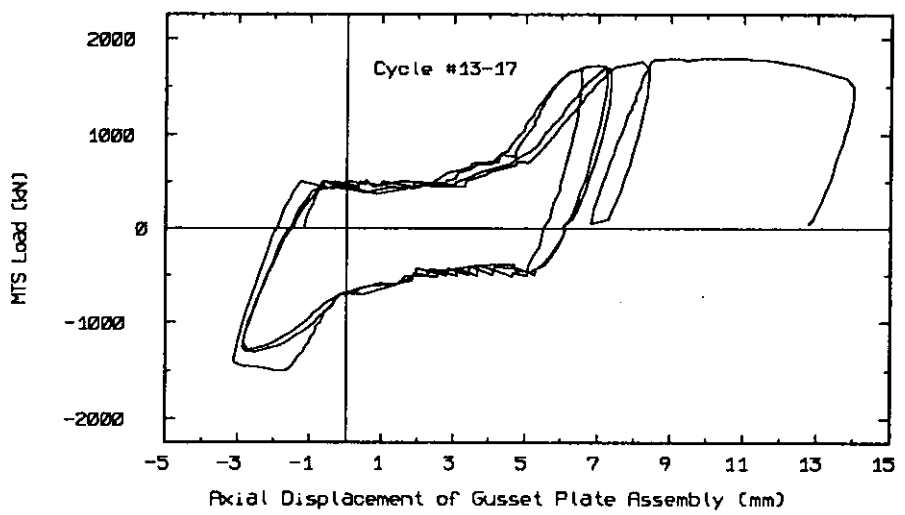

(c)

Figure 4.4. Load vs. Axial Displacement Response - Specimen A-1
(a) Cycle #1-7; (b) Cycle #8-13; (c) Cycle #13-17

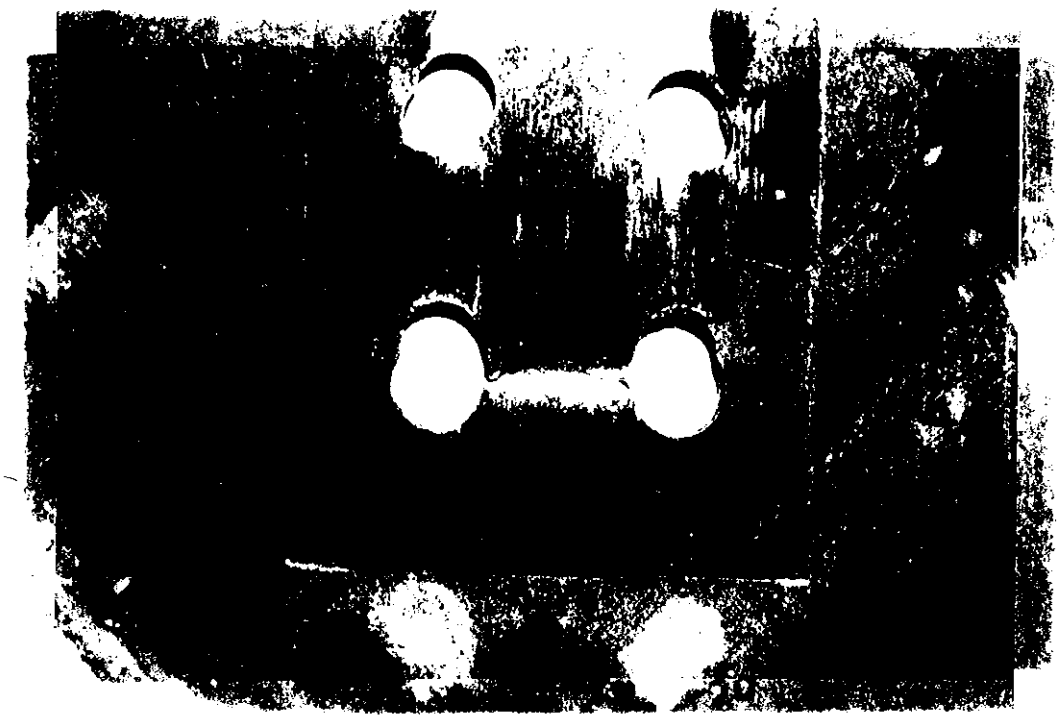

Figure 4.5. Plate Fracture in Bolted Connection - Specimen A-1

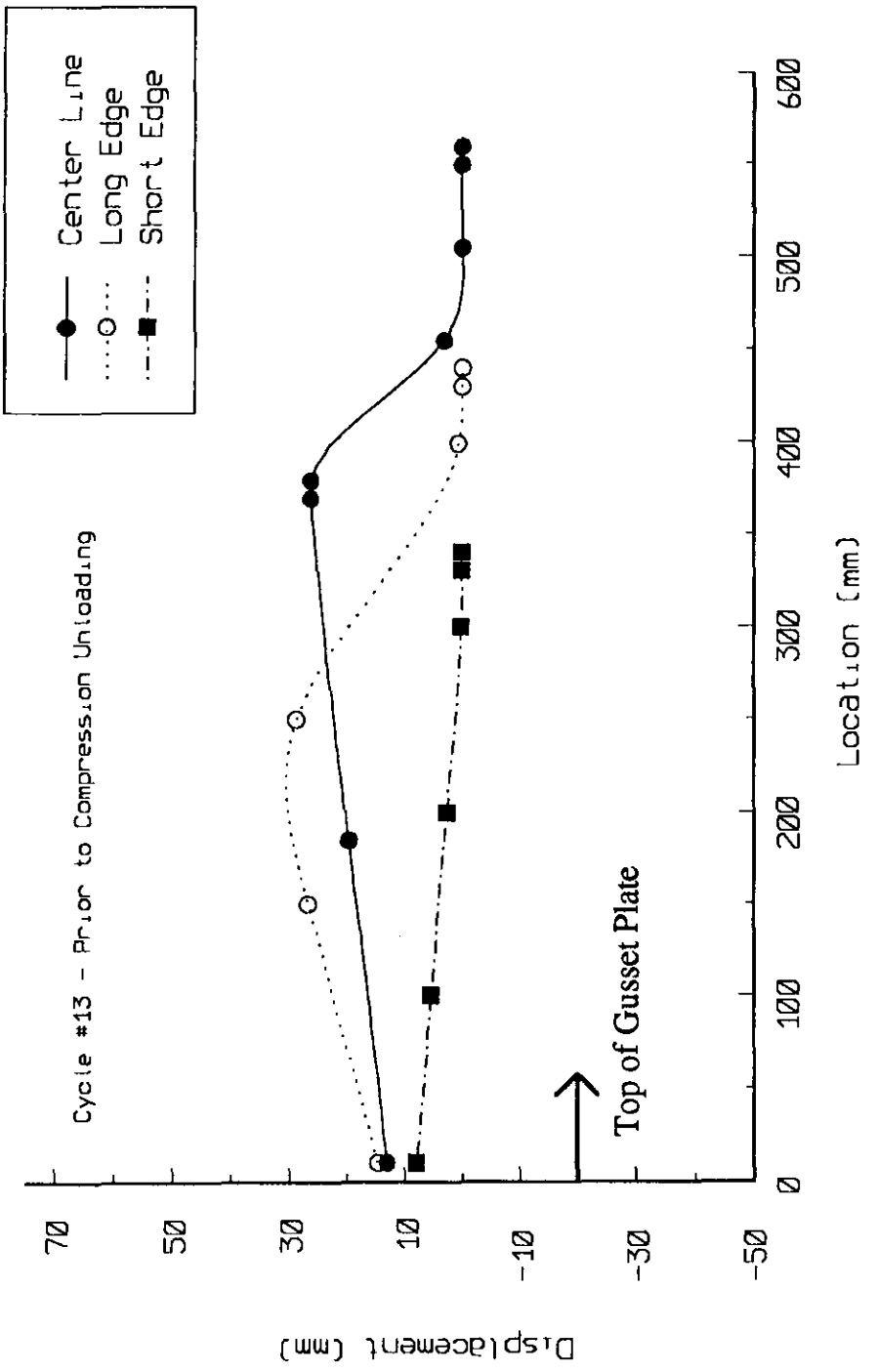

Figure 4.6. Out-of-plane Displacements - Specimen A-1

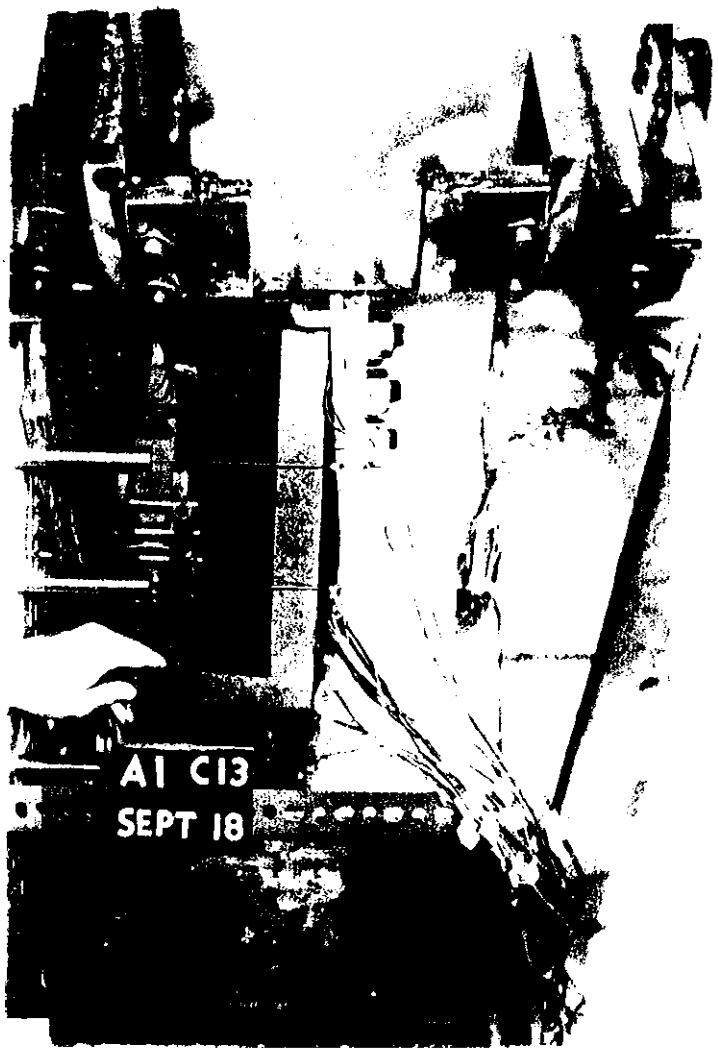

Figure 4.7. Buckled Long Free Edge - Specimen A-1

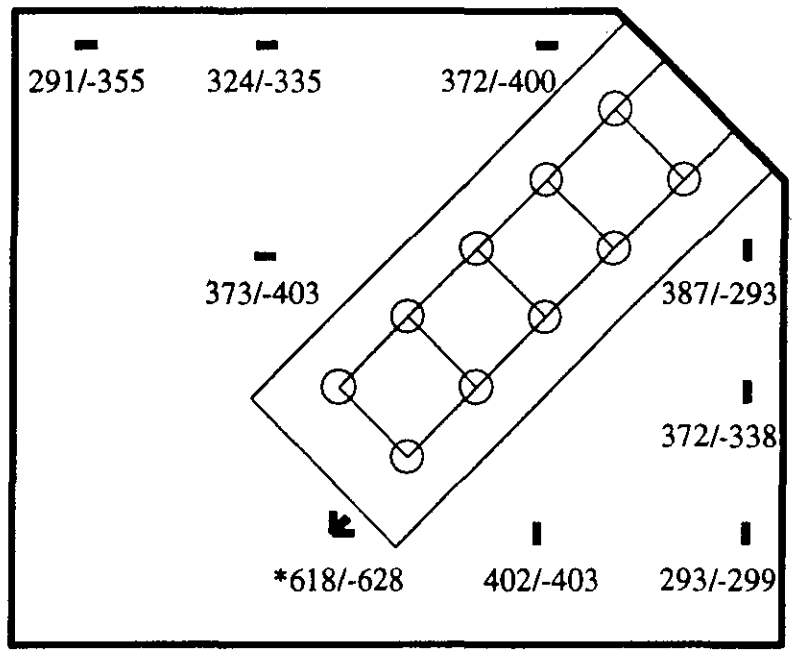

Load Level
+/- 530 kN

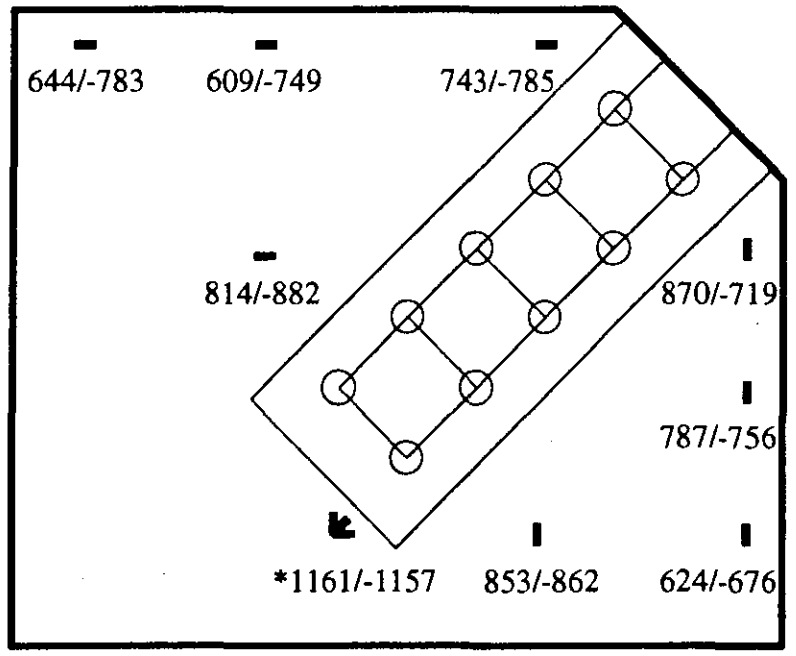

Load Level
+/- 1060 kN

* Strains at rosette locations are principal strain values

Figure 4.8. Strain Distribution - Specimen A-1

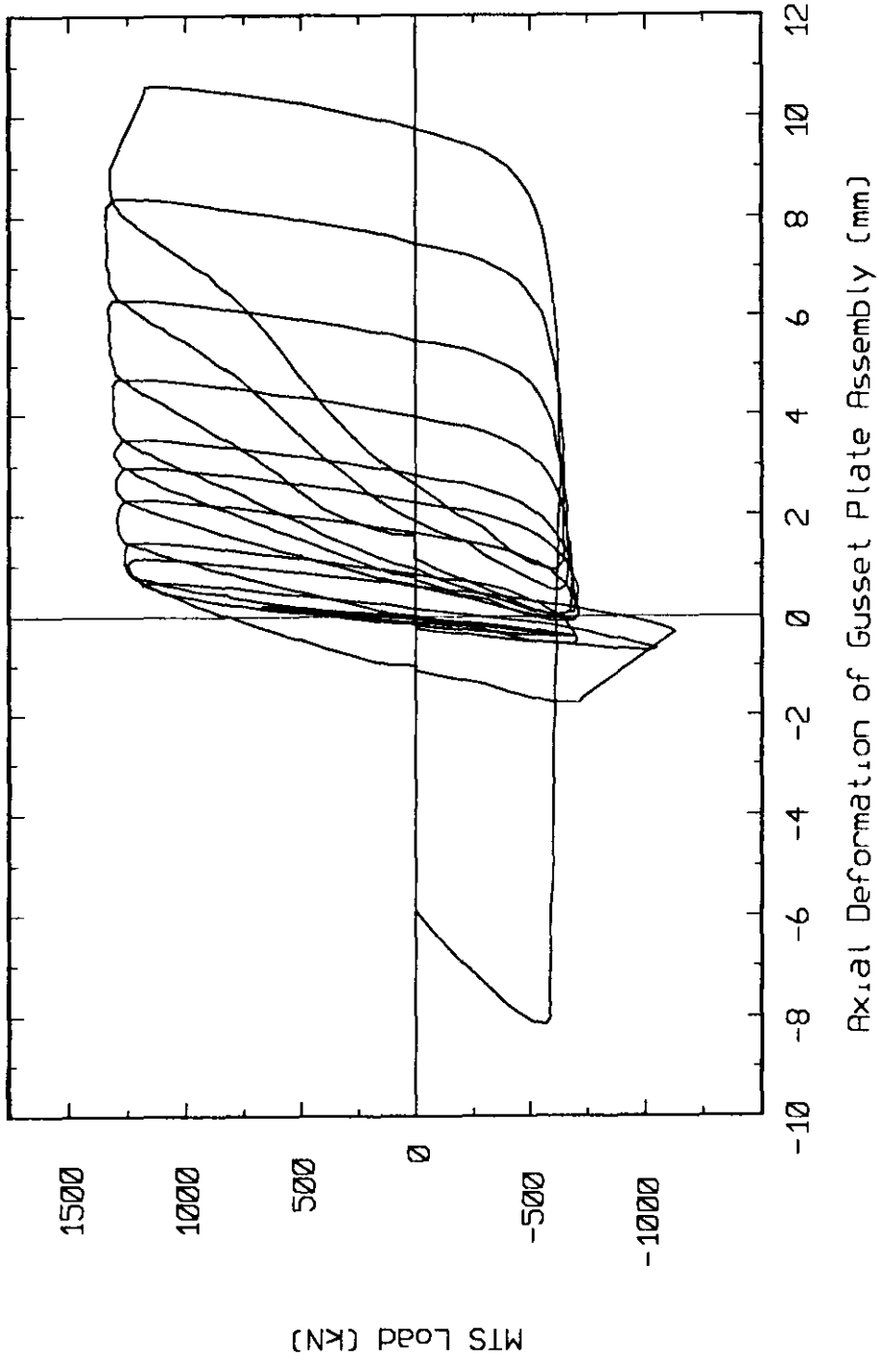

Figure 4.9. Load vs. Axial Displacement Response of the Gusset Plate Assembly - Specimen A-2

Figure 4.10. Final Specimen Yield Line Pattern - Specimen A-2

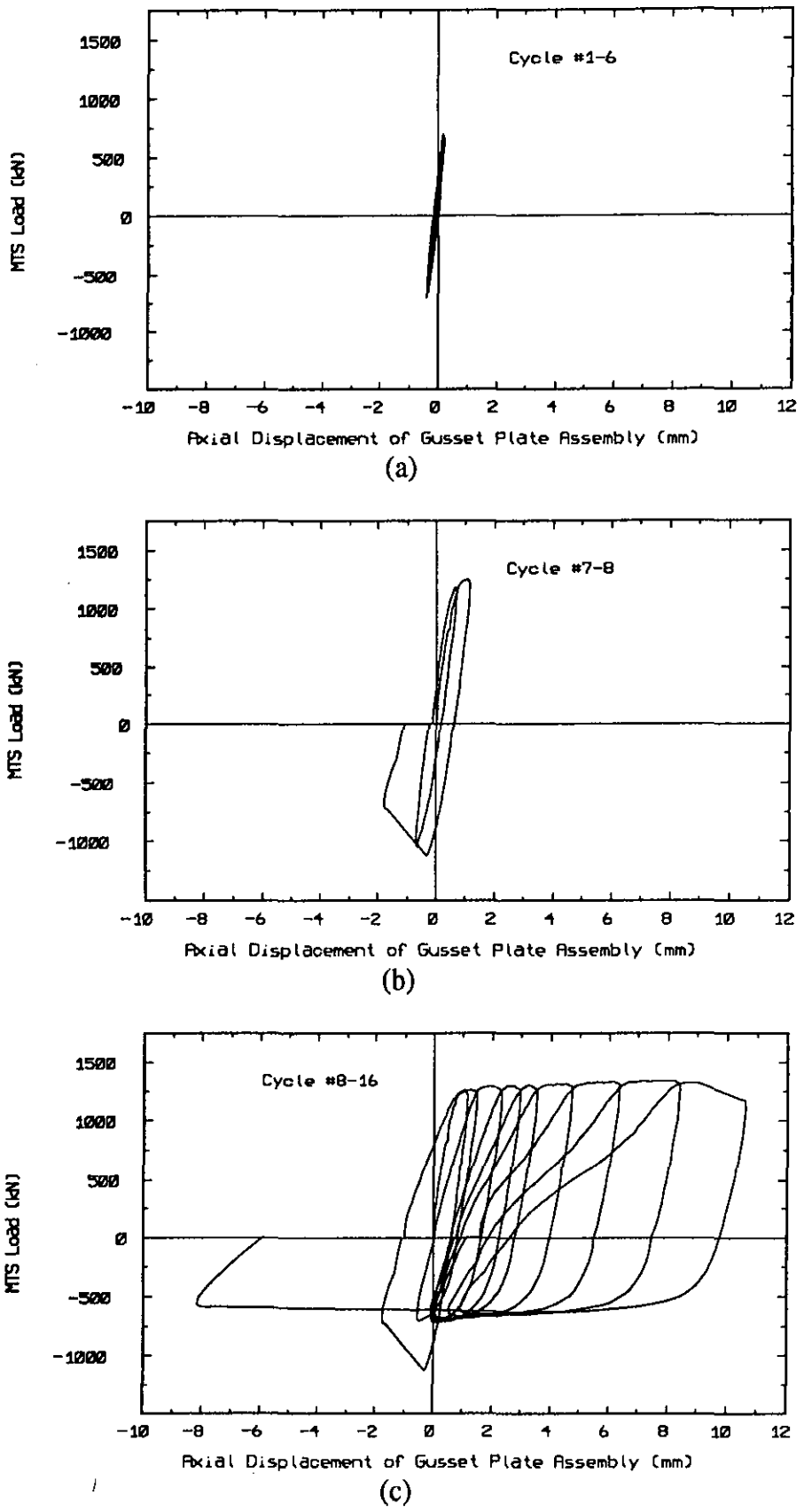

Figure 4.11. Load vs. Axial Displacement Response - Specimen A-2
(a) Cycle #1-6; (b) Cycle #7-8; (c) Cycle #8-16

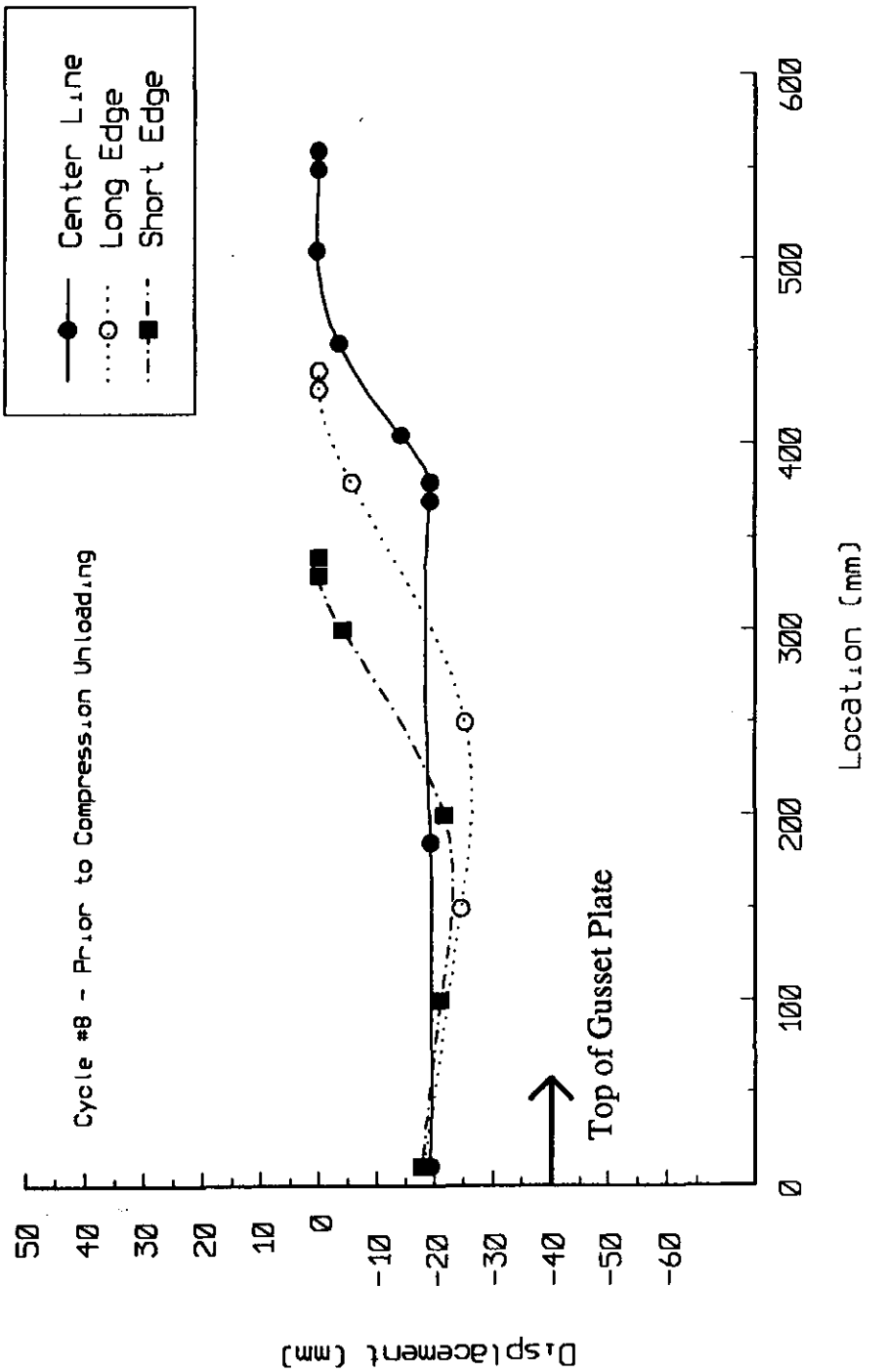

Figure 4.12. Out-of-plane Displacements - Specimen A-2

Figure 4.13. Buckled Plate Free Edges - Specimen A-2

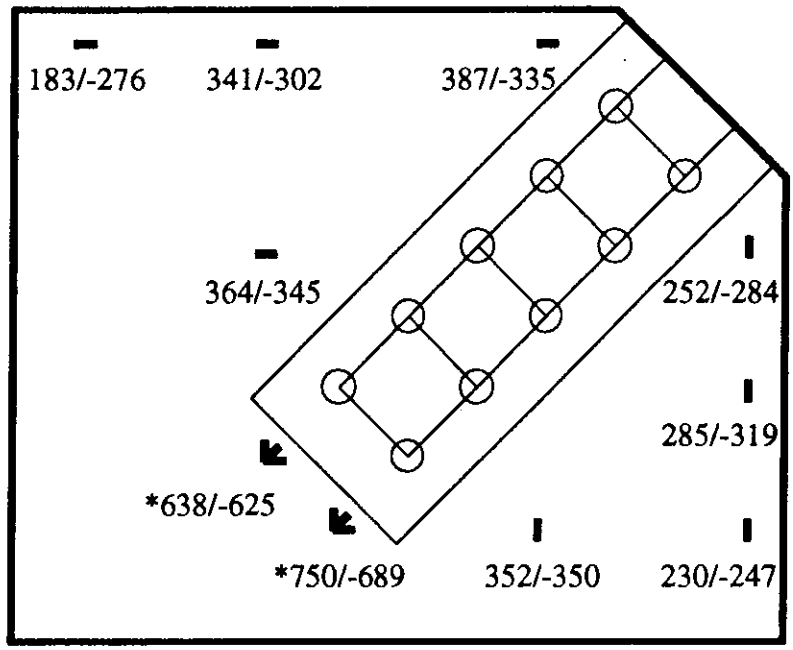

Load Level
+/- 353 kN

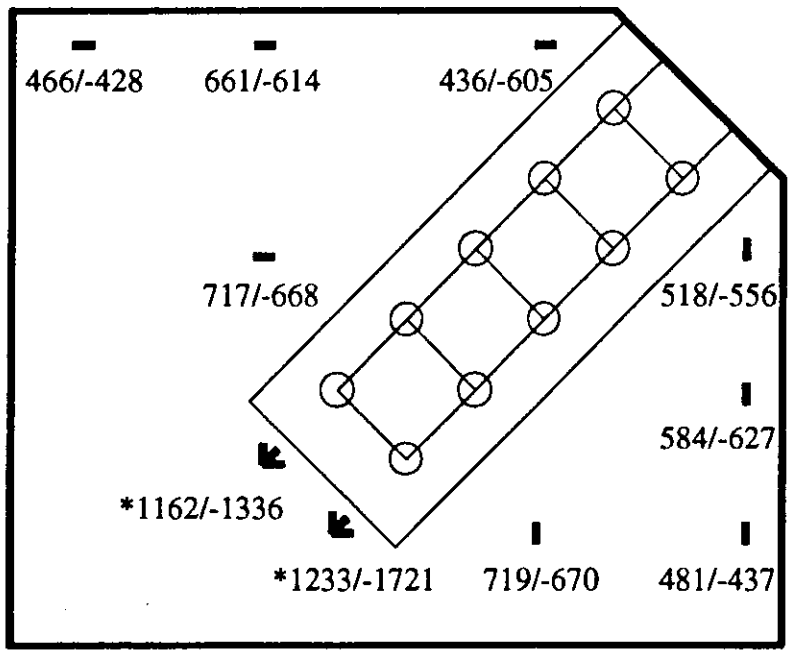

Load Level
+/- 707 kN

* Strains at rosette locations are principal strain values

Figure 4.14. Strain Distribution - Specimen A-2

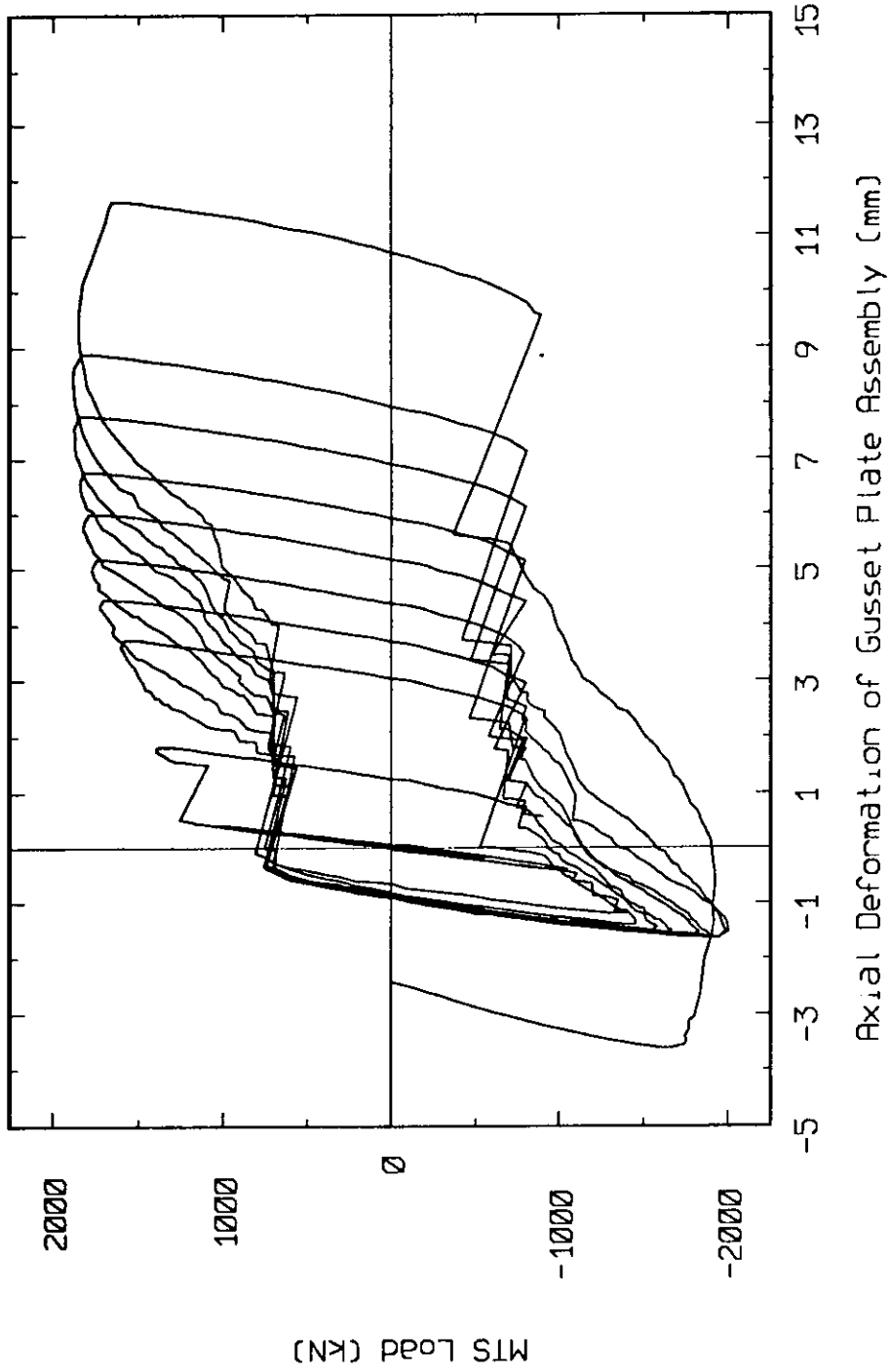

Figure 4.15. Load vs. Axial Displacement Response of the Gusset Plate Assembly - Specimen A-3

Figure 4.16. Final Specimen Yield Line Pattern - Specimen A-3

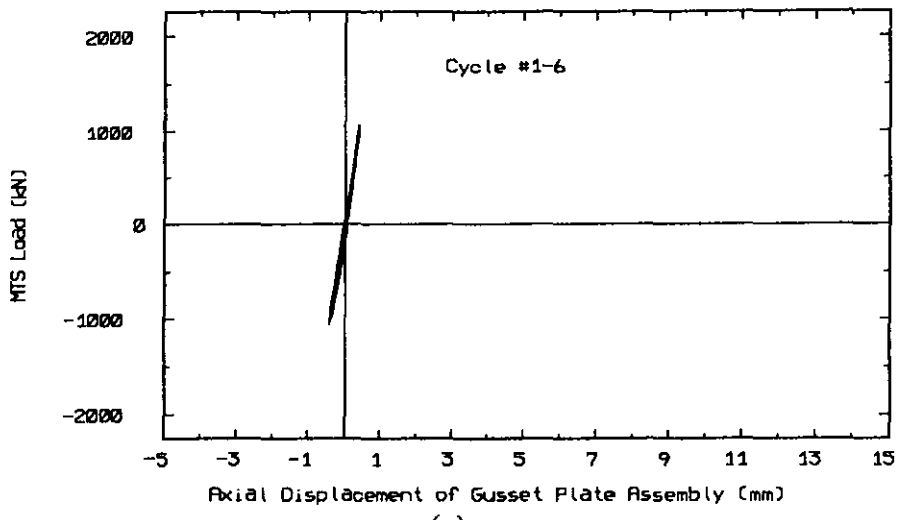

(a)

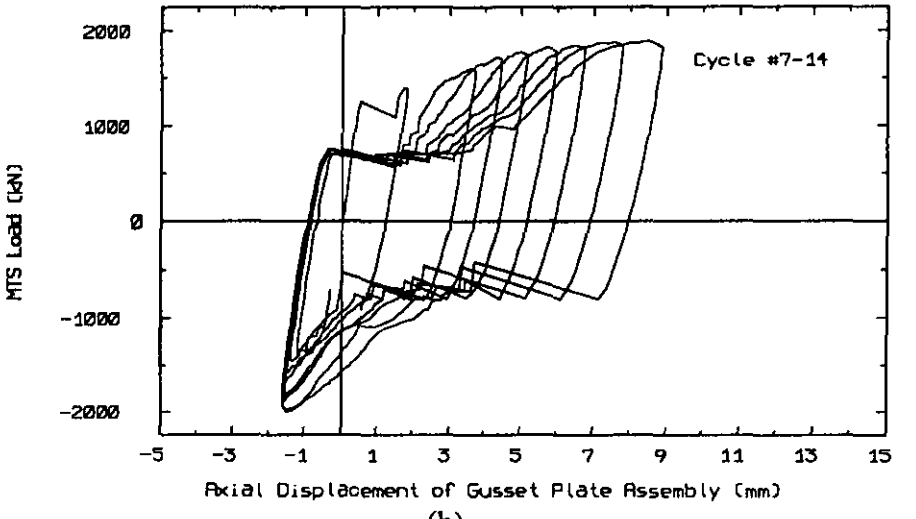

(b)

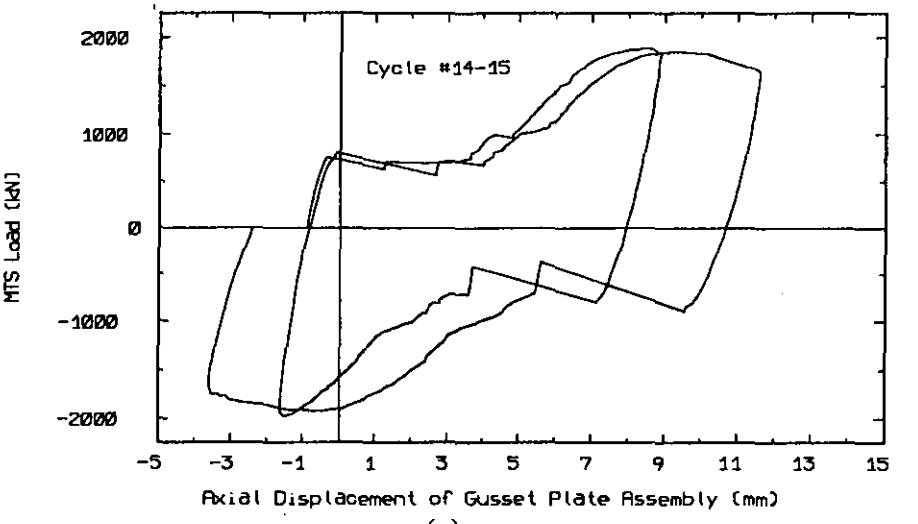

(c)

Figure 4.17. Load vs. Axial Displacement Response - Specimen A-3
(a) Cycle #1-6; (b) Cycle #7-14; (c) Cycle #14-15

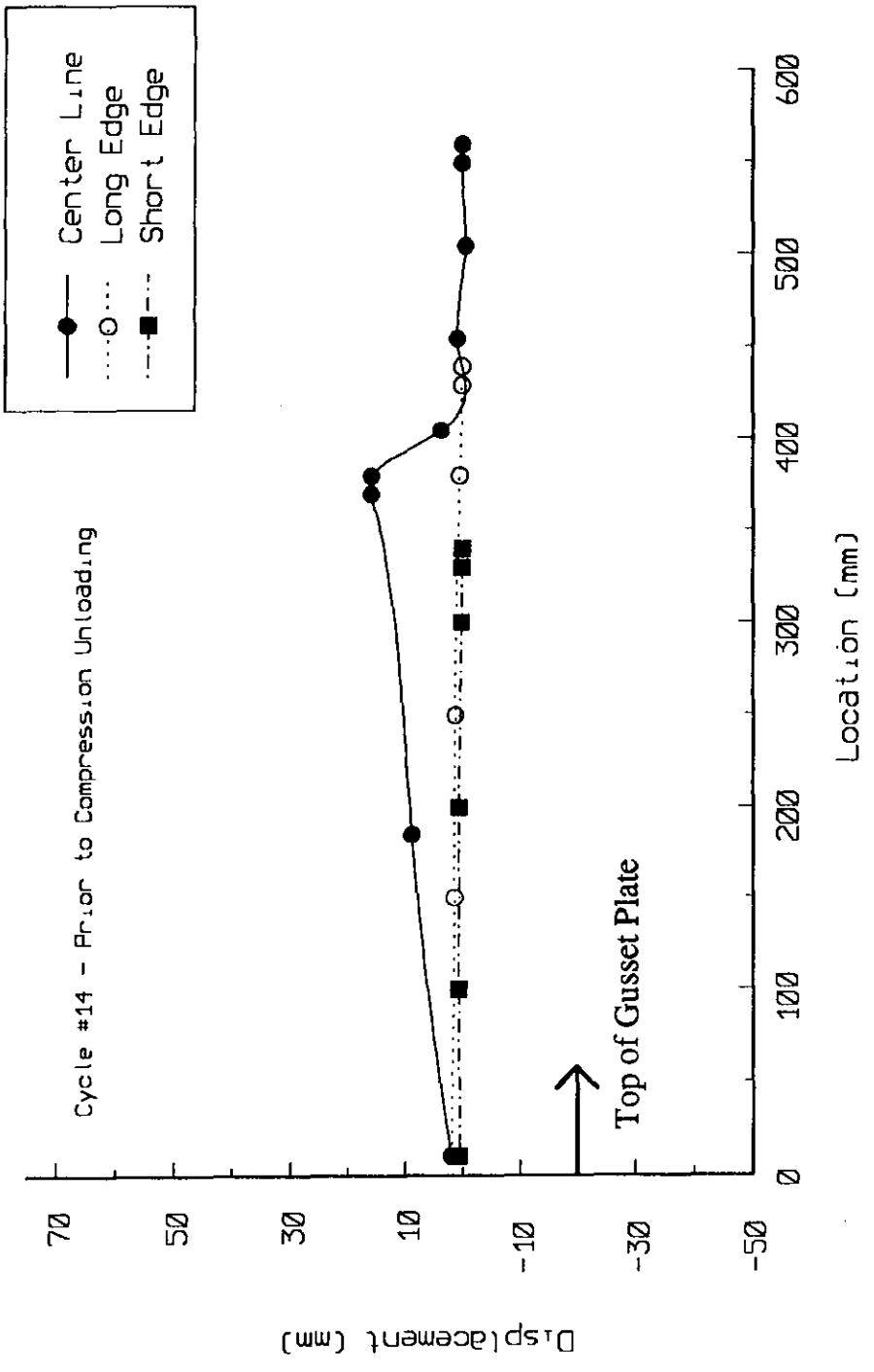

Figure 4.18. Out-of-plane Displacements - Specimen A-3

Figure 4.19. Deformed Plate Edge Stiffeners - Specimen A-3

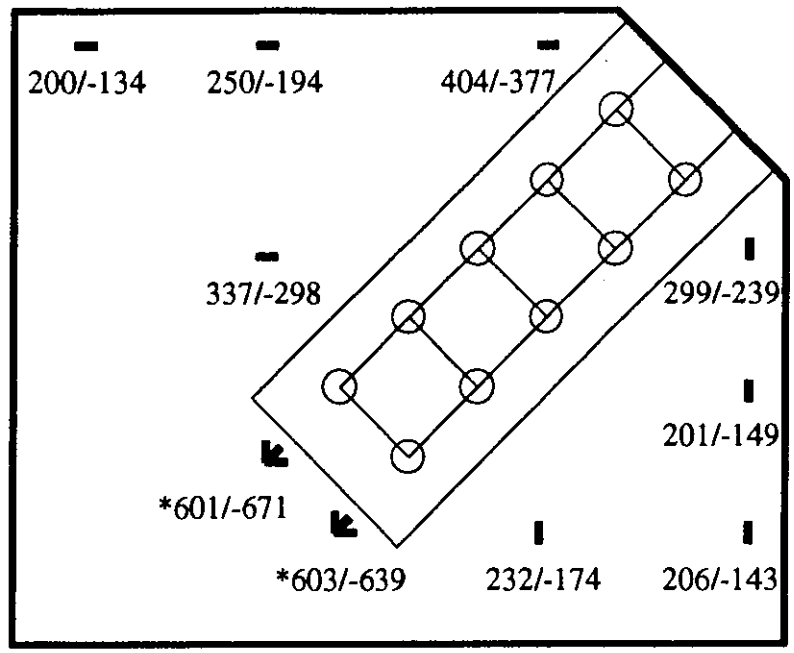

Load Level
+/- 530 kN

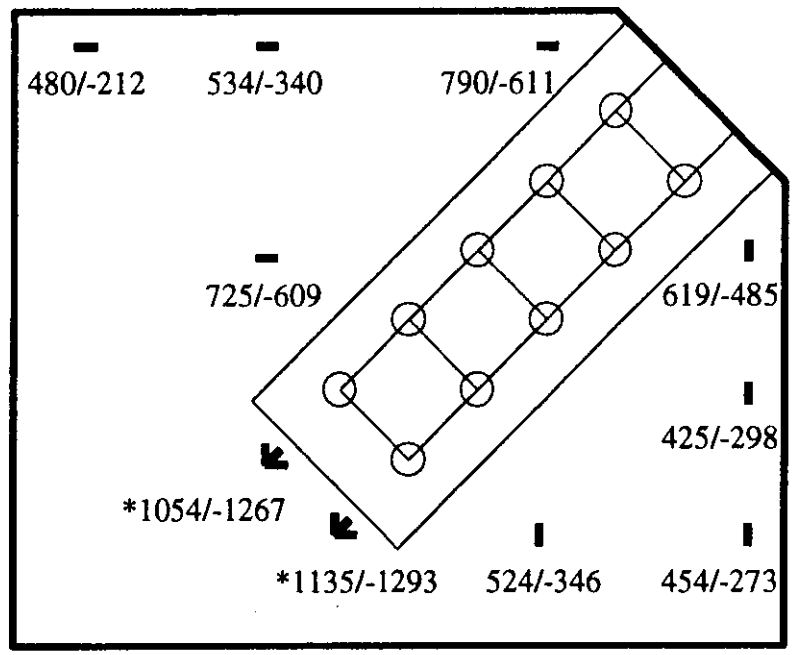

Load Level
+/- 1060 kN

* Strains at rosette locations are principal strain values

Figure 4.20. Strain Distribution - Specimen A-3

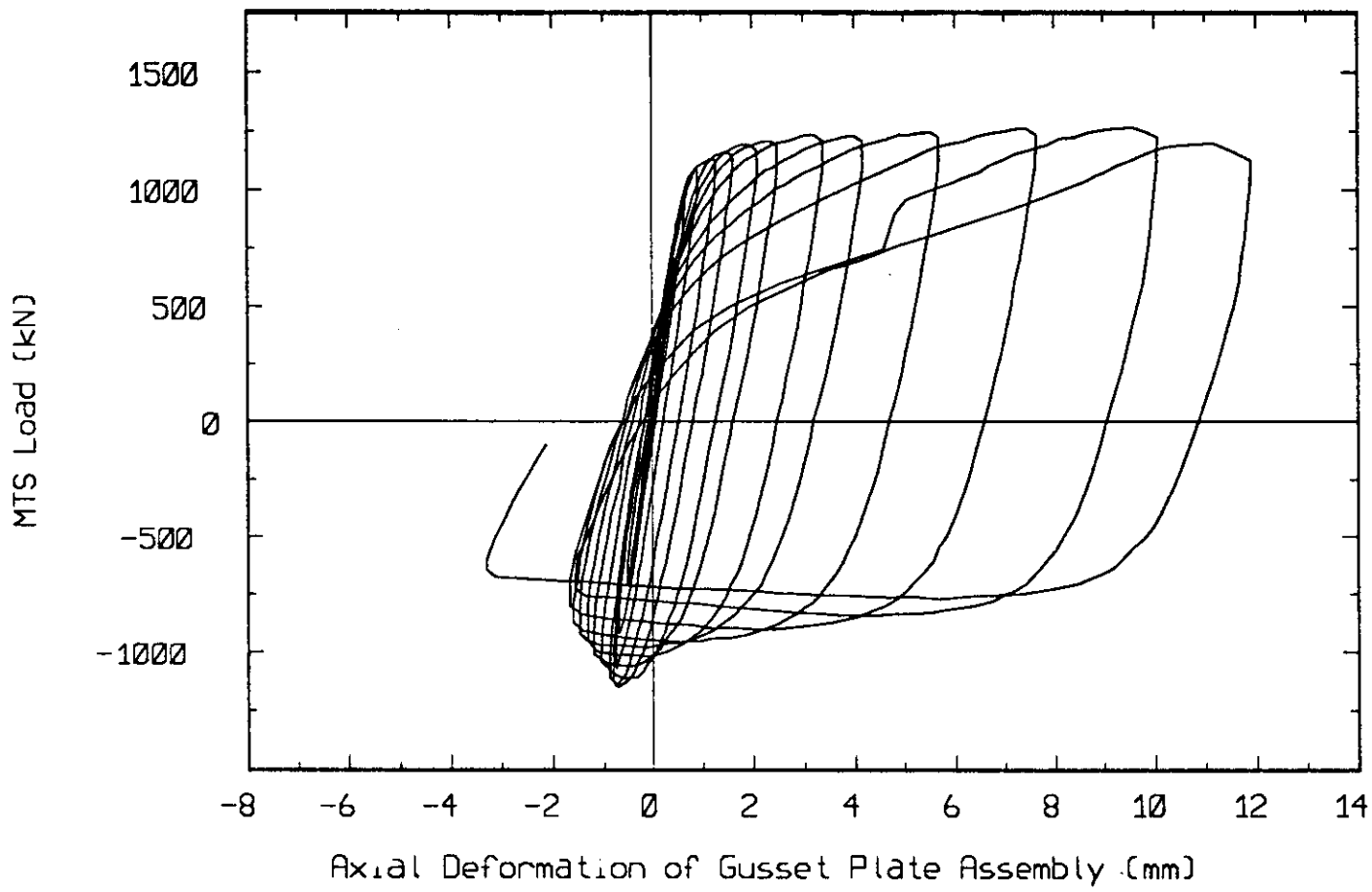

Figure 4.21. Load vs. Axial Displacement Response of the Gusset Plate Assembly - Specimen A-4

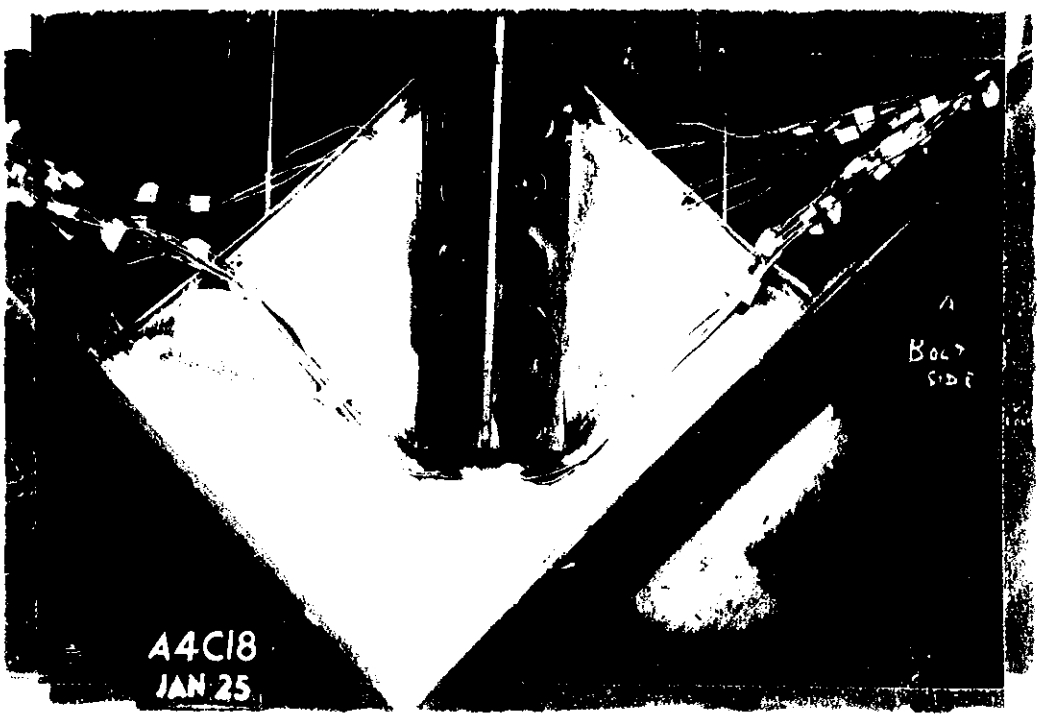

Figure 4.22. Final Specimen Yield Line Pattern - Specimen A-4

Figure 4.23. Deformed Plate Edge Stiffeners - Specimen A-4

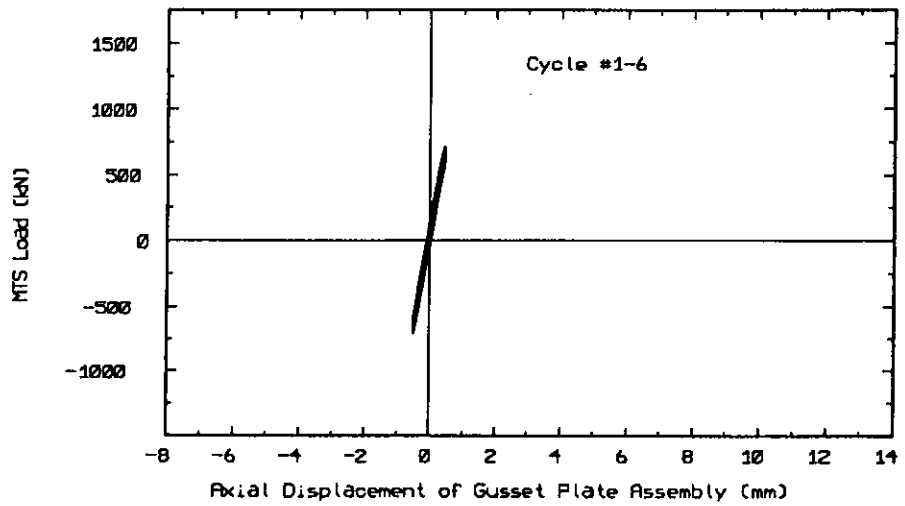

(a)

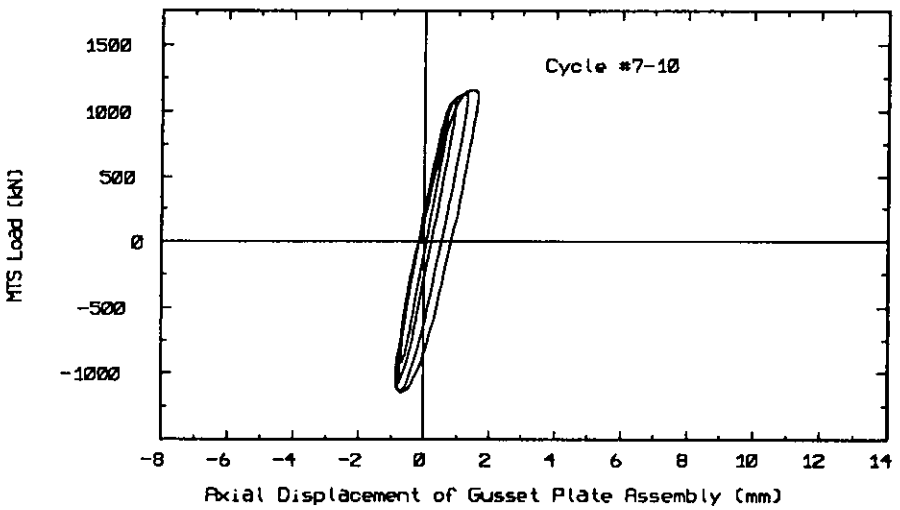

(b)

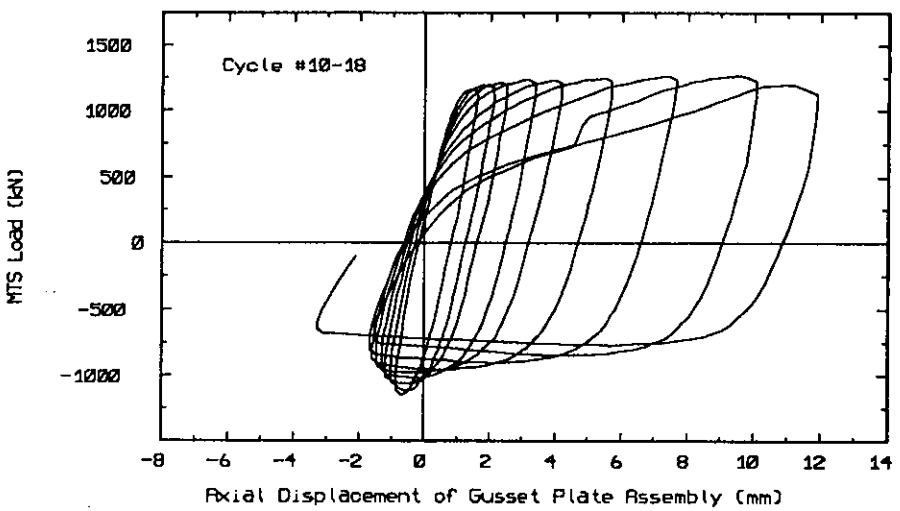

(c)

Figure 4.24. Load vs. Axial Displacement Response - Specimen A-4
(a) Cycle #1-6; (b) Cycle #7-10; (c) Cycle #10-18

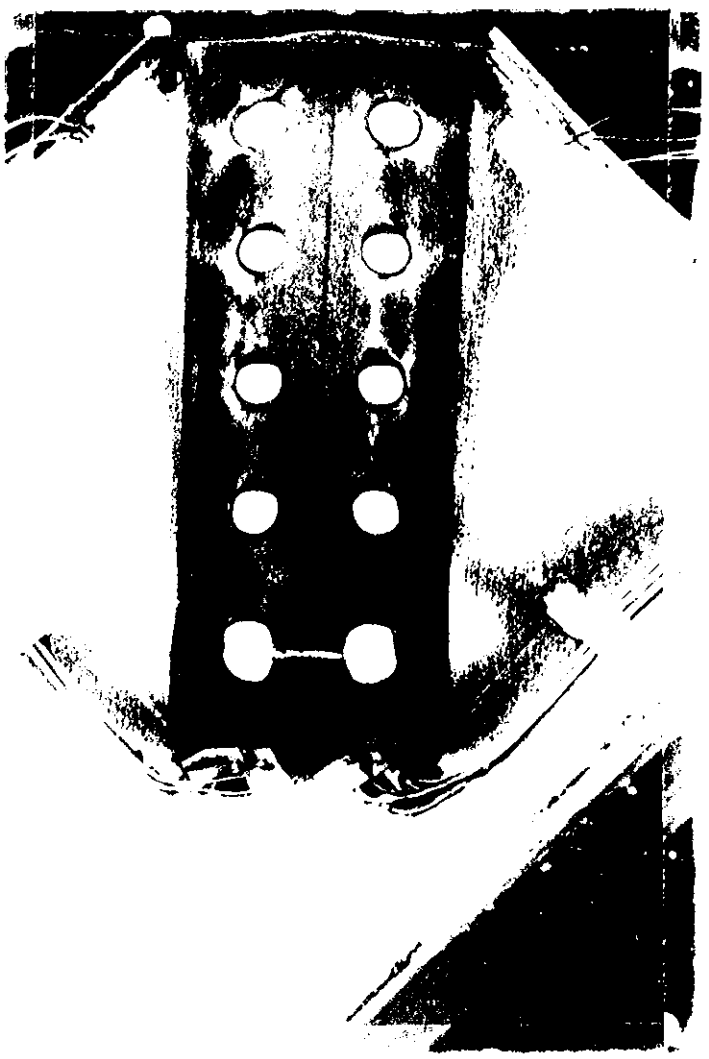

Figure 4.25. Plate Deformations in Bolted Connection - Specimen A-4

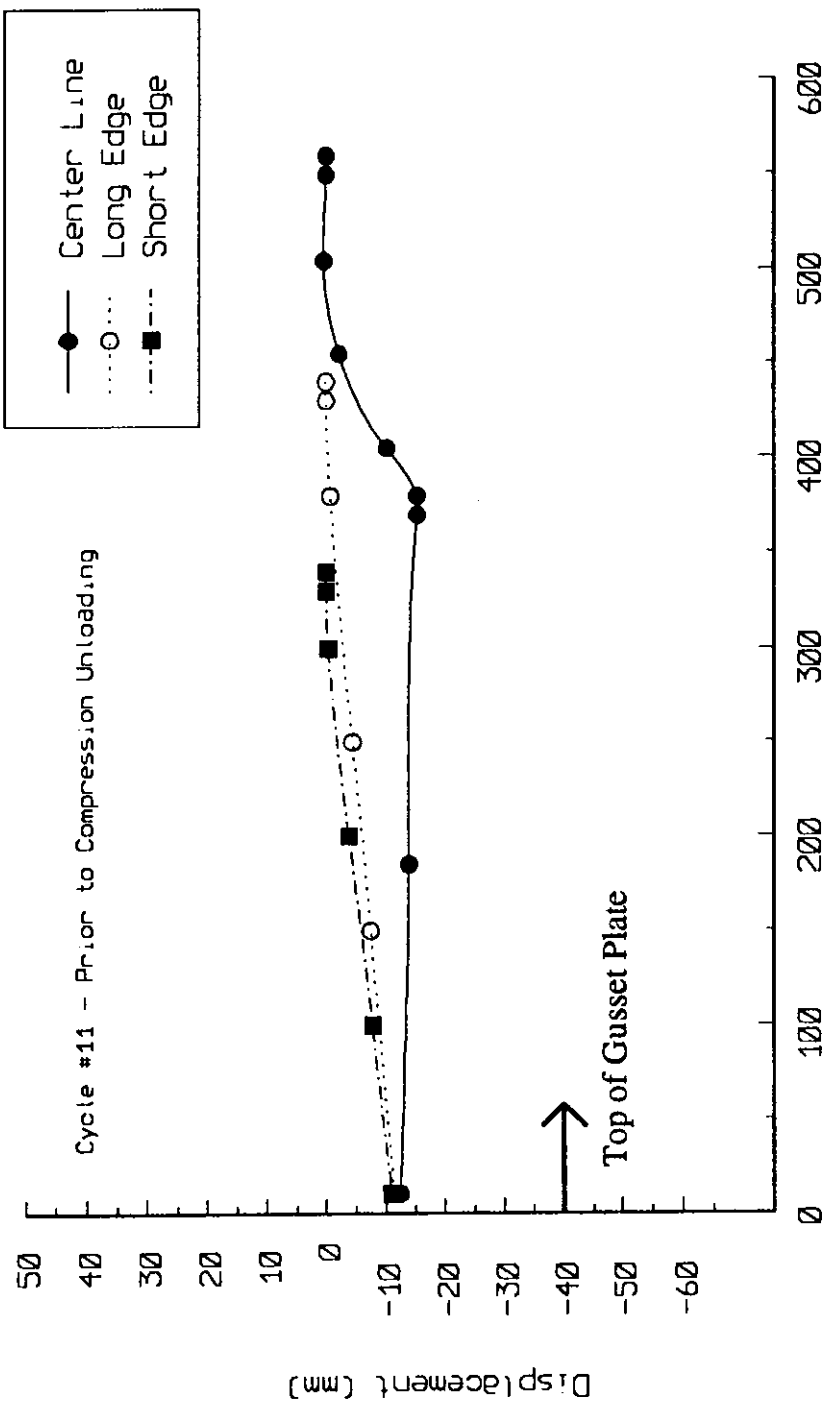

Figure 4.26. Out-of-plane Displacements - Specimen A-4

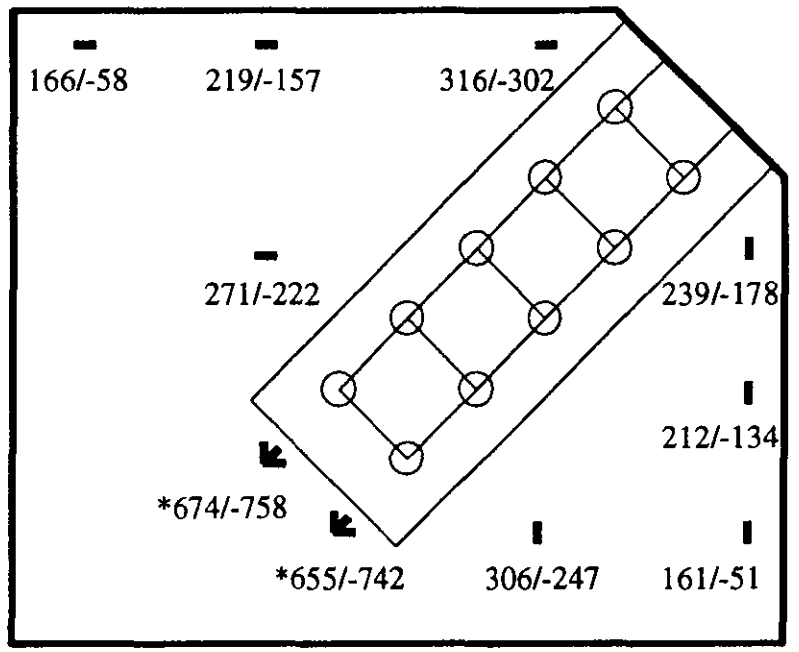

Load Level
+/- 353 kN

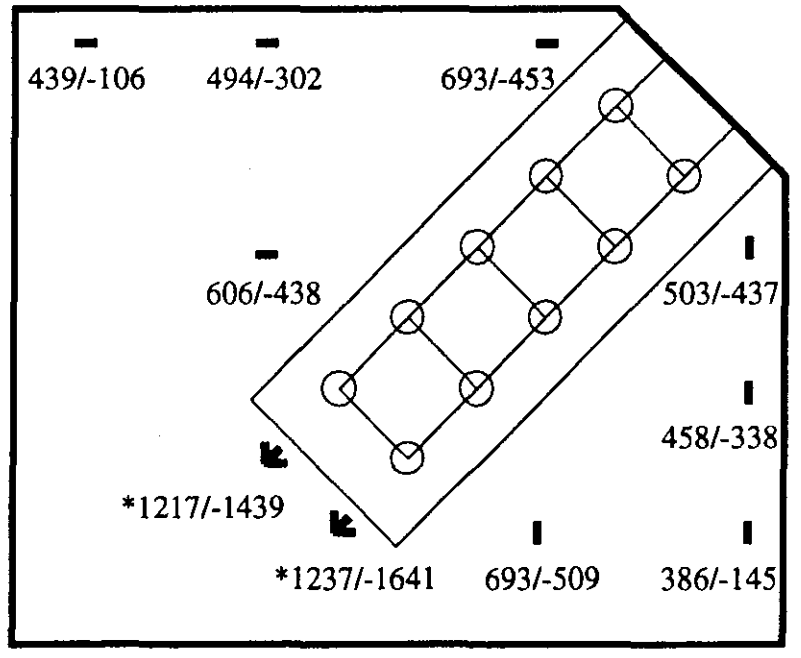

Load Level
+/- 707 kN

* Strains at rosette locations are principal strain values

Figure 4.27. Strain Distribution - Specimen A-4

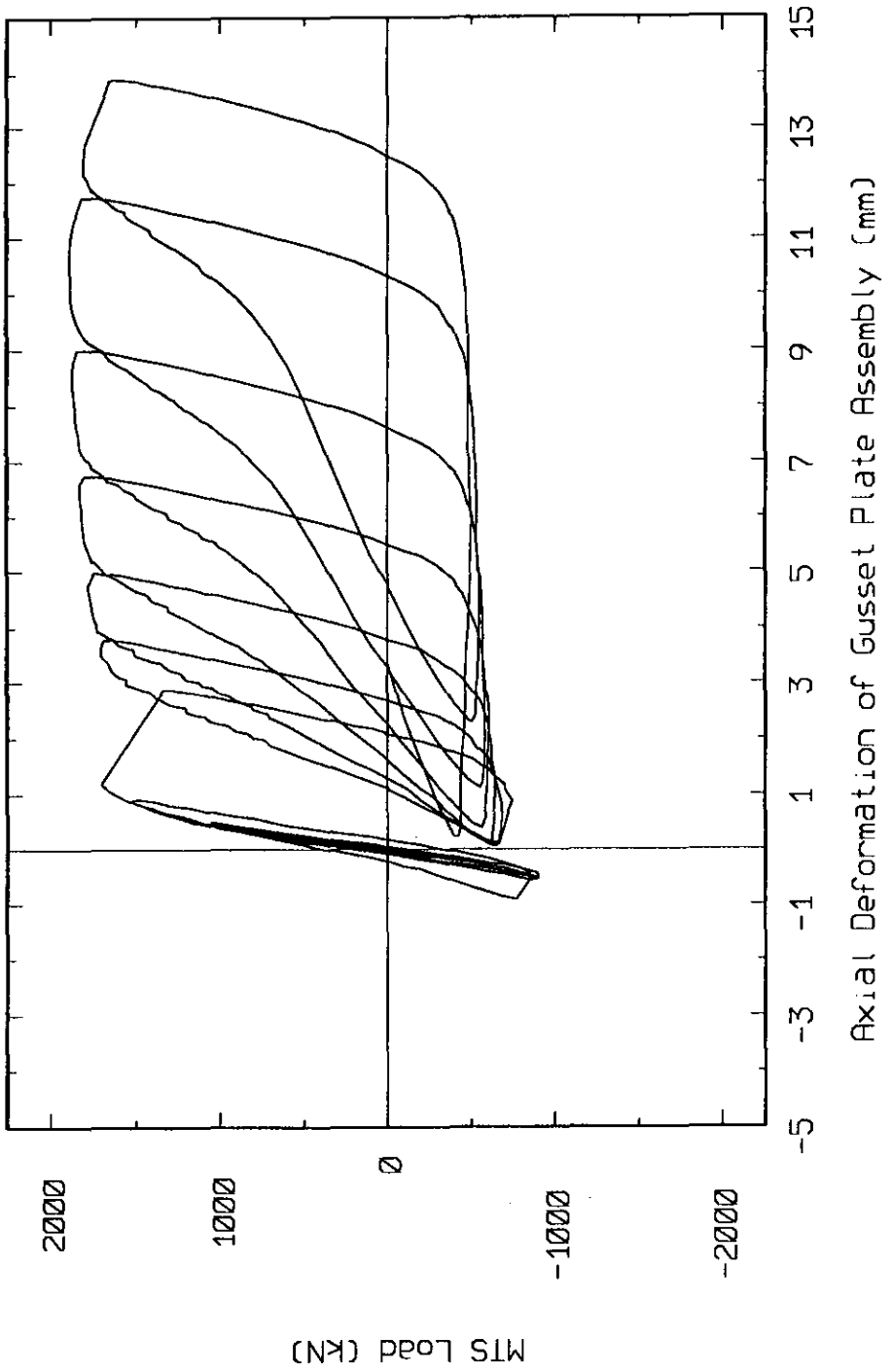

Figure 4.28. Load vs. Axial Displacement Response of the Gusset Plate Assembly- Specimen A-5

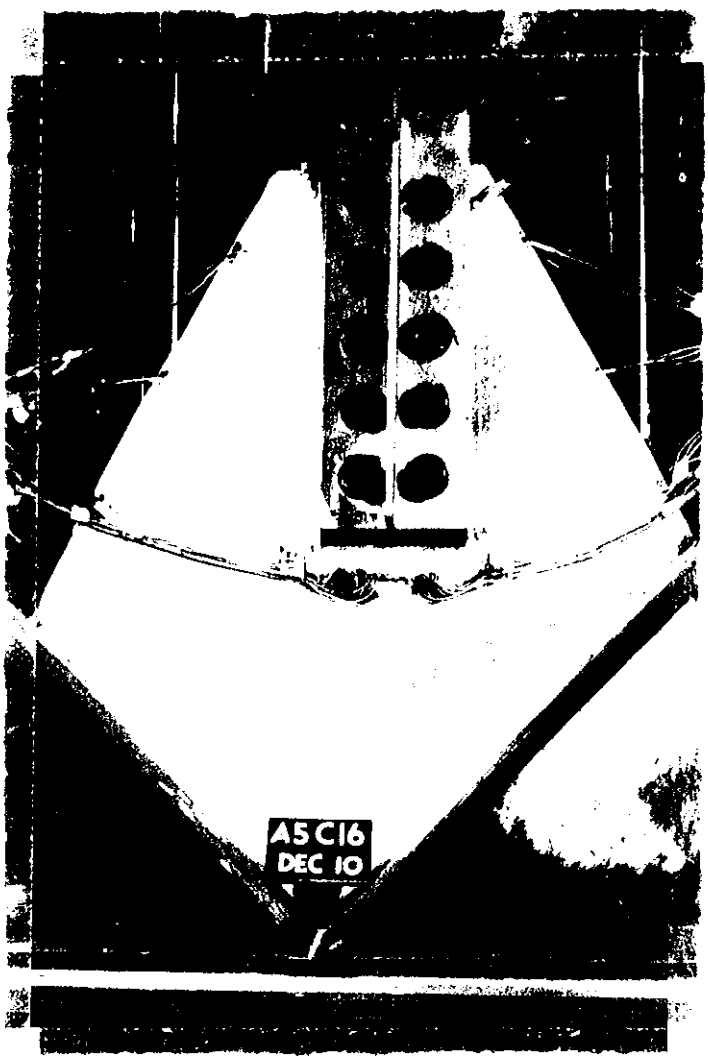

Figure 4.29. Final Specimen Yield Line Pattern - Specimen A-5

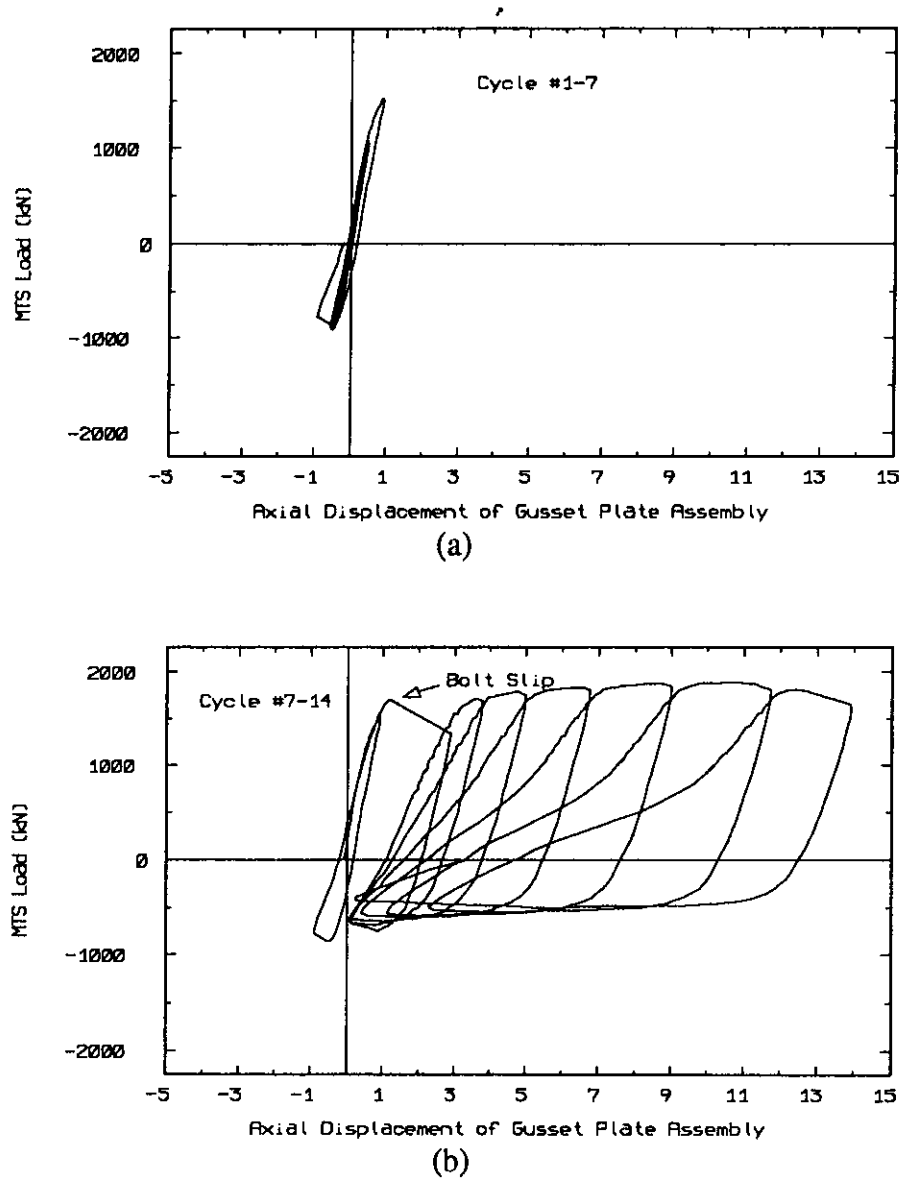

Figure 4.30. Load vs. Axial Displacement Response - Specimen A-5 (a) Cycle #1-7; (b) Cycle #7-14

Figure 4.31. Weld Fracture at Plate Boundary - Specimen A-5

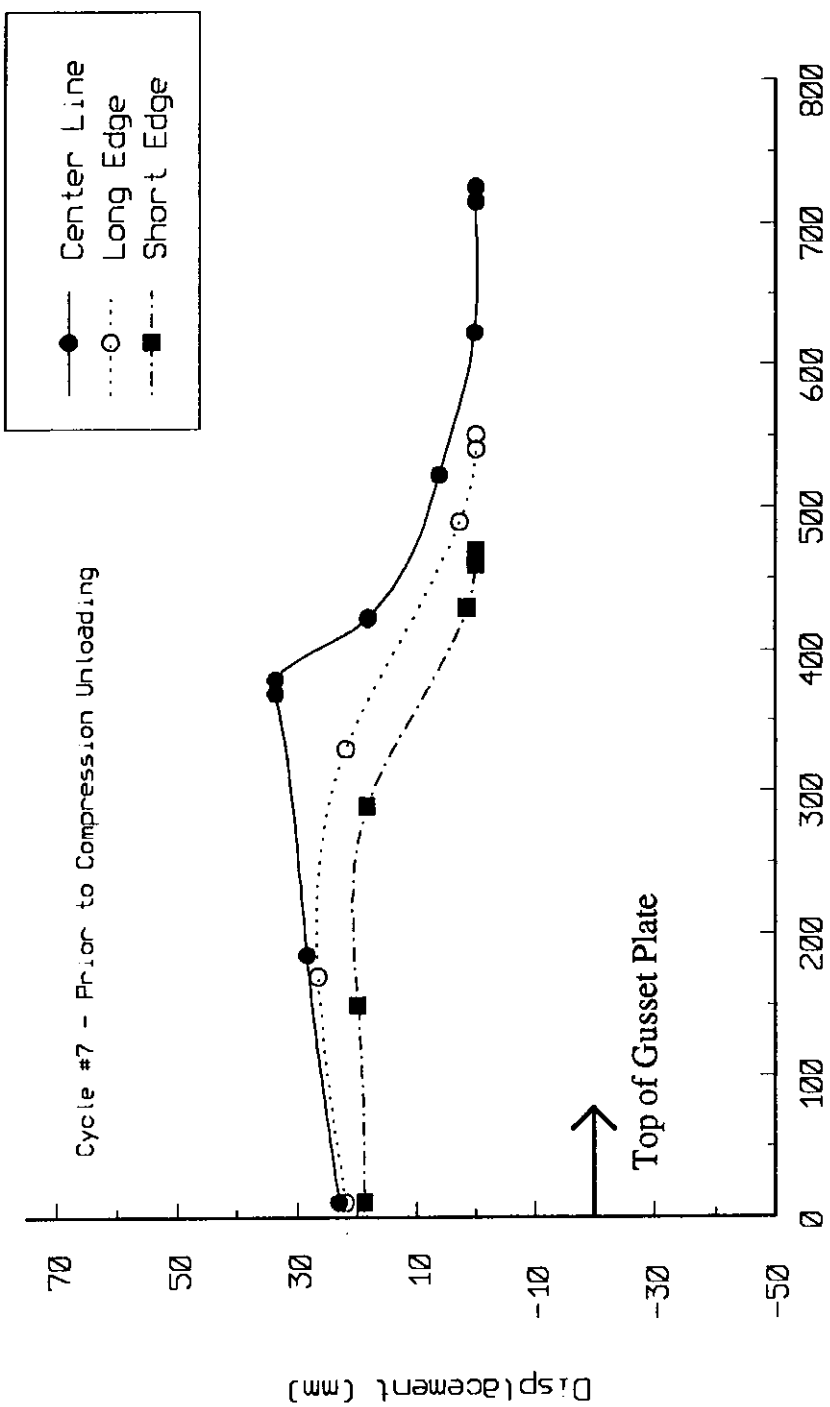

Figure 4.32. Out-of-plane Displacements - Specimen A-5

Figure 4.33. Buckled Plate Free Edges - Specimen A-5

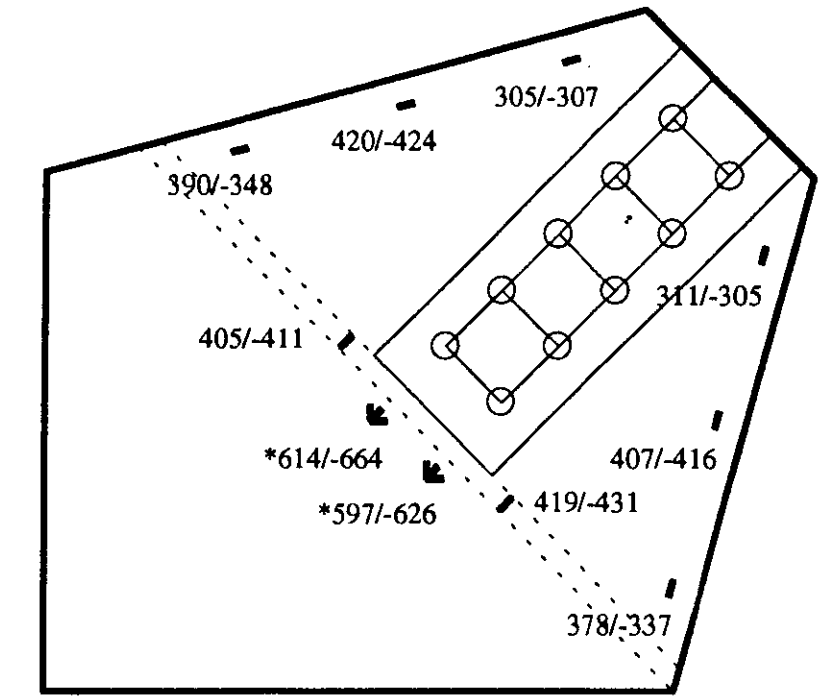

Load Level
+/- 530 kN

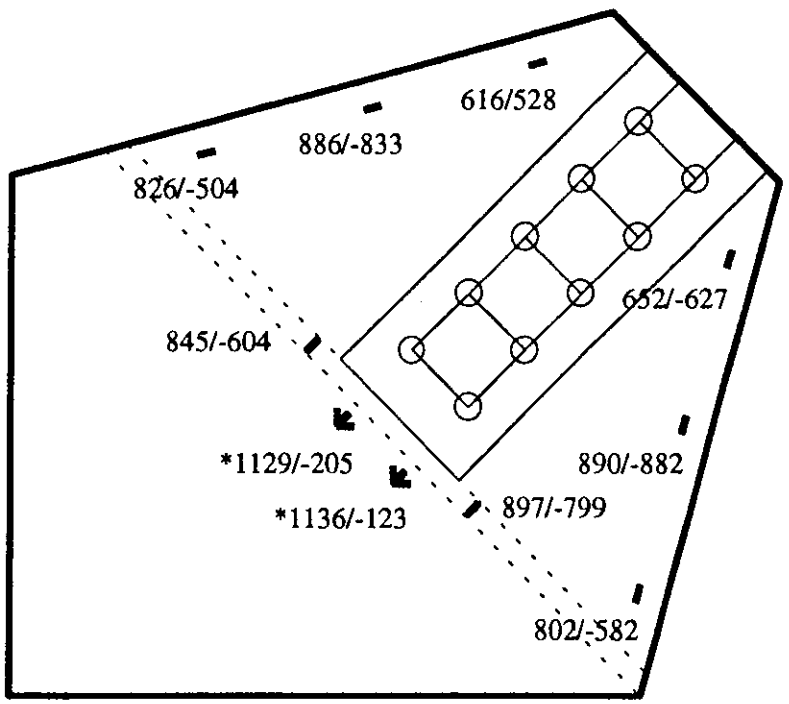

Load Level
+1060/-907 kN

* Strains at rosette locations are principal strain values

Figure 4.34. Strain Distribution - Specimen A-5

5. DISCUSSION OF TEST RESULTS

5.1 Introduction

This chapter discusses the test results in relation to the gusset plate parameters investigated in the test program. Section 5.2 considers the effect of the gusset plate thickness, plate edge stiffeners, gusset plate geometry, and connection bolt slip on the energy absorption characteristics of the test specimens. Section 5.3 examines current design theories for gusset plates under tensile and compressive loading and compares the present cyclic test results to monotonic tests performed at the University of Alberta on similar gusset plate specimens. Finally, the results of an elastic finite element analysis are presented in Section 5.4. An elastic finite element analysis was performed to provide an analytical reference to the plate strain distribution data discussed in Chapter 4.

5.2 Parameters Affecting Energy Absorption

The test parameters considered in the design of the test specimens were gusset plate thickness, stiffness of the free edge of the gusset plate, and the geometry of the gusset plate such that the free formation of a plastic hinge is facilitated. In addition, by providing slip-resistant fasteners in the gusset plate to splice member connection, the effect of bolt slip could be investigated. The effect of these test parameters on the energy absorption characteristics of the gusset plate specimens will be discussed in turn.

5.2.1 Gusset Plate Thickness

The effect of plate thickness on the energy absorption behavior of gusset plates can be considered by comparing the behavior of the 9.32 mm specimens and the 6.18 mm specimens. Specimen A-1, A-3, and A-5 are all 9.32 mm thick, while Specimen A-2 and A-4 are 6.18 mm thick.

The ultimate compressive load behavior of Specimen A-1 and A-2 appears to be roughly proportional to the thickness of the specimen. The specimens are both basic gusset plates of identical geometry with the exception of plate thickness. The ultimate compressive capacity of Specimen A-1 is 1.49 times greater than the compressive capacity of Specimen A-2. The ratio of the specimen thicknesses, 9.32 mm to 6.18 mm, is 1.51. Therefore, a strong linear relationship exists between the compressive capacity and the specimen thickness. The observed relationship between the ultimate compressive load behavior and the specimen thickness is only applicable to the basic gusset plates tested, Specimen A-1 and A-2. The addition of plate edge stiffeners to Specimen A-3 and A-4, and the modifications to the specimen geometry of Specimen A-5, greatly affect the specimen behavior under the compressive portion of the cyclic loading. The effect of the addition of plate edge stiffeners and the specimen geometry on the compressive capacity of the gusset plate specimens will be considered in detail in subsequent sections.

In tension, plate thickness appears to be the primary variable affecting the ultimate tensile capacity of the specimens. It is observed that all specimens with the same plate thickness and the same connection geometry reached approximately the same ultimate load level in tension. From the test loads recorded in Table 5.1, it is evident that the ultimate tensile capacity was not significantly affected by either the addition of plate edge stiffeners to Specimen A-3 and A-4, or the modified plate geometry of Specimen A-5. In addition, the relationship between plate thickness and specimen response is again roughly linear.

5.2.2 Plate Edge Stiffeners

The effect of the addition of plate edge stiffeners on the energy absorption capacity of gusset plates can be examined by comparing the behavior of the stiffened specimens, Specimen A-3 and A-4, with the unstiffened basic specimens, Specimen A-1 and A-2. Since it has been determined that the tensile behavior of the specimens is governed by the

connection geometry and the plate thickness, only the compressive behavior of the specimens will be considered presently.

Specimen A-3 is a stiffened specimen of 9.32 mm thickness. During the test, yielding initially progressed in a pattern similar to that of the unstiffened specimen, Specimen A-1. However, the presence of the plate edge stiffeners prevented the specimen from undergoing overall plate buckling at the same load level as Specimen A-1. Initially, the specimen buckled locally in a confined region beneath the splice member. Only when the plate edge stiffeners began to yield, was the ultimate compressive capacity reached. The ultimate compressive capacity of Specimen A-3 is almost 20% greater than that recorded for Specimen A-1. In addition, the presence of the plate edge stiffeners prevented the specimen load carrying capacity from dropping significantly once buckling occurred. The unstiffened specimen experienced a sharp drop in load carrying capacity once overall plate buckling occurred, while the response of Specimen A-3 showed a gradual decrease in load carrying capacity under cycles of increasing axial compressive deformation. Figure 5.1 shows the load versus displacement response of the gusset plate assembly for Specimen A-1 and A-3. Although slightly different test loading schemes were employed for each specimen, the enhanced energy absorption behavior of Specimen A-3 is evident.

Specimen A-4 is a stiffened specimen of 6.18 mm thickness. Although the ultimate compressive load reached was not significantly different than that obtained during the testing of the unstiffened specimen, Specimen A-2, the presence of the plate edge stiffeners affected the post-buckling behavior of the specimen. Initially, as the axial compressive deformation level increased, the plate edge stiffeners prevented the specimen from undergoing overall plate buckling. As the axial deformation level increased further, the plate edge stiffeners themselves ultimately buckled both in-plane and out-of-plane, allowing overall plate buckling to occur. Unlike the unstiffened Specimen A-2, the

buckling of the specimen was not immediately followed by a significant drop in specimen load carrying capacity. Instead, as the axial deformation level and the out-of-plane deformations increased, the load carrying capacity slowly deteriorated from the ultimate compressive load reached. The increased load carrying capacity under post-buckling deformations improves the hysteresis response of the stiffened specimen. This can be observed in Figure 5.2 where the load versus axial deformation response of Specimen A-2 and A-4 are plotted.

It is observed that the addition of plate edge stiffeners does not have a consistent effect on the ultimate compressive capacity obtained by a test specimen under cyclic loads. The 9.32 mm thick specimen, Specimen A-3, reached a significantly higher ultimate load than the unstiffened Specimen A-1. In comparison, the ultimate capacity of the 6.18 mm specimens, Specimen A-2 and A-4, was relatively unaffected by the presence of the plate edge stiffeners. However, the above observation can not automatically lead to the conclusion that the addition of plate edge stiffeners does not improve the compressive capacity of gusset plates. It must be noted that different thicknesses of stiffeners were used for each specimen. The slenderness ratio, b/t, for the unsupported edge of the stiffener of Specimen A-3 was 2.68, while the stiffeners of Specimen A-4 had a b/t of 4.05. In addition, the behavior of the stiffeners varied between the tests. In the testing of Specimen A-3, the stiffeners remained mostly elastic. In contrast, during the testing of Specimen A-4, the stiffeners yielded and eventually buckled in both the in-plane and out-of-plane directions. If a thicker stiffener was applied to Specimen A-4, an improved compressive capacity may have been observed.

It is interesting to note that the Canadian highway bridge design code, CAN/CSA-S6-88 - Design of Highway Bridges (CSA, 1988), makes a distinction based on the unsupported length of a gusset plate free edge. Clause 7.26.4.4 specifies that a gusset plate under

compression must be stiffened if the length of an unsupported edge is greater than $945/\sqrt{F_y}$ times its thickness. Both unsupported edges of the 6.18 mm specimens and the long edge of 9.32 mm specimens would fail the above criterion. The current test results on gusset plates of concentric braced frames indicate that stiffeners are beneficial regardless of the unsupported length of the plate free edges. The addition of plate edge stiffeners significantly improved the energy absorption behavior of the gusset plates tested.

5.2.3 Gusset Plate Geometry

The effect of the gusset plate geometry on the energy absorption behavior of gusset plates can be considered by examining the behavior of Specimen A-5. All the test specimens were rectangular in shape with the exception of Specimen A-5. As outlined in Section 3.3, the geometry of Specimen A-5 was modified to accommodate the free formation of a plastic hinge (Figure 3.2).

In order to accommodate the free formation of a plastic hinge in the specimen geometry, the splice member had to be placed further away from the base of the gusset plate. The change in specimen geometry significantly affected the compressive response of the specimen. Although the specimen yield pattern was similar to the other specimens of the same plate thickness, yielding and plate buckling occurred at significantly lower load and axial deformation levels. The geometry required to accommodate the plastic hinge region greatly lowered the stiffness and buckling load of the specimen. As seen in Table 5.2, the ultimate compressive capacity of Specimen A-5 was approximately one-half of the other specimens of the same plate thickness. In the post-buckling range, the specimen capacity continued to deteriorate under cycles of increasing axial plate deformation. In addition, the inherent flexibility of the specimen caused the weld at the gusset plate to frame boundary connection to fracture as the axial deformation level, and the resulting out-of-plane deformations, increased.

The test results from Specimen A-5 clearly indicate that there is no rationale for providing for the free formation of a plastic hinge in the geometry of the type of gusset plate investigated in this study. Astaneh-Asl's investigation (Astaneh-Asl, et al., 1985) considered the cyclic out-of-plane buckling of double angle bracing where the gusset plates were connected to the frame along one plate edge only (Figure 2.5). He concluded that restraints on the free formation and the rotation of plastic hinges leads to premature fracture in the gusset plate. It is apparent that this conclusion does not apply when the gusset plate is connected to the framing members along two plate edges, as was the case in the current investigation.

The conclusions from the experimental investigation by Astaneh, et al. (1986) are adopted by the AISC seismic design code (AISC, 1992) and are used as a reference for Clause 27.4.4.4 in the seismic design provisions of the current Canadian limit states design code, CAN/CSA-S16.1-M89 (CSA, 1989). Clause 27.4.4.4 states:

> Brace connections including gusset plates shall be detailed to avoid brittle failures due to rotation of the brace when it buckles. This ductile rotational behavior shall be allowed for, either in the plane of the frame or out of it, depending on the slenderness ratio.

Based on the observed test results of Specimen A-5, it is believed that the ductility requirements of Clause 27.4.4.4 may need to be clarified. The current test program reveals that no special provisions need to be made to avoid the brittle failure of gusset plates connected to the beam and column framing members along two plate edges. The free formation of a plastic hinge was not provided for in the geometry of Specimen A-1 to A-4 and no premature fracture was observed. It appears that the rotational restraint provided by the specimen boundary causes the plastic strains to be distributed more evenly over a wide region of the gusset plate. The testing of Specimen A-5 indicates that if a

gusset plate is designed to be overly ductile in the out-of-plane direction, a deteriorated behavior is observed.

5.2.4 Connection Bolt Slip

All 9.32 mm specimens, Specimen A-1, A-3, and A-5, used 7/8" diameter ASTM A325 high strength bolts designed for bearing in the splice member to gusset plate connection. Due to loads anticipated in the connection, all 9.32 mm specimens were expected to experience bolt slip at some point during the cyclic loading history. The mechanism of connection bolt slip will first be considered, followed by the possible influence of bolt slip on the energy absorption behavior of a braced frame.

The process of initial bolt slip in a connection likely proceeds as follows. Initially, the load is transferred by friction forces between the contacting surfaces at the ends of connection. As the load is increased, the maximum frictional resistance is eventually exceeded at the ends, and small displacements of contact points on the faying surfaces take place. As the load is increased further, the slip zone proceeds inward from the ends towards the center of the connection. When the applied load exceeds the frictional resistance over the entire faying surface of the connection, large relative displacements occur, major slip. When major slip occurs, only the end bolts may come into bearing against the gusset plate and the splice members. As the applied load is increased, the end bolts and holes deform further until the succeeding bolts come into bearing. This process continues until all of the bolts are brought into bearing. (Kulak, et al., 1987)

In Specimen A-1 and A-3, connection slip occurred twice during every cycle subsequent to the initial bolt slip. As seen in Figures 4.2 and 4.15, the connection slip that occurs under repeated loading cycles occurs at a lower load level than the initial slip experienced in the connection. The initial bolt slip that occurs is due to the overcoming of static

friction. At this point, the original contact between the members of the connection has been altered and subsequent slip under cycles of repeated loading occurs as the level of dynamic friction is exceeded. It is this repeated connection slip that is of interest when assessing the importance of bolt slip in the energy absorption behavior of the gusset plate. Since the area under the load versus axial displacement curve is a measure of the energy absorbed by the test specimen, it is apparent that slip displacements in the splice member connection can contribute significantly to the energy absorption capacity of the gusset plate assembly.

To consider the effect of connection slip on the energy absorption capacity in the design of a braced frame, it must be ensured that connection slip will occur during every loading cycle. This may not always be the case, as was observed in the testing of Specimen A-5. The initial connection slip occurred during the tension portion of a loading cycle. The compressive capacity of the specimen, however, was not sufficient to cause the connection to slip from tension bearing into compressive bearing. As such, the connection remained in tension bearing throughout the remainder of the loading history and no further bolt slip was experienced.

The present investigation centered around the behavior of the gusset plate itself and connection slip was only investigated as a secondary consideration. The reliance on repeated connection slip throughout the cyclic loading puts into questions the suitability of considering the energy absorbed by the connection. As such, it is believed that further study focusing on connection slip would be required before the energy absorbed by the connection slip could be relied on to improve the design of a braced frame.

5.3 Comparison of Test Results

This section will examine some current design theories for both the tensile and

compressive strength of gusset plates under monotonic loading. The present cyclic test results will be compared to the current design theories to determine their applicability in predicting the capacity of gusset plates under cyclic loads. In addition, the cyclic test results will be compared to a monotonic test series performed at the University of Alberta on similar gusset plate specimens.

5.3.1 Monotonic Tension

Table 5.1 lists the ultimate tensile capacity of each test specimen. The ultimate tensile load is defined as the maximum tensile load level reached by a specimen throughout its cyclic loading history. Table 5.1 also lists a Whitmore yield load and a tension tear-out load for each specimen. The Whitmore yield load is calculated by applying the Whitmore critical stress theory (Whitmore, 1952) at the actual material yield level (see Section 2.2). The tension tear-out load is based on a block shear tear-out model proposed by Hardash and Bjorhovde (1985). It was determined that gusset plates in tension are governed by a block shear failure consisting of a tensile failure on the net cross section of the plate between the rows of bolts, and shear yielding on the gross section along the line of the applied force from the last row of bolts to the top edge of the plate (Hardash and Bjorhovde, 1985). A schematic drawing of the proposed tear-out model is shown in Figure 2.4. Additionally, Table 5.1 lists the nominal tensile capacity of the gusset plate specimens as computed according to the seismic design provisions of CAN/CSA-S16.1-M89 (CSA, 1989). Clause 27.4.4.3 considers the block shear failure of the gusset plate to splice member bolted connection based on the ultimate capacity of the net section. In calculating the present theoretical specimen capacities dynamic material properties were used since the gusset plate specimen were tested under continuous loading conditions.

By examining Table 5.1 it is revealed that the Whitmore load underestimates the ultimate tensile capacity of the test specimens. Since the Whitmore load is a material yield

approach, it is expected that it will provide a conservative estimate of the ultimate specimen capacity. The seismic design provisions of CAN/CSA-S16.1-M89 also provide a conservative estimate of the ultimate tensile capacity of the test specimens. In comparison, the tension tear-out load proposed by Hardash and Bjorhovde provides a very accurate estimate of the ultimate tensile capacity. For the specimens tested, the ratio of ultimate test capacity to predicted tear-out capacity ranges from 0.92 to 1.05, with a mean value of 0.97 and a coefficient of variation of 0.043.

Hardash and Bjorhovde's block shear analysis was based on the experimental test results of monotonically loaded specimens. Still, it is shown that the test results from the current cyclic test program are in relatively strong agreement with the predicted capacities. Therefore, it can be concluded that the ultimate tensile behavior of the test specimens was not significantly adversely affected by the cyclic loading history and the extreme compressive deformations that resulted. In addition, the block shear theory is based entirely on a tear-out failure of the gusset plate to splice member connection. There is no reference to the overall geometry of the gusset plate or the stiffness of the plate free edges. Therefore, the correlation between the predicted tension tear-out load and the actual test capacities reinforces the previous conclusion (Section 5.2.1) that the tensile behavior of a gusset plate under cyclic loading is governed by the connection geometry and the plate thickness.

5.3.2 Monotonic Compression

The compressive capacity of the cyclic test specimens will be compared with two current design approaches. Table 5.2 list the ultimate compressive capacity of each test specimen. The ultimate compressive capacity is defined as the maximum compressive load level reached by a specimen throughout its cyclic loading history. The test capacities are compared to a Whitmore yield load and a Thornton load for each specimen. The

Whitmore yield load for compression is defined as for tension in Section 5.3.1. The Thornton load (Thornton, 1984) attempts to estimate the buckling load of the gusset plate by considering an imaginary fixed-fixed column strip of unit width below the Whitmore effective width in the gusset plate. The process for determining the buckling capacity of a gusset plate by the Thornton equivalent column method is outlined in Section 2.3.

The ratios of the actual compressive test capacity to the Whitmore load and to the Thornton load are recorded in Table 5.2. It is observed that the Whitmore load is ineffective in estimating the ultimate capacity of the test specimens. The Whitmore load does not account for the effect of the stiffness of the plate edges or the overall gusset plate geometry in its formulation. As a material yield approach, the Whitmore load attempts to estimate the load at which material yielding will occur at the critical section. From the Whitmore load data, it is seen that Specimen A-5 reached its ultimate capacity well before material yielding occurred at the critical section. All other specimens reached their ultimate compressive capacity once material yielding at the critical sections had occurred. The ultimate capacity of all test specimens was accompanied by gusset plate buckling.

In all cases the Thornton load produced conservative estimates of the ultimate compressive capacity of the test specimens. By accounting for the overall geometry of the gusset plate, the Thornton load provides a more rational estimate of the ultimate compressive capacity. The calculation of the Thornton load does not, however, account for the presence of the plate edge stiffeners. The average test specimen capacity to Thornton load predicted capacity is 1.24.

Table 5.2 also presents the results from a test series performed at the University of Alberta on similar gusset plate specimens tested under monotonic loading conditions (Cheng and Yam, 1991). 500 mm x 400 mm rectangular specimens with four rows of bolts were

tested under monotonic compression. All specimens were unstiffened and ranged in thickness from 6.51 mm to 13.3 mm. The average test to predicted ratios based on the Whitmore load theory and the Thornton load theory for the specimens tested are presented in Table 5.2. By comparing the monotonic test to predicted ratios with the current test results, it is observed that cyclic loading significantly reduces the ultimate compressive strength of steel gusset plates. Some possible explanations to this observed effect will be discussed in the next section. Due to the modified gusset plate geometry of Specimen A-5, no comparison with the monotonic test results was made.

It is important to note that both the Whitmore yield load and the Thornton equivalent column load theories are provided for monotonic loading conditions. Under monotonic loading, the Thornton load is shown to greatly underestimate the inelastic buckling capacity of gusset plates (Cheng and Yam, 1991). Therefore, the relative effectiveness of the Thornton load in estimating the ultimate compressive capacity under cyclic loads may be a result of the deteriorated specimen behavior observed under the imposed cyclic loading.

5.3.3 Cyclic Load Behavior

In Section 5.3.2 it was observed that cyclic loading significantly reduces the ultimate compressive strength of steel gusset plates. It is believed that the cyclic loading history, and the resulting residual strains, are responsible for altering the mechanical properties of the test specimens. The material phenomena that may be responsible for the observed specimen response include: the effect of stress reversal, Bauschinger Effect; the effect of prior cycles on reversed loading curves, cyclic hardening or softening; and the effect of aging (Singh, et al., 1965).

The Bauschinger Effect is described as a phenomenon that results in an increase in the

proportional limit and yield strength by reloading a plastically deformed specimen in the same direction, tension after prestretching, or in a decrease by reloading it in the opposite direction, compression after prestretching (Chajes, et al., 1963). It is the latter case that is of interest to the current testing program. All test specimens were initially loaded in tension during each loading cycle. In all cases, with the exception of the testing of Specimen A-5, significant plastic straining had occurred under tensile loading prior to reaching the ultimate compressive capacity of the specimen. As such, it would be expected that the compressive yield strength would be reduced under the imposed test loading. A reduction in the compressive yield strength would lead to an increase in compressive plate deformations at reduced load levels, resulting in a reduced plate buckling capacity.

Due to plastic deformation, modifications to the microstructure occur during cyclic straining. Depending on the initial state and test conditions, the deformation resistance of the material may increase, decrease, or remain essentially unchanged: cyclic hardening, cyclic softening, or cyclic stability (Starke and Lutjering, 1978). The loading procedure unique to Specimen A-1 allows an assessment of this phenomenon. The loading scheme for Specimen A-1 involved a set of three identical cycles at each axial deformation level in the inelastic range. Figure 5.3 shows the hysteresis loops for Cycles #8-10. All three cycles involved testing the specimen to roughly the same axial deformation level. From the figure, it is observed that the maximum tensile loads reached decreased with each repeated cycle of loading. Therefore, the material used in this investigation undergoes cyclic softening under cyclic loading conditions. The magnitude of this cyclic softening has not been quantified, but it is evident that this behavior contributed to the observed specimen behavior under cyclic loading.

The effect of aging on the behavior of a material subject to cyclic loading appears to vary

with the type of steel and the nature of the plastic straining history. An investigation into the behavior of reinforcing steel under reversed loading (Singh, et al., 1965) revealed that the reversed strain curves showed a recovery of stiffness and strength with time, as the cyclic material response tended towards the virgin response curve. Conversely, research into the effects of cold-straining on structural sheet steels (Chajes, et al., 1963) showed an increase in the yield strength and proportional limit, above the virgin curve, as a result of aging. The effect of aging on the cyclic behavior in the current investigation is unknown. However, it is believed that the magnitude of prior plastic straining and the duration of time between successive loading cycles might not have been sufficient to produce any significant effects due to aging.

The above discussion has only attempted to provide an insight into the possible factors that may be responsible for the observed gusset plate compressive behavior. A detailed investigation would be required to isolate the relative effects under the type of cyclic loading employed in the current test program. Such an investigation is beyond the scope of this test program.

5.4 Finite Element Analysis

An elastic finite element analysis was performed to provide an analytical reference to the recorded test strain data. The finite element program ANSYS was used to determine the in-plane principal stress distribution of a typical gusset plate specimen within the elastic loading range. Specimen A-1 and A-2, both unstiffened specimens, were selected to provide a comparison to the observed test results.

In the analysis, the gusset plate and splice member were modeled by a series of three-dimensional shell elements. The finite element mesh used to model the gusset plate is shown in Figure 5.4. The gusset plate was assumed to be fixed along the welded

boundary to the beam and column members. The top of the gusset plate, at the conjunction of the gusset plate and splice members, is assumed to be fixed in rotation but free to move in both the in-plane and out-of-plane directions. The test load was applied as a constant pressure over the cross-section of the splice member at the top of the specimen. The bolted connection between the splice members and the gusset plate was modeled as a series of rigid-link connections at the bolt locations. This configuration was believed to best represent the design prototype and the actual conditions under testing.

The analytical stress distribution for Specimen A-1 at the 530 kN load level, 50% of the nominal Whitmore yield level, is shown in Figure 5.5. The stress analysis for Specimen A-2 was likewise performed at 50% of the nominal Whitmore yield level, 353 kN. Due to the similarity of the results, only the analytical stress distribution for Specimen A-2 will be considered in detail.

The analytical principal stress distribution for Specimen A-2 is shown in Figure 5.6. The observed stress distribution can be converted to strains by applying Hook's Law. It is observed that the elastic strains recorded during the cyclic testing of the specimen (Figure 4.14) are in good agreement with the analytical results. The recorded principal strains at the rosette locations near the base of the splice member are in particularly strong agreement with the analytical results, while the overall finite element stress distribution pattern corresponds with that observed during testing. The actual principal stress at the rosette locations during testing at the +353 kN load level were computed to be 162.1 MPa and 155.6 MPa, with the higher stress recorded at the rosette location nearest to the plate boundary. To allow a comparison with the analytical results, the location of the rosette gages are shown on Figure 5.6. The comparison of data must be viewed in light of the ideal conditions modeled by the finite element analysis. The model assumes perfect boundary conditions and no initial imperfection. Since an elastic finite element analysis

was performed, the gusset plate stress distribution presented are applicable to either tension or compression at the 353 kN load level.

The finite element analysis also produced data on the fastener force distribution in the splice member to gusset plate connection. Figure 5.7 shows the relative magnitude of the force components in the splice member connection for Specimen A-1 at the 530 kN load level. The distribution of fastener forces can be compared with the bolt hole deformations observed during the testing of Specimen A-1. Careful observation of Figure 4.3 reveals that the pattern of bolt hole deformations corresponds with the fastener force distribution obtained from the finite element analysis.

Table 5.1. Comparison of Test Results - Tension

Specimen	Plate Size (mm)	Ultimate Tensile Load (kN)	Whitmore Load (kN)	Tension Tear-Out (kN)	S16.1-M89 Block Shear (kN)
A-1	550x450x9.32	1794	1718	1960	1499
A-2	550x450x6.18	1340	1122	1282	981
A-3	550x450x9.32	1884	1718	1960	1499
A-4	550x450x6.18	1265	1122	1282	981
A-5	550x450x9.32	1887	1718	1960	1499

Table 5.2. Comparison of Test Results - Compression

Specimen	Plate Size (mm)	Ultimate Compressive Load P_u (kN)	Whitmore Load P_w (kN)	Thornton Load P_t (kN) k = 0.65	$\frac{P_u}{P_w}$	$\frac{P_u}{P_t}$
A-1	550x450x9.32	1682	1718	1500	0.98	1.12
A-2	550x450x6.18	1128	1122	841	1.01	1.34
A-3	550x450x9.32	2004	1718	1500	1.17	1.34
A-4	550x450x6.18	1149	1122	841	1.02	1.37
A-5	550x450x9.32	907	1718	898	0.53	1.01
				Average	0.94	1.23

Average Ratios from Monotonic Testing: (Cheng and Yam, 1991)

$$\frac{P_u}{P_w} = 1.47 \qquad \frac{P_u}{P_t} = 1.68$$

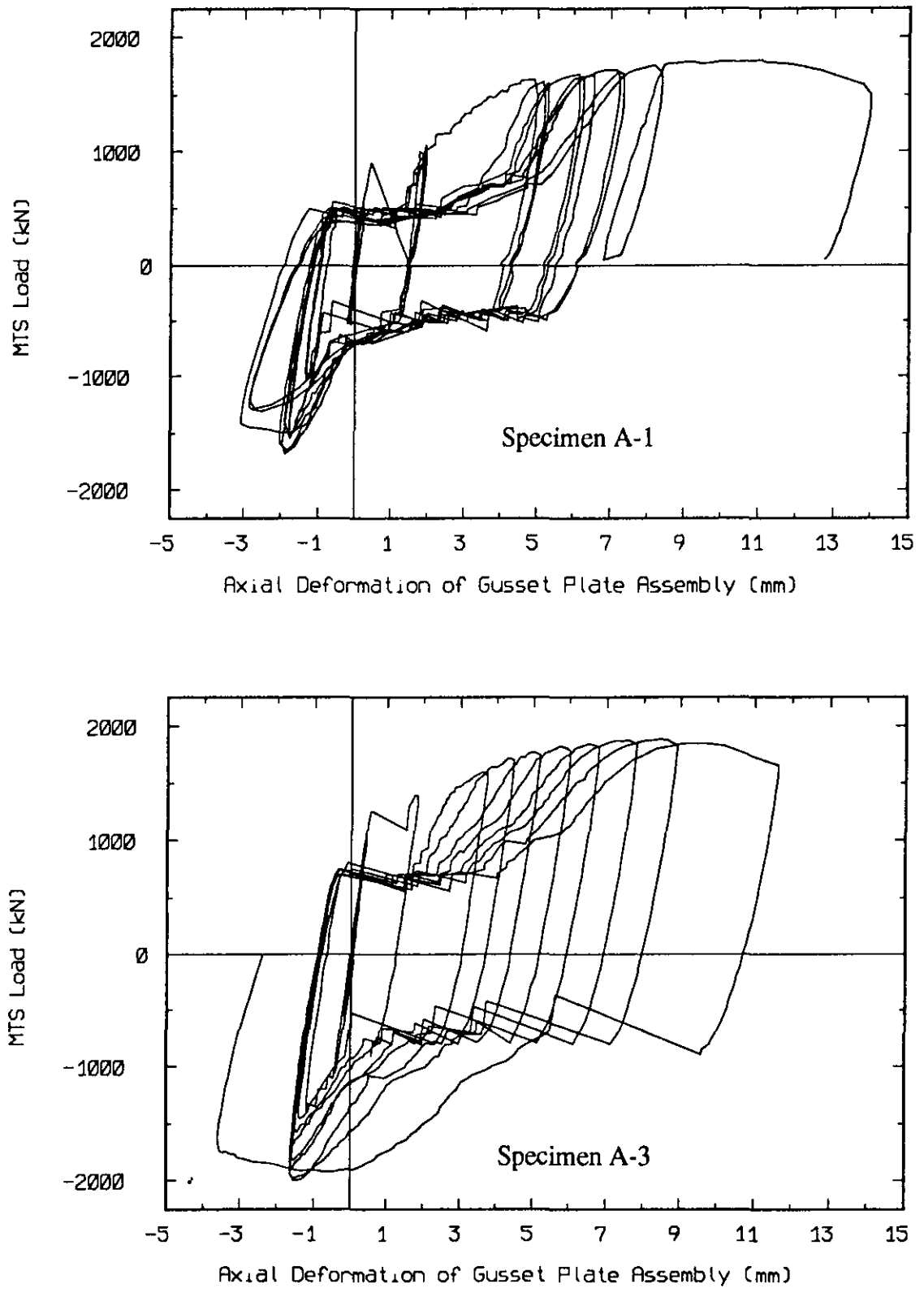

Figure 5.1. Influence of Plate Edge Stiffeners - 9.32 mm Specimens

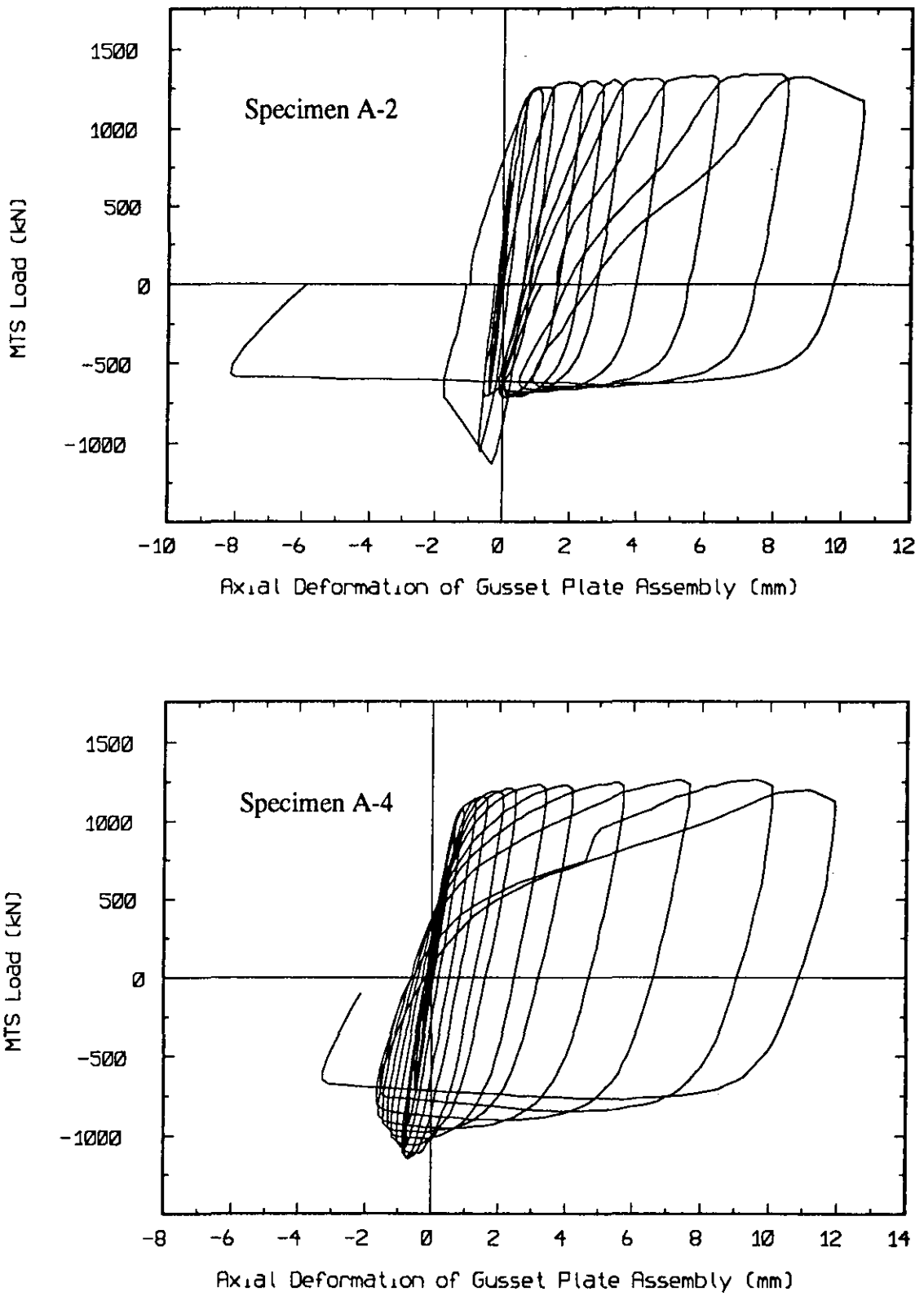

Figure 5.2. Influence of Plate Edge Stiffeners - 6.18 mm Specimens

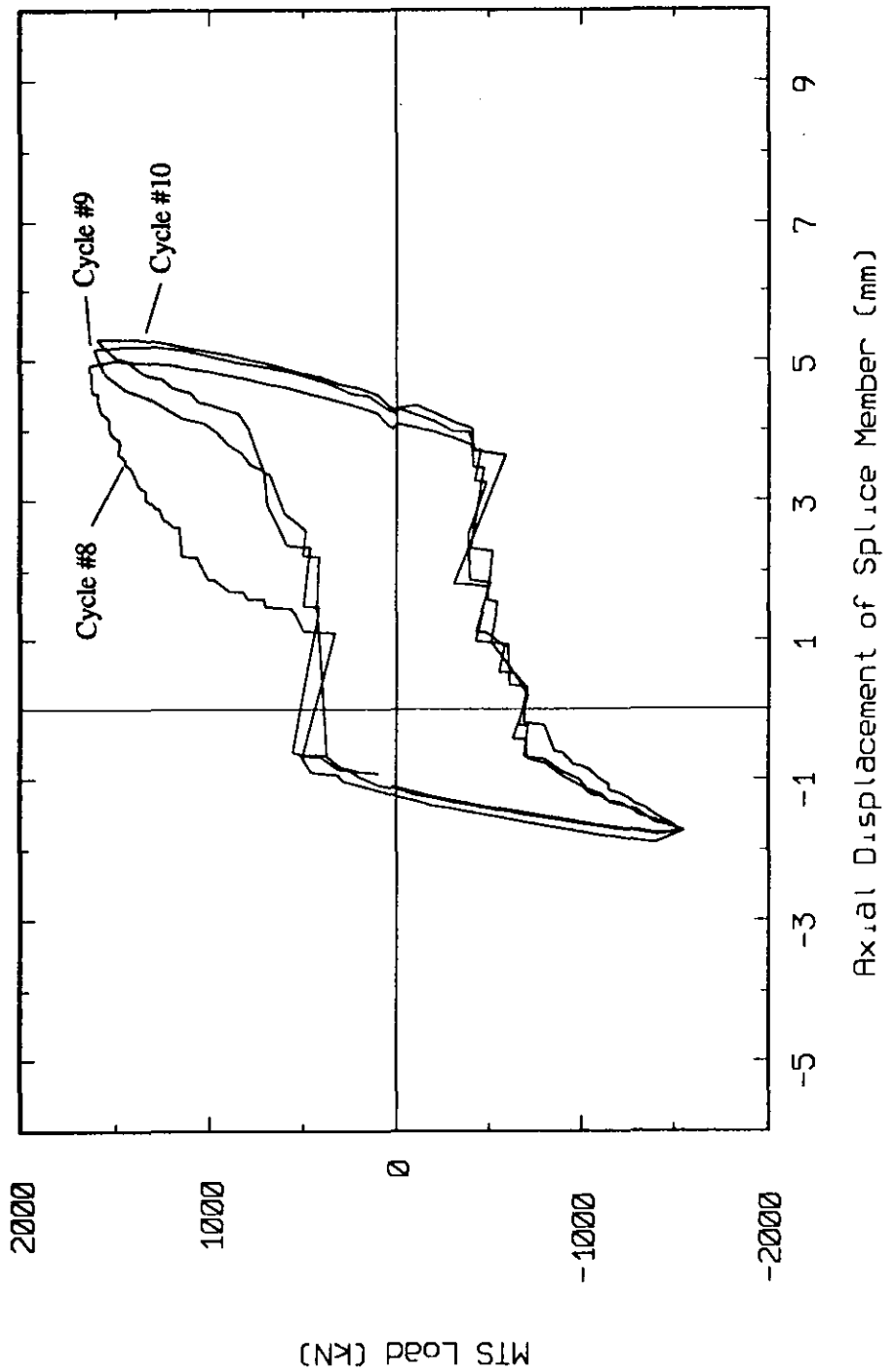

Figure 5.3. Cyclic Softening - Specimen A-1

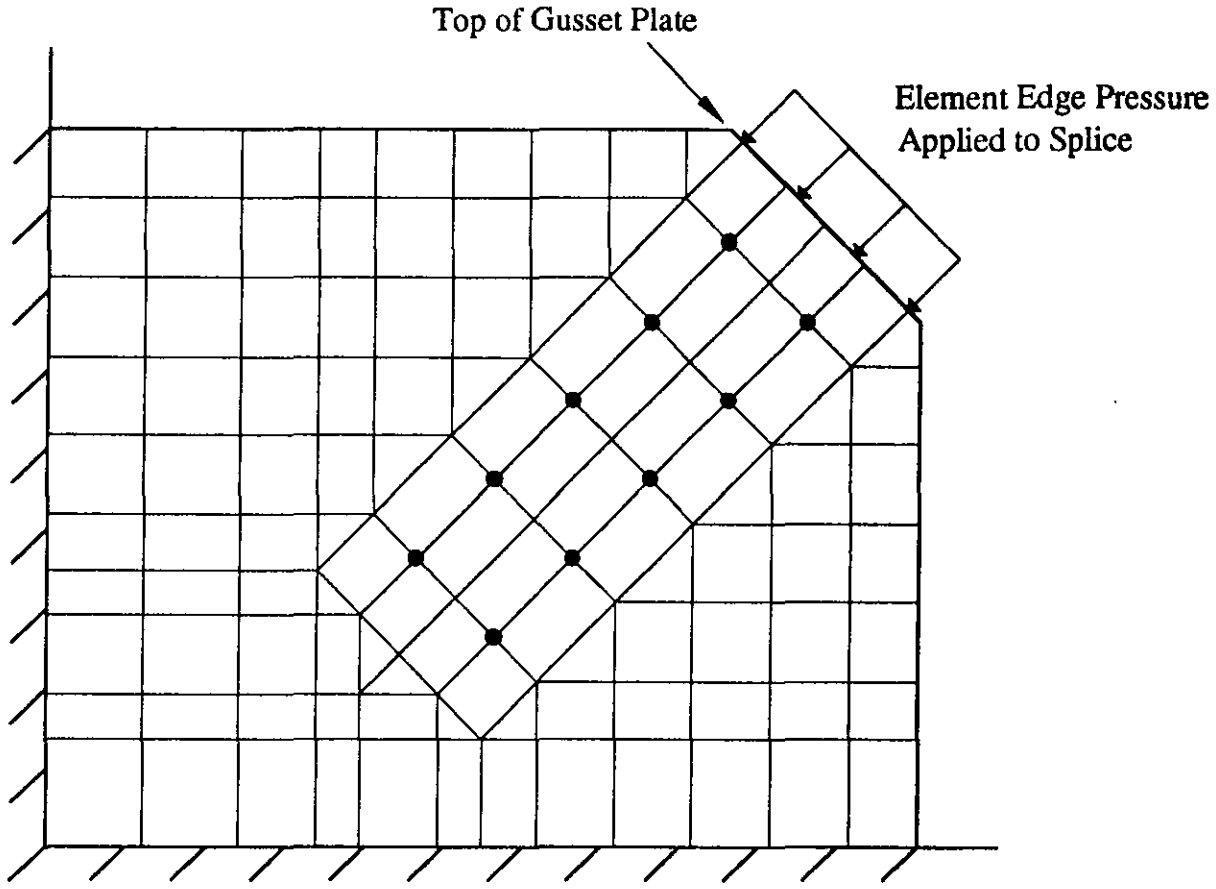

Figure 5.4. Finite Element Mesh

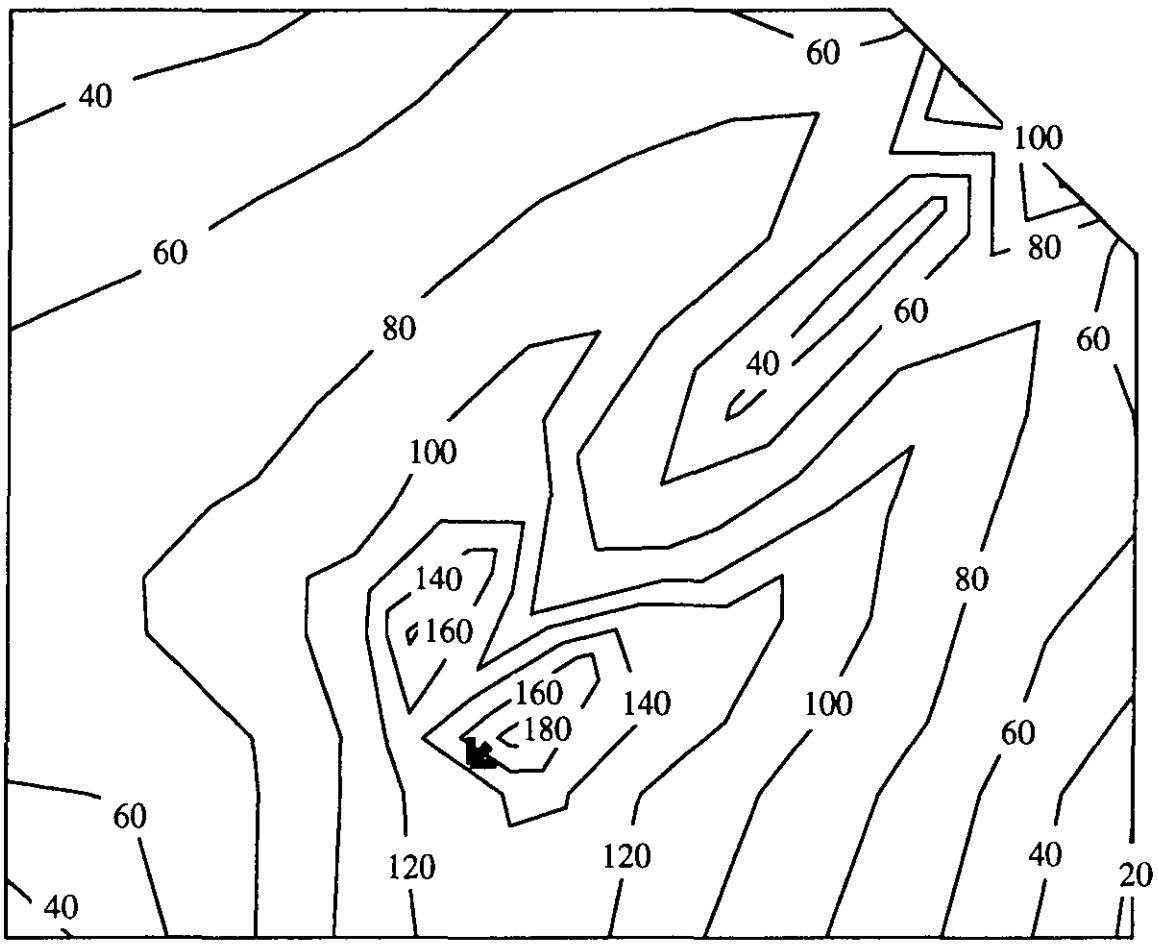

(stress in MPa)
Maximum Stress = 187.0 MPa

Figure 5.5. Analytical Stress Distribution - Specimen A-1

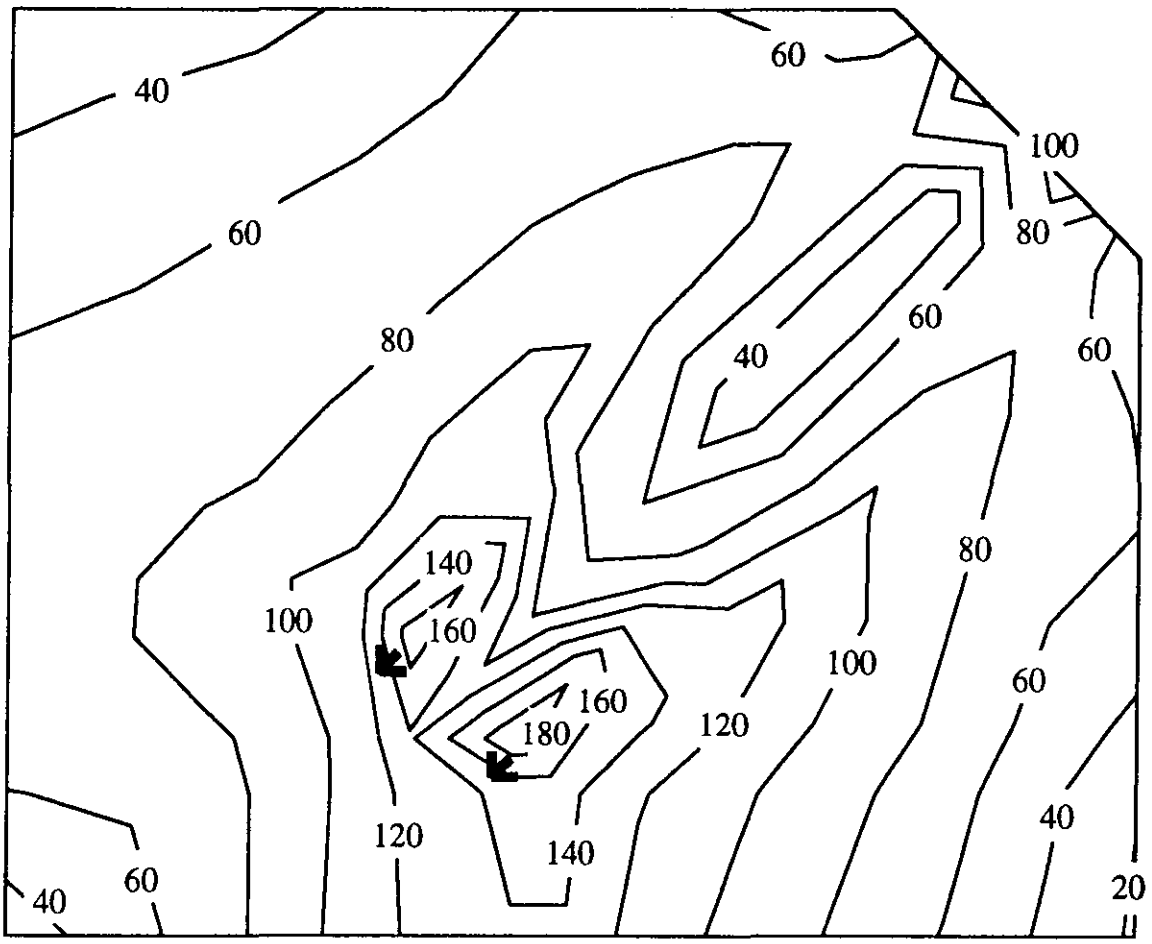

(stress in MPa)
Maximum Stress = 195.2 MPa

Figure 5.6. Analytical Stress Distribution - Specimen A-2

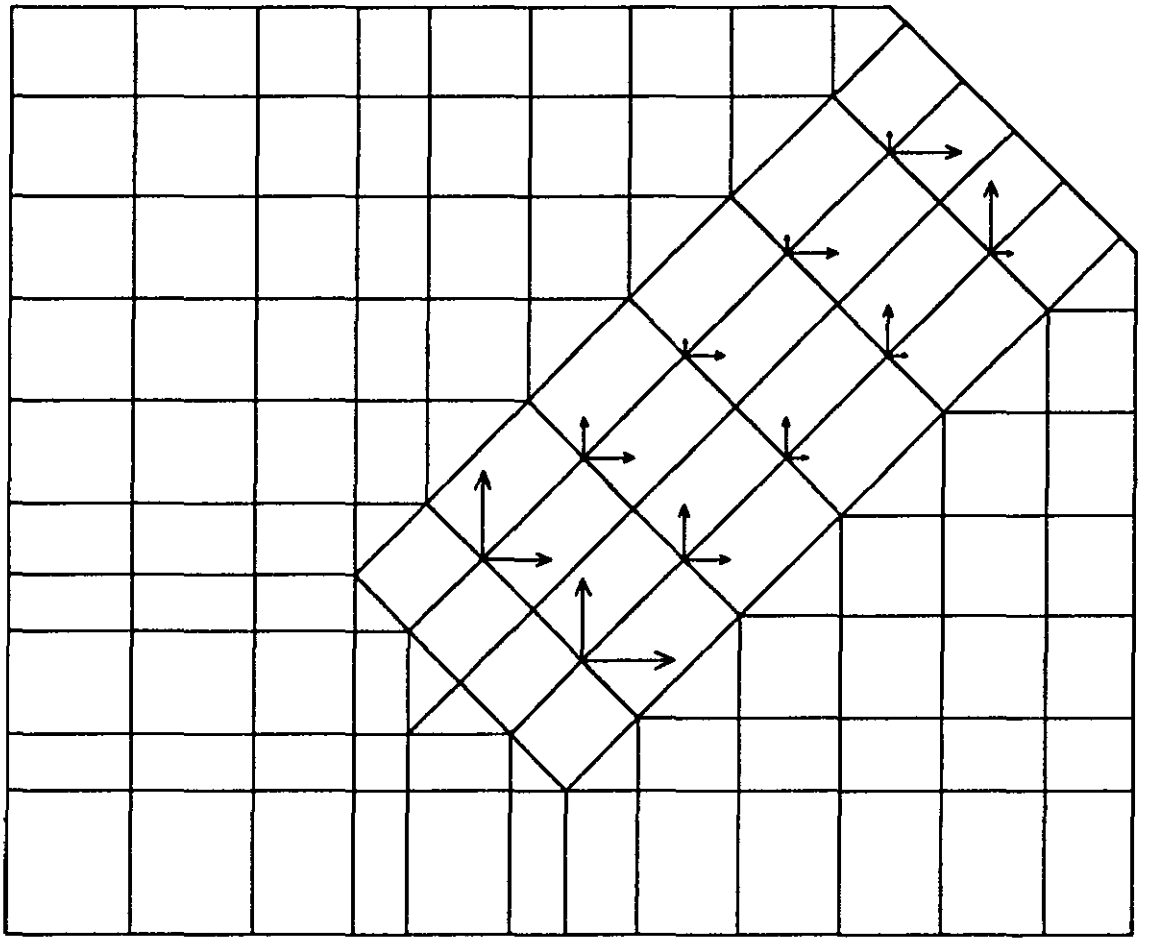

Figure 5.7. Analytical Fastener Force Distribution - Specimen A-1

6. SUMMARY AND DESIGN GUIDELINE

6.1 Summary

The cyclic behavior of steel gusset plates has been examined by an experimental investigation of full-scale gusset plate connections of a diagonal bracing member at the joint of a beam and column. The frame model examined considers a concentric braced frame where the brace member is designed not to buckle. The energy of the system is designed to be absorbed by the gusset plate connection. The experimental program considered the effect of the gusset plate thickness, plate edge stiffeners, gusset plate geometry, and connection bolt slip on the energy absorption characteristics of the system. A total of five gusset plate specimens were tested under reverse loading conditions. The brace member was connected to the gusset plate by means of a bolted splice member connection. The gusset plate was directly welded to the beam and column members of the frame. The test results were analyzed and compared to current design practices and to the results of a monotonic gusset plate test series. The finite element program ANSYS was used to provide an analytical reference to the observed test results. The following is a summary of the most significant findings from this investigation.

1. The ultimate tensile and compressive capacity of the unstiffened gusset plate specimens is roughly proportional to the thickness of the specimen.
2. The ultimate tensile capacity was governed by the plate thickness and the connection geometry. The tensile capacity was not affected by either the addition of plate edge stiffeners to Specimen A-3 and A-4, or the modified plate geometry of Specimen A-5. All specimens with the same plate thickness and the same connection geometry reached approximately the same ultimate load level in tension.
3. The addition of plate edge stiffeners significantly improved the energy absorption

behavior of the gusset plates tested. The effect of plate edge stiffeners on the ultimate compressive capacity of gusset plates is dependent on the size and stiffness of the stiffener.

4. Unstiffened gusset plates experience a sudden drop in compressive load carrying capacity once overall plate buckling occurs. In contrast, stiffened gusset plates experience a stable post-buckling response; there is only a gradual decrease in compressive load carrying capacity under cycles of increasing axial compressive deformation.

5. The test results from Specimen A-5 indicate that there is no rationale for providing for the free formation of a plastic hinge in the geometry of a gusset plate connected to the main framing members on two sides. The gusset plate geometry required to accommodate the free formation of a plastic hinge under compressive deformations results in a reduced stiffness and buckling load.

6. Slip displacements in the gusset plate to splice member bolted connection can contribute significantly to the energy absorption capacity of the gusset plate assembly. However, to be able to consider the energy absorbed through connection slip, it must be assured that connection slip will occur during every loading cycle.

7. The Whitmore yield load (Whitmore, 1952) underestimates the ultimate tensile capacity of the test specimens. The tension tear-out load proposed by Hardash and Bjorhovde (1985) provides a very good estimate of the ultimate tensile capacity of the test specimens.

8. The Whitmore yield load (Whitmore, 1952) is ineffective in estimating the ultimate compressive capacity of the test specimens. The Thornton equivalent column load (Thornton, 1984) produced conservative estimates of the ultimate compressive capacity of the test specimens. The Thornton method accounts for the overall

geometry of the gusset plate, but does not account for the presence of plate edge stiffeners.

9. The ultimate tensile behavior of the test specimens does not appear to be significantly adversely affected by the cyclic loading history and the extreme compressive deformations that resulted. However, when the ultimate compressive behavior is compared to gusset plates tested under monotonic loading conditions, it is observed that cyclic loading significantly reduces the ultimate compressive strength of gusset plates.

10. The tensile failure mode of all gusset plate specimens was a fracture of the plate material between the bolt holes in the bottom row of the splice member connection. The compressive failure mode of all gusset plate specimens was ultimately an overall buckling of the gusset plate. For the stiffened specimens, overall buckling of the gusset plate was delayed until the stiffeners began to yield.

11. The peak gusset plate strains recorded during the elastic portion of loading were beneath the base of the splice member. The general elastic distribution of gusset plate strains recorded during testing are in good agreement with the results obtained from the finite element analysis.

6.2 Design Guideline for Gusset Plates Under Cyclic Loads

Properly designed and detailed gusset plate connections appear capable of absorbing significant amounts of energy to validate the proposed 'strong brace, weak gusset' concentric braced frame model. The brace member is designed not to buckle. The energy of the system is designed to be absorbed by the inelastic deformation of the gusset plate connection.

Based on the test results, a design guideline for gusset plates subjected to cyclic loading

conditions is recommended as below. However, it should be noted that the present recommendations are based on the limited results of the current investigation. Further research as outlined in the next section is required for the improvement of the proposed design recommendation.

1. Plate edge stiffeners should be added to all gusset plates in order to improve their behavior under cyclic loads. The size and stiffness of the edge stiffener should be sufficient to delay the onset of overall plate buckling of the gusset plate and to provide a stable post-buckling response.
2. The tensile strength of gusset plates under cyclic loads can be accurately determined using the block shear tear-out model proposed by Hardash and Bjorhovde (1985).
3. Prior to the development of a more refined design approach, the Thornton equivalent column method (Thornton, 1984) can be used to provide a conservative estimate of the ultimate compressive capacity of gusset plates under cyclic loads.
4. A defined free plastic hinge width should not be provided for in the geometry of the gusset plate when the gusset plate is connected to the main framing members along two plate edges. No special provisions need to be made to accommodate the formation of a plastic hinge in the gusset plate.
5. The end of the splice member should be located within the region of the gusset plate constrained by the plate boundary to the beam and column frame members.

6.3 Recommendations for Future Research

Further research should be conducted on the cyclic behavior of steel gusset plate connections in the following areas:

1. A parametric study should be performed to determine the optimum size and stiffness

of plate edge stiffener required to improve the buckling strength and energy absorption characteristics of gusset plates under cyclic loads.

2. Further study is required to develop a more refined design method for the compressive capacity of gusset plates under cyclic loads. Such a study should attempt to evaluate the loss in gusset plate compressive capacity due to cyclic loading effects.

3. A full scale test program should be undertaken to determine the ability of bolt slip in the gusset plate to splice member connection to partake in the energy absorption mechanism of a concentric braced frame.

4. Further tests should be conducted to investigate the optimum location for placing the end of the splice member (or brace member) in order to maximize the compressive strength and overall ductility of the connection.

5. Full frame tests should be performed to better assess the energy absorption characteristics of the proposed 'strong brace, weak gusset' concentric braced frame model. A comparison with the energy absorption characteristics of other types of braced frames would be beneficial.

REFERENCES

AASHTO, 1989. Standard Specification for Highway Bridges - Fourteenth Edition. The American Association of State Highway and Transportation Officials, Washington, D.C.

AISC, 1986. Load and Resistance Factor Design Specification for Structural Steel Buildings. American Institute of Steel Construction (AISC), Chicago, Illinois.

AISC, 1992. Seismic Provisions for Structural Steel Buildings. American Institute of Steel Construction (AISC), Chicago, Illinois.

Akay, H.U., Johnson, C.P., and Will, K.M., 1977. "Lateral and Local Buckling of Beams and Frames." Journal of the Structural Division, Proceedings of the American Society of Civil Engineers, Vol. 103, No. ST9, September, pp. 1821-1832.

Astaneh, A., 1992. "Cyclic Behavior of Gusset Plate Connections in V-Braced Frames." Stability and Ductility of Steel Structures Under Cyclic Loading, ed. Y. Fukumoto and G.C. Lee, CRC Press, Boca Raton, Florida, pp. 63-74.

Astaneh, A., Goel, S.C., and Hanson, R.D., 1986. "Earthquake Resistant Design of Double-Angle Bracing." Engineering Journal, AISC, Vol. 23, No. 4, Fourth Quarter, pp. 133-147.

Astaneh-Asl, A., Goel, S.C., and Hanson, R.D., 1981. "Behavior of Steel Diagonal Bracing." ASCE Conference, October 26-31, St. Louis, Missouri.

Astaneh-Asl, A., Goel, S.C., and Hanson, R.D., 1985. "Cyclic Out-of-plane Buckling of Double Angle Bracing." Journal of Structural Engineering, ASCE, Vol. 111, No. 5, May, pp. 1135-1153.

ASTM, 1992. "A370-92 - Standard Test Methods and Definitions for Mechanical Testing of Steel Products." 1992 Annual Book of ASTM Standards, Vol. 03.01.

Bjorhovde, R. and Chakrabarti, S.K., 1985. "Tests of Full-Size Gusset Plate Connections." Journal of Structural Engineering, ASCE, Vol. 111, No. 3, March, pp. 667-684.

Chajes, A., Britvec, S.J., and Winter, G., 1963. "Effects of Cold-Straining on Structural Sheet Steels." Journal of the Structural Division, Proceedings of the American Society of Civil Engineers, Vol. 89, No. ST2, April, pp. 1-32.

Cheng, J.J.R. and Hu, S.Z., 1987. "Compressive Tests of Gusset Plate Connections." SSRC 1987 Annual Conference, March 24-25, Houston, Texas.

Cheng, J.J.R. and Yam, M., 1991. "Buckling Strength of Gusset Plate Connections." 1991 Annual Conference of the Canadian Society for Civil Engineers, May 29-31, Vancouver, pp. 83-92.

Cheng, J.J.R, Yam, M., and Hu, S.Z., 1993. "Elastic Buckling Strength of Gusset Plate Connections." Accepted for publication by Journal of Structural Engineering, ASCE.

CSA, 1988. CAN/CSA-S6-88 - Design of Highway Bridges. Canadian Standards Association (CSA), Rexdale, Ontario.

CSA, 1989. CAN/CSA-S16.1-M89 - Limit States Design of Steel Structures. Canadian Standards Association (CSA), Rexdale, Ontario.

Davis, C.S., 1967. "Computer Analysis of the Stresses in a Gusset Plate." Thesis presented to the University of Washington, at Seattle, in partial fulfillment of the requirements for the degree of Master of Science.

Davis, H.E., Troxell, G.E., and Hauck, G.F.W., 1982. The Testing of Engineering Materials. McGraw-Hill Book Company, Fourth Edition, New York.

Engelhardt, M.D. and Popov, E.P., 1989. "Tests on Brace and Link Connections for EBFs." Steel Structures - Proceedings of the Sessions Related to Steel Structures at Structures Congress '89, ASCE, ed. Jerome S.B. Iffland, May 1-5, San Francisco, pp. 549-558.

Gross, J.L., 1990. "Experimental Study of Gusseted Connections." Engineering Journal, AISC, Vol. 27, No. 3, Third Quarter, pp. 89-97.

Hardash, S.G. and Bjorhovde, R., 1985. "New Design Criteria for Gusset Plates in Tension." Engineering Journal, AISC, Vol. 22, No. 2, pp. 77-94.

Hardin, B.O. 1958. "Experimental Investigation of the Primary Stress Distribution in the Gusset Plates of a Double Plane Pratt Truss Joint with Chord Splice at the Joint." University of Kentucky Engineering Experiment Station, Bulletin No. 49.

Irvan, W.G., 1957. "Experimental Study of Primary Stresses in Gusset Plates of a Double Plane Pratt Truss." University of Kentucky Engineering Experiment Station, Bulletin No. 46.

Kulak, G.L., Fisher, J.W., and Struik, J.H.A., 1987. Guide to Design Criteria for Bolted and Riveted Joints. John Wiley and Sons, Second Edition, New York.

NRCC, 1990. National Building Code of Canada 1990. Associate Committee on the National Building Code, National Research Council of Canada, Ottawa, Ontario.

Popov, E.P. and Engelhardt, M.D., 1988. "Seismic Eccentrically Braced Frames." Journal of Construction Steel Research, Vol. 10, pp. 321-354.

Singh, A., Gerstle, K.H., and Tulin, L.G., 1965. "The Behavior of Reinforcing Steel Under Reversed Loading." Material Research and Standards, ASTM, Vol. 5, No. 1, January, pp. 12-17.

Starke, E.A. Jr. and Lutjering, G, 1978. "Cyclic Plastic Deformation and Microstructure." Fatigue and Microstructure, Papers presented at the 1978 ASM Materials Science Seminar, October 14-15, St. Louis, Missouri, pp. 205-243.

Thornton, W.A., 1984. "Bracing Connections for Heavy Construction." Engineering Journal, AISC, Vol. 21, No. 3, pp. 139-148.

Vasarhelyi, D.D., 1971. "Tests of Gusset Plate Models." Journal of the Structural Division, Proceedings of the American Society of Civil Engineers, February, pp. 665-678.

Wakabayashi, M., Matsui, C., Minami, K., and Mitani, I, 1974. "Inelastic Behavior of Full-Scale Steel Frames with and without Bracings." Bulletin. Disaster Prevention Research Institute, Kyoto University, Vol. 24, Part I, No. 216, March, pp. 1-23.

Whitmore, R.E., 1952. "Experimental Investigation of Stresses in Gusset Plates." Bulletin No. 16, Engineering Experiment Station, University of Tennessee.

Williams, G.C. and Richard, R.M., 1986. "Steel Connection Design Based on Inelastic Finite Element Analysis." Report of the Department of Civil Engineering and Engineering Mechanics, The University of Arizona.

APPENDIX A. Additional Test Data

Figures A.1 to A.5 show the load versus axial displacement response of the gusset plate for the specimens tested. The displacement is recorded by the LVDTs attached to the top of the gusset plate adjacent to the splice member connection. The observed displacement is that of the gusset plate itself. The deformations in the splice member, the local bearing deformations in the gusset plate bolted connection, and the connection slip in the splice member to gusset plate connection, if any, are not included. For the purpose of comparison, Figures A.1 to A.5 are plotted to the same scale as the load versus displacement curves presented in Chapter 4.

Figures A.6 to A.10 show the out-of-plane displacement response of the test frame. The displacement is recorded by the LVDT attached the distributing beam. The displacement represents the out-of-plane sway of the test frame and the lower end of the gusset plate. The test frame was allowed to displace out-of-plane to simulate the desired plate boundary condition.

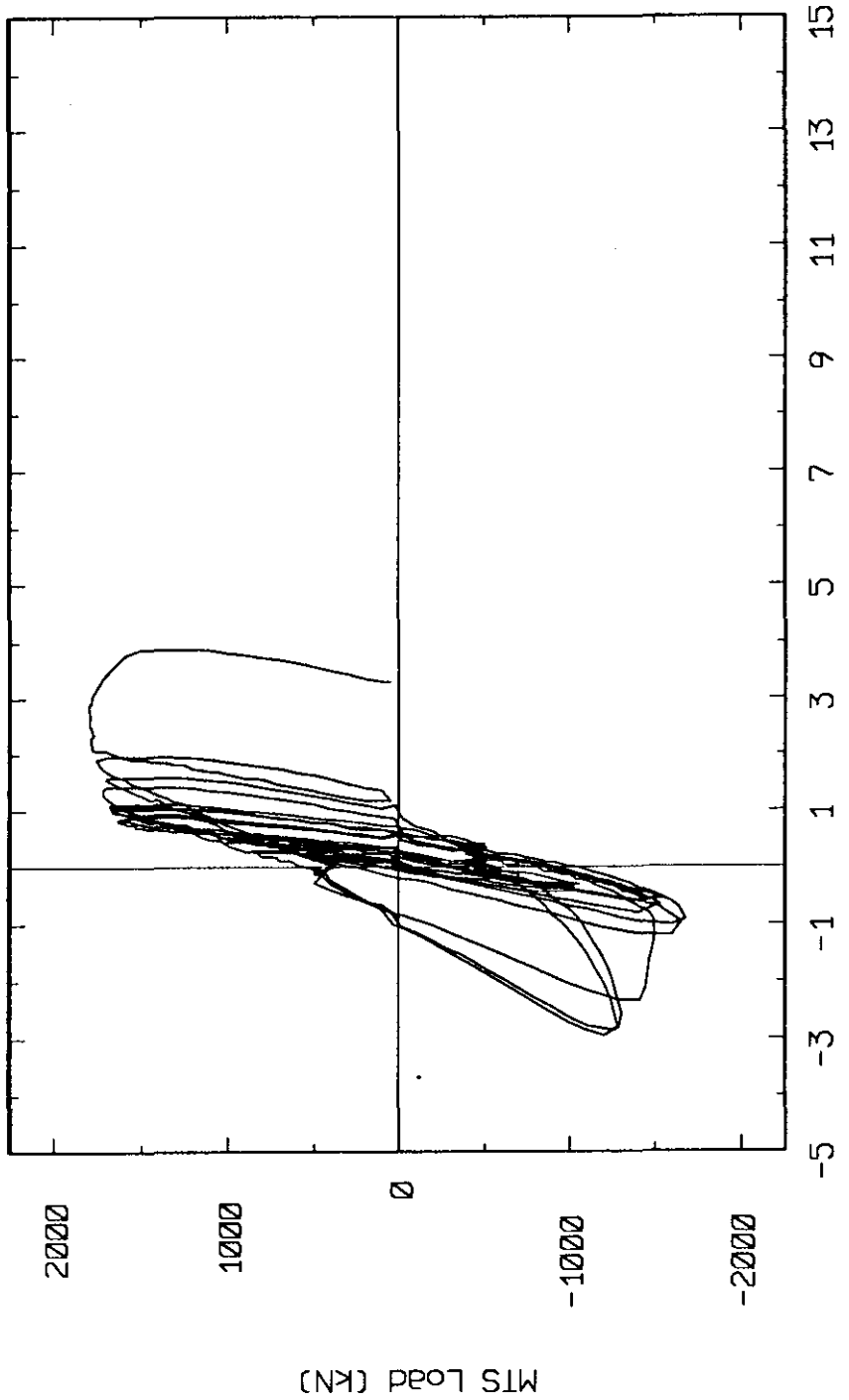

Figure A.1. Load vs. Axial Displacement Response of the Gusset Plate - Specimen A-1

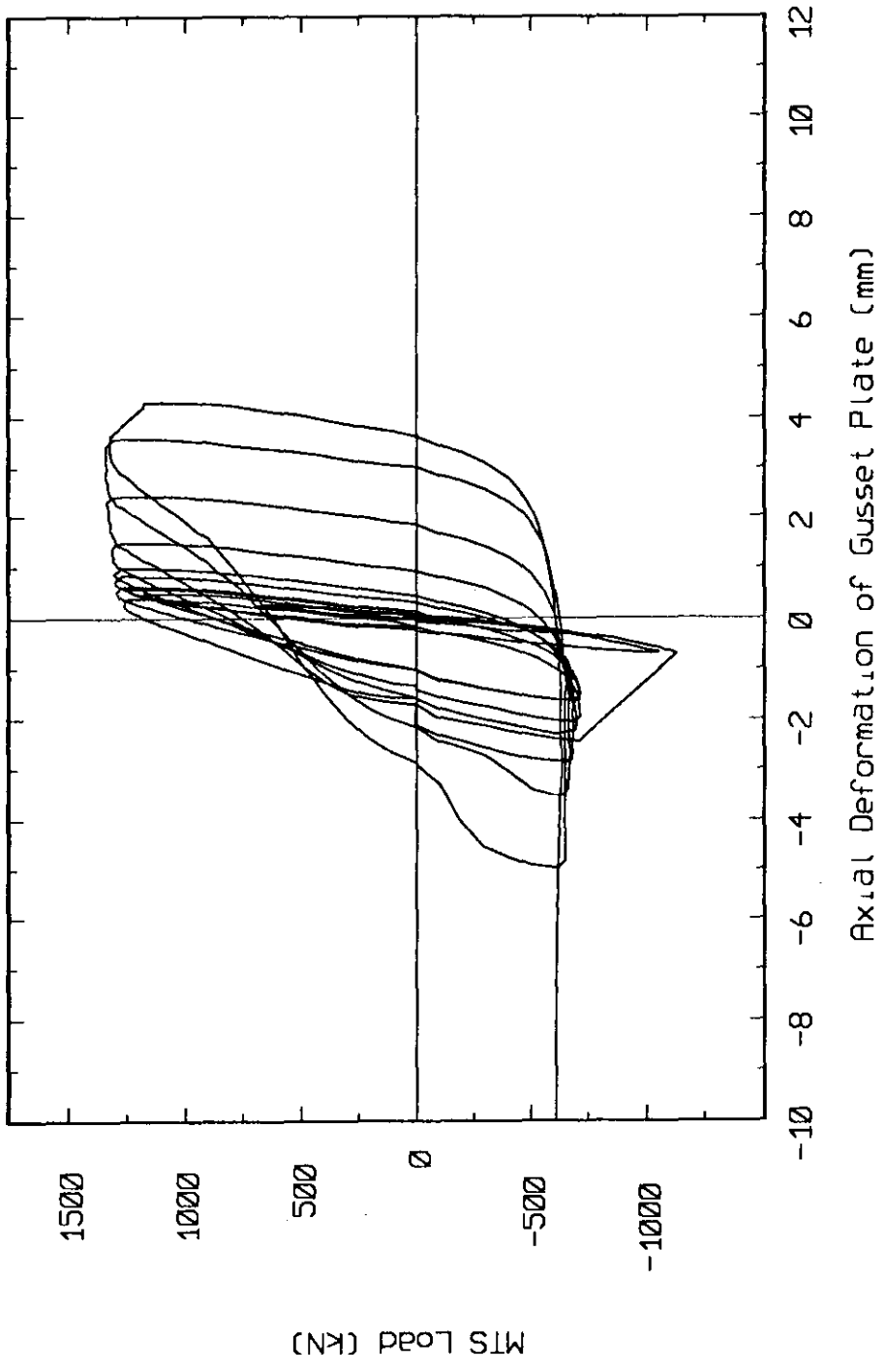

Figure A.2. Load vs. Axial Displacement Response of the Gusset Plate - Specimen A-2

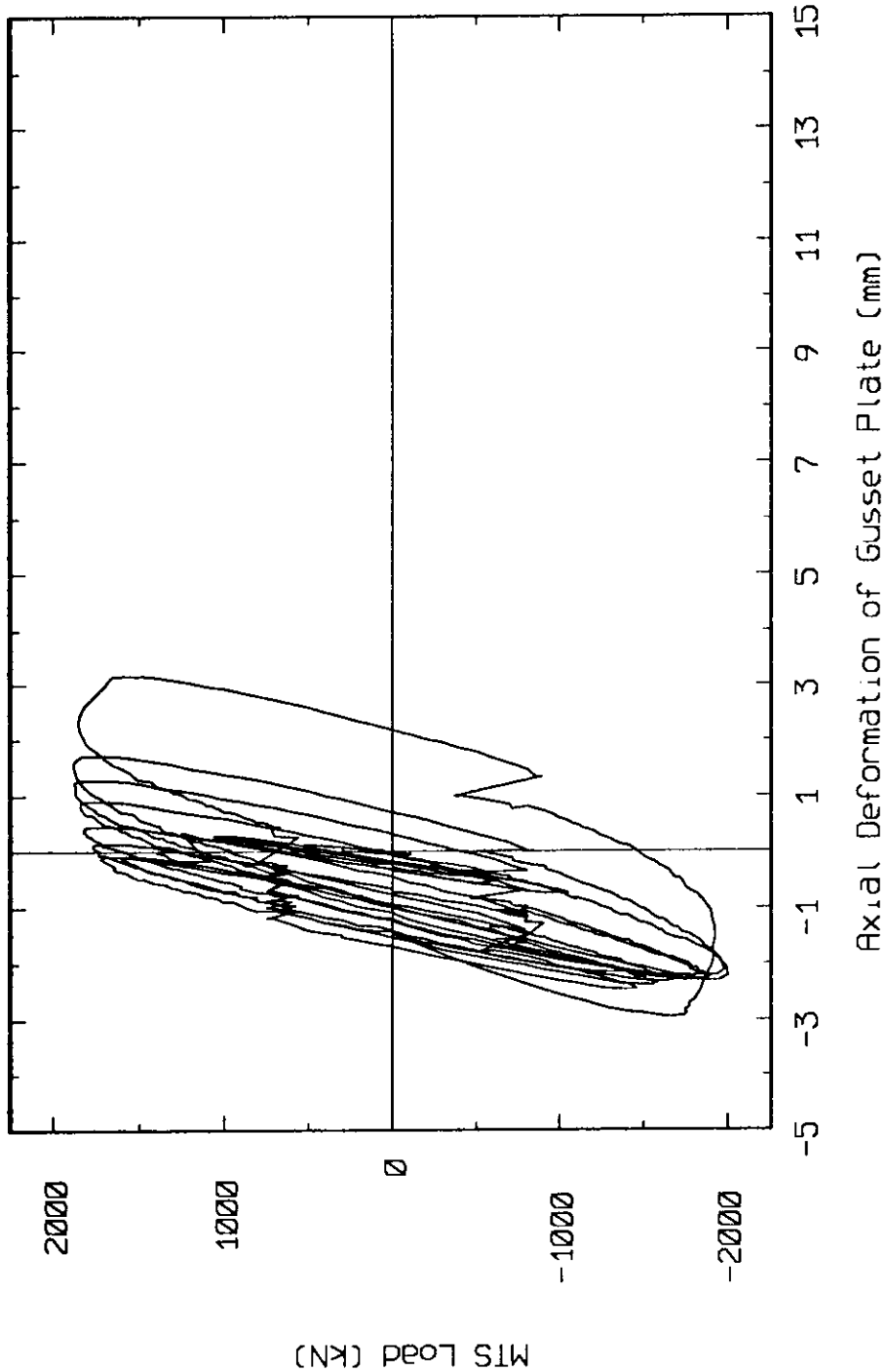

Figure A.3. Load vs. Axial Displacement Response of the Gusset Plate - Specimen A-3

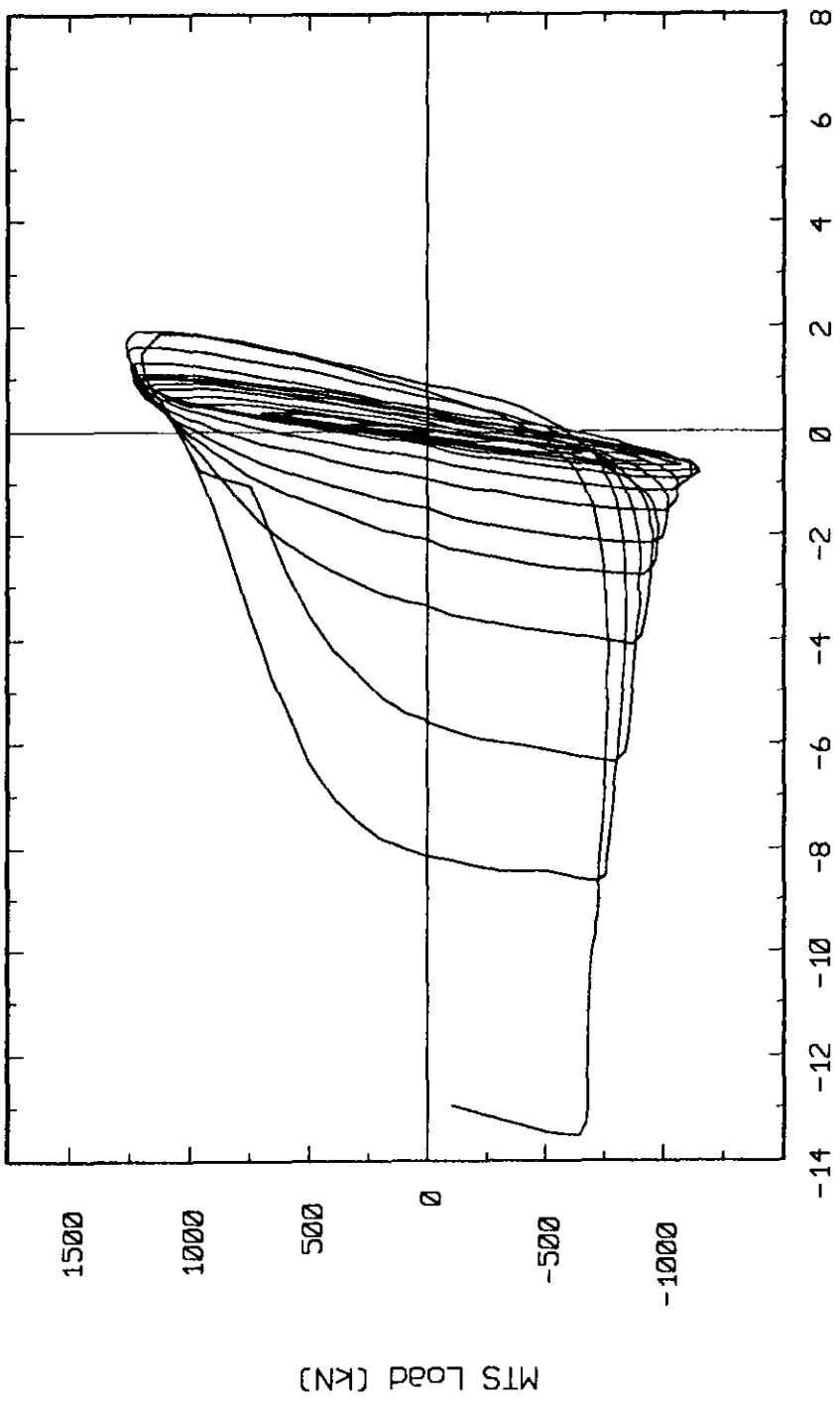

Figure A.4. Load vs. Axial Displacement Response of the Gusset Plate - Specimen A-4

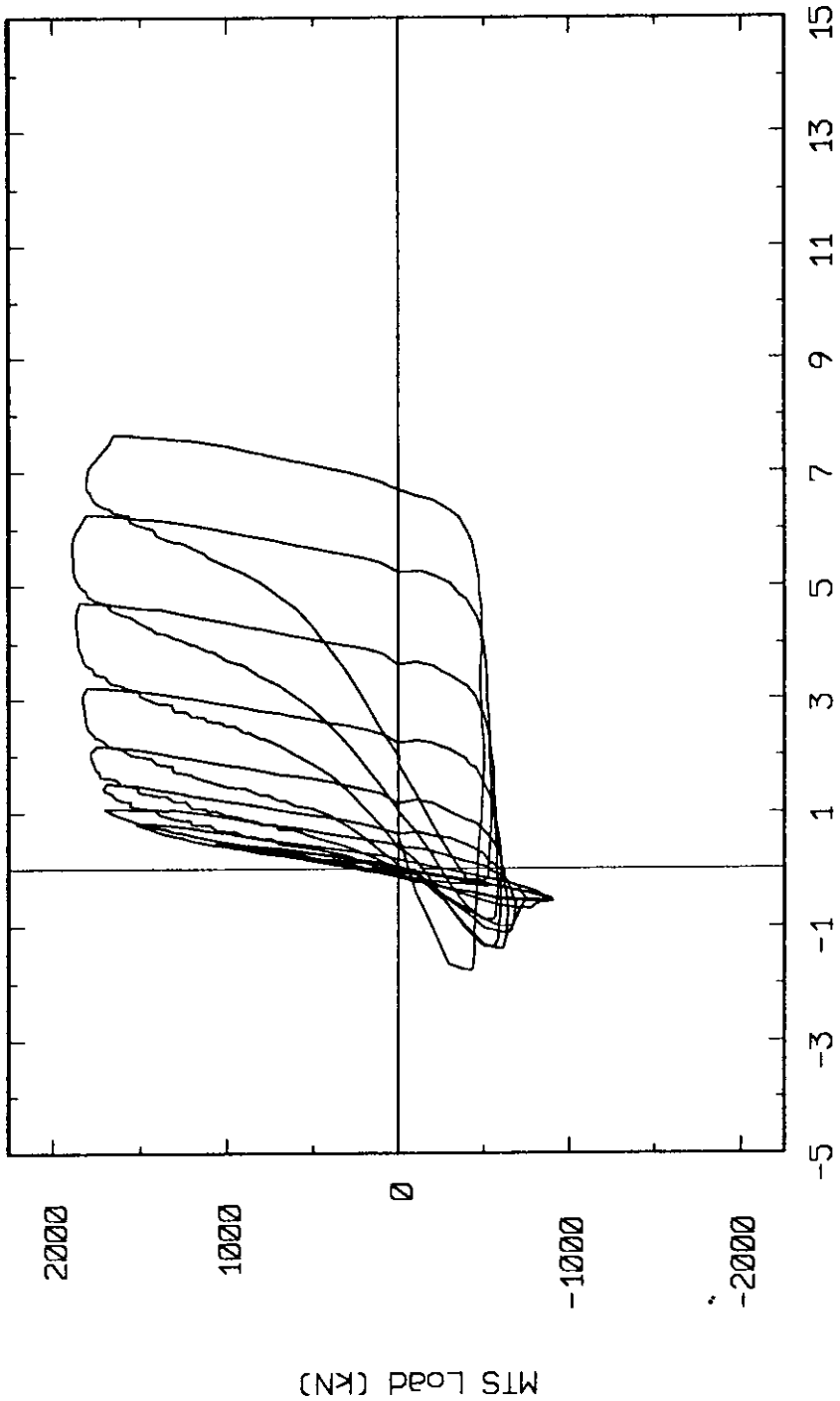

Figure A.5. Load vs. Axial Displacement Response of the Gusset Plate - Specimen A-5

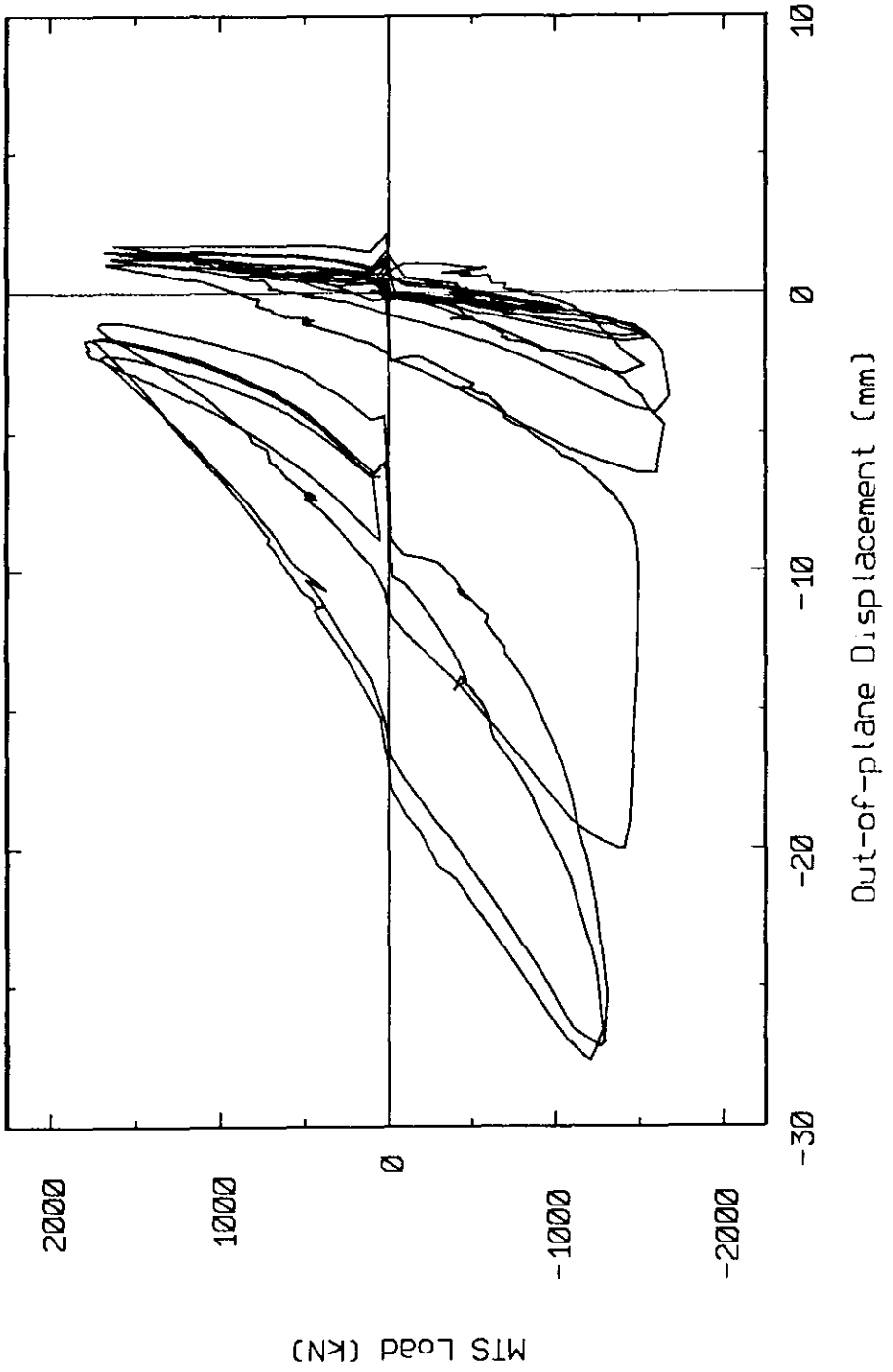

Figure A.6. Out-of-plane Displacement of Test Frame - Specimen A-1

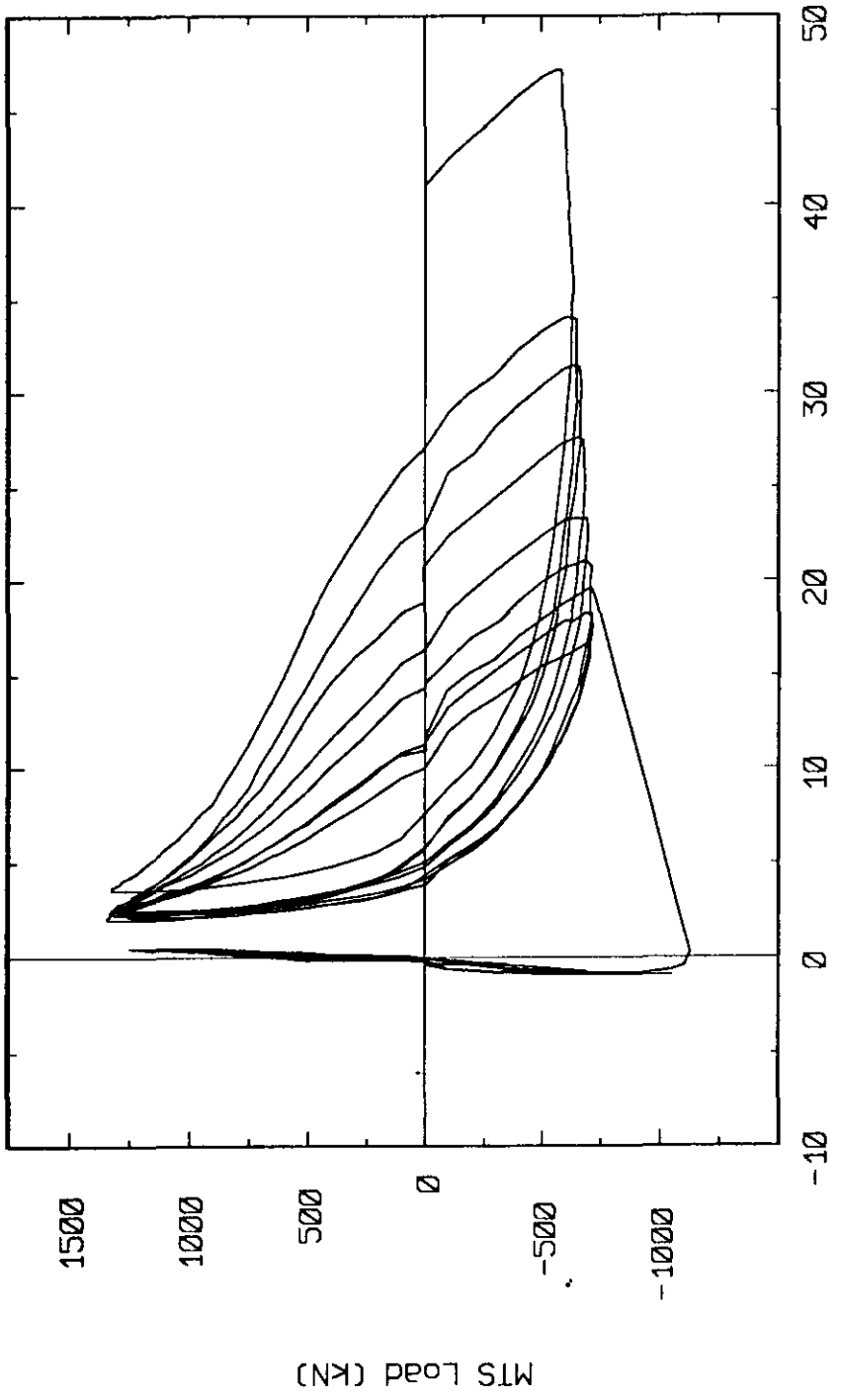

Figure A.7. Out-of-plane Displacement of Test Frame - Specimen A-2

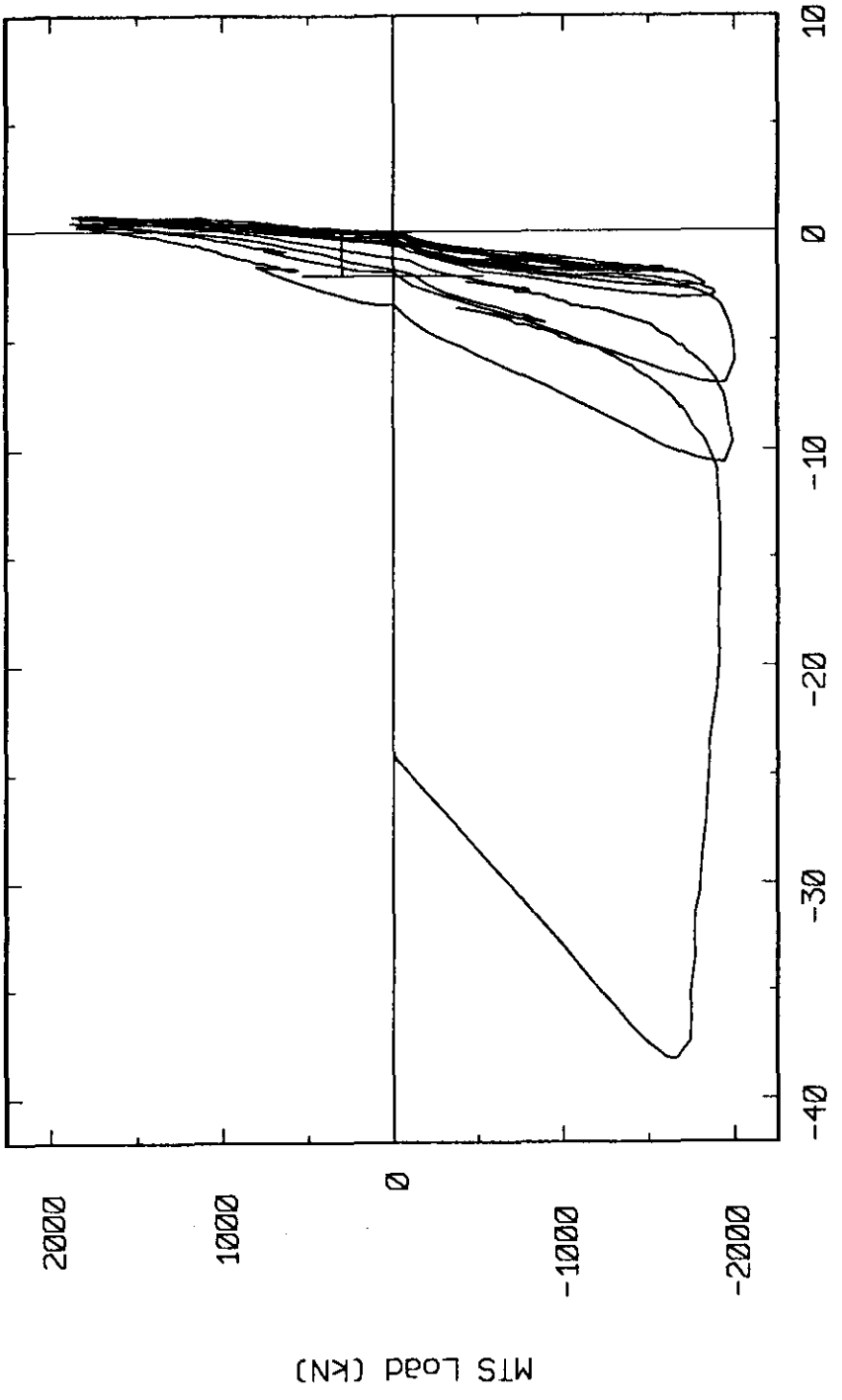

Figure A.8. Out-of-plane Displacement of Test Frame - Specimen A-3

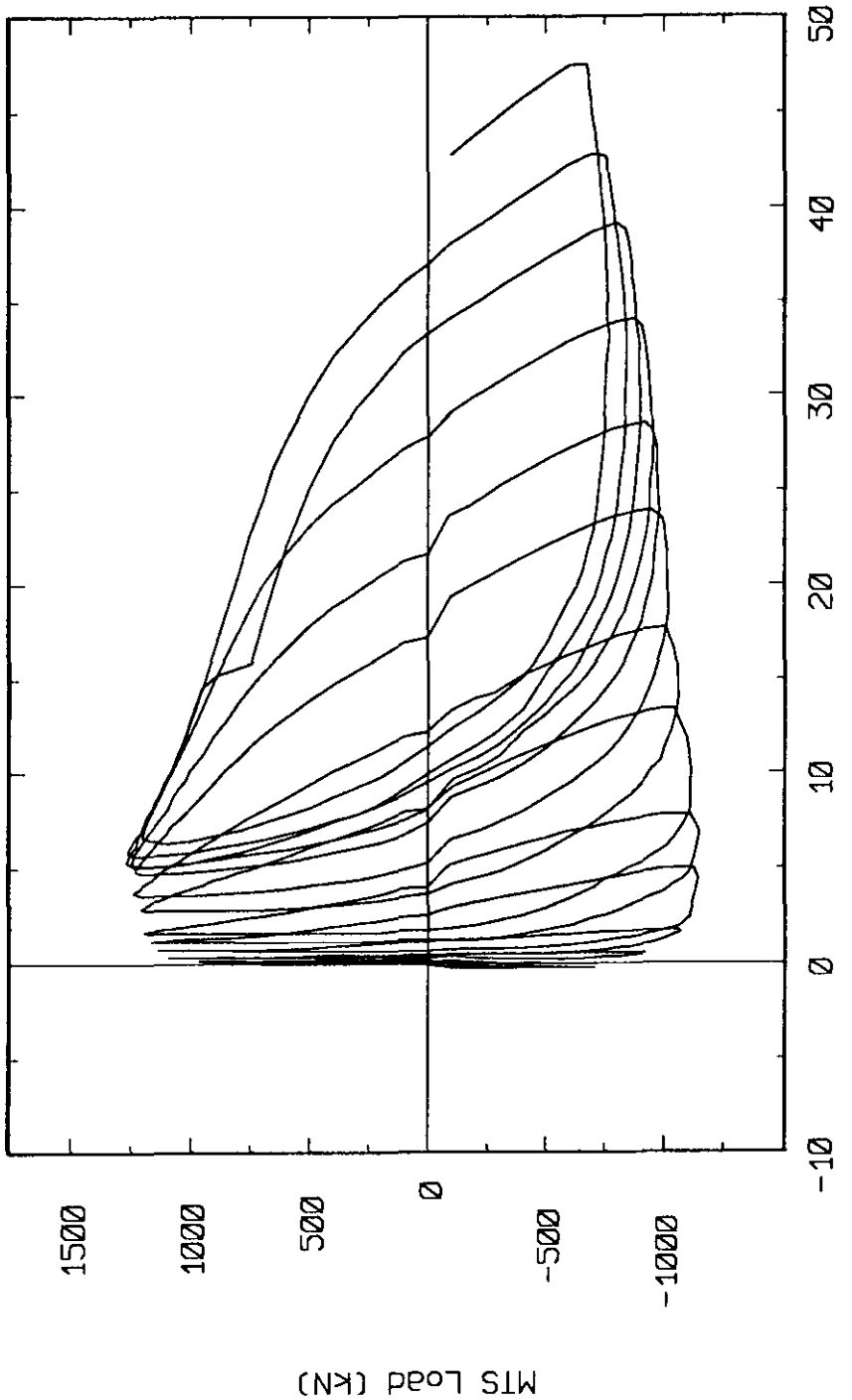

Figure A.9. Out-of-plane Displacement of Test Frame - Specimen A-4

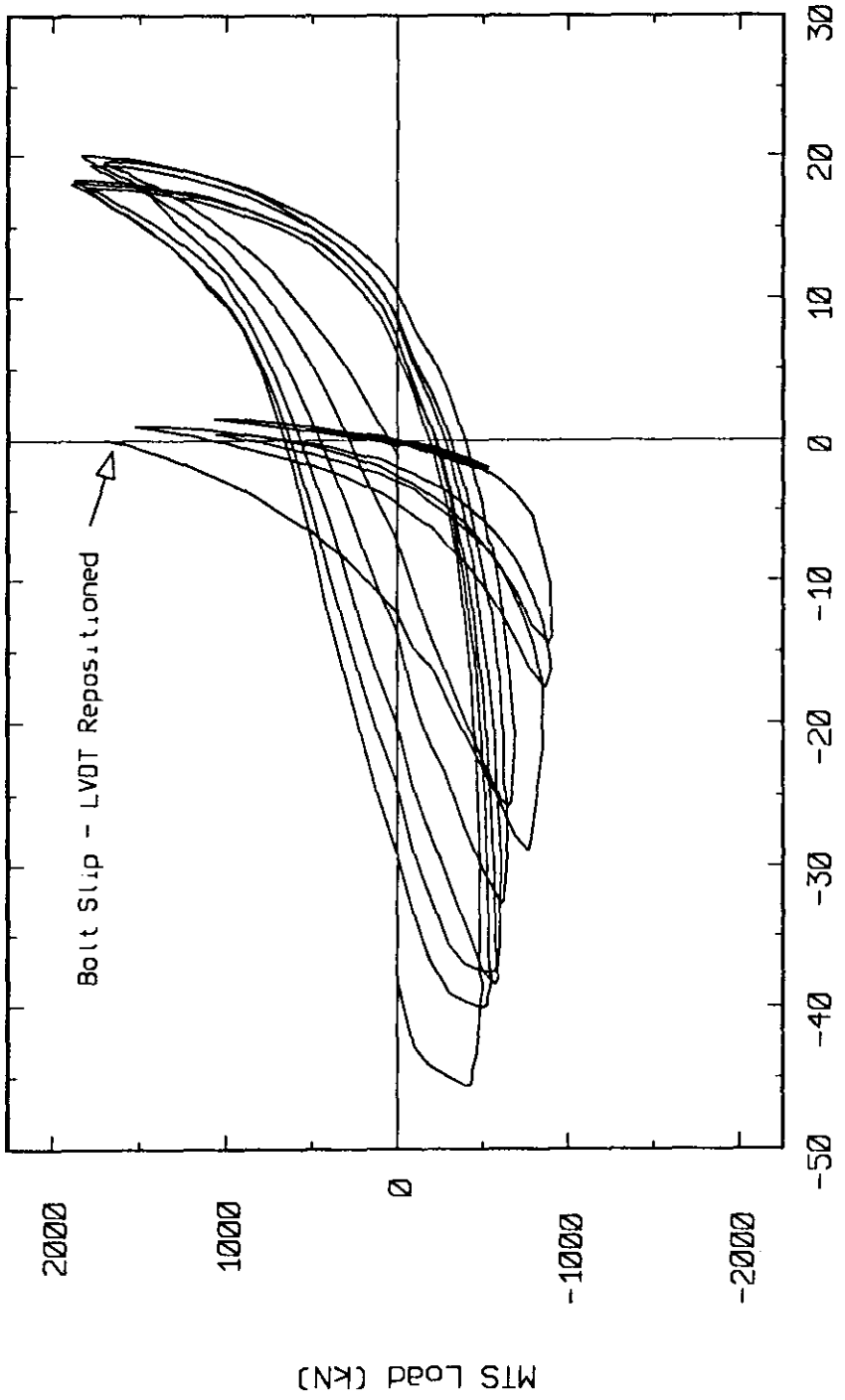

Figure A.10. Out-of-plane Displacement of Test Frame - Specimen A-5